Durham University

Durham E-Theses

The petrology and structure of the country around Julianehaab, South-West Greenland

Robert William Nesbitt

How to cite:

Nesbitt, Robert William (1961) The petrology and structure of the country around Julianehaab, South-West Greenland. Doctoral thesis, Durham University.

Use policy

The full-text may be used and/or reproduced, and given to third parties in any format or medium, without prior permission or charge, for personal research or study, educational, or not-for-profit purposes provided that:

- a full bibliographic reference is made to the original source
- a https://etheses.durham.ac.uk/id/eprint/10356/ is made to the metadata record in Durham E-Theses
- the full-text is not changed in any way

The full-text must not be sold in any format or medium without the formal permission of the copyright holders.

Please consult the full Durham E-Theses policy for further details.

Academic Support Office, The Palatine Centre, Durham University, Stockton Road, Durham, DH1 3LE
e-mail: e-theses.admin@durham.ac.uk Tel: +44 0191 334 6107
https://etheses.durham.ac.uk

THE

PETROLOGY AND STRUCTURE

OF

THE COUNTRY AROUND JULIANEHAAB,

SOUTH-WEST GREENLAND.

by

Robert William Nesbitt, B.Sc., F.G.S.

A thesis submitted for the Degree of Doctor of Philosophy in the University of Durham.

University College.

November 1961.

VOLUME TWO.

ILLUSTRATIONS

List of Figures.

		Facing page.
Fig. 1.1....	General geology of S.W.Greenland.....	2.
1.2....	Map of S. Greenland.	2.
1.3....	Locality map of the area studies.....	3.
2.1....	Veins of Sanerutian Granite cutting Porphyritic Granite.	4.
2.2....	Block of Ketilidian Granite in Sanerutian Granite.	4.
2.3....	Banding in the Sanerutian Granite.....	5.
2.4....	Sanerutian Granite-dioritic gneiss contact.	5.
2.5....	Contact of Sanerutian Granite and Ketilidian Granite	6.
2.6....	"Flow banding"	6.
2.7....	Fault breccia.	7.
3.1....	Gneiss band feature, Trekant Sø	8.
3.2....	Acid veins in the gneiss band	8.
3.3....	Banding in amphibolitic gneiss	9.
3.4....	Acid gneiss- amphibolitic gneiss contact.	9.
3.5....	Acid wedges in amphibolitic gneiss.....	10.
3.6....	Folded amphibolitic gneiss	10.
3.7....	Sketch of folded axial planes in gneiss band.	11.
3.8....	Broken aplitic vein in gneiss	11.
3.9....	Partially digested gneiss block in granite.	12.
3.10...	Migmatitic contact between gneiss and granite.	12.
3.11...	Ptygmatically folded acid veins in the gneiss band	13.
3.12...	Central part of a breccia zone	13.
3.13...	Specimen from the breccia zone	14.
3.14...	Northern margin of the breccia zone	14.

(list of figures, continued) Facing page.

Fig. 3.15.... View of gabbro knolls ..... 15.

3.17.... Contact between the dioritic amphibolite and granite. ..... 15.

3.16.... Geological sketch map of the gabbro-norite mass. ..... 16.

3.18.... Contact between granite and dioritic amphibolite, Arpatsivik 17

3.19.... Blocks of diorite etc. in basified granite. ..... 17.

3.20.... Contact between Sanerutian Granite and dioritic amphibolite ..... 18.

3.21.... Schlerion in amphibolite ..... 18.

3.22.... "Raft" of amphibolite. 19

3.23.... Field sketch of Fig.3.22. ..... 19.

3.24.... Aerial view of amphibolite mass north end of Karrarmiut ..... 20.

5.1..... Kuanitic dykes in Ketilidian Granite. ..... 20.

5.2..... Kuanitic dyke cutting xenoliths in the granite ..... 21.

5.3..... Blocks of granite in Kuanitic dyke ..... 21.

5.4..... Granite block with quartz vein, lying in Kuanitic dyke ..... 22.

5.5..... Kuanitic dyke veinlet in granite inclusion ..... 22.

5.6..... Kuanitic dyke ..... 23.

5.7..... Kuanitic dykes in Sanerutian Granite..... 23.

5.8..... Intersection of dolerite dykes with sill and amphibolitic band ..... 24.

5.9..... Sketch of locality in Fig. 5.8. ..... 24.

5.10.... Junction between Kuanitic dykes ..... 25.

5.11.... "Pseudo-agmatites" ..... 25.

(list of figures, continued). Facing page

Fig. 5.12.... "Pseudo-agmatites" Karrarmiut..... 26.
5.13.... Alkaline dyke classification ..... 26.
5.14.... Nepheline microsyenite dyke ..... 27.
5.15.... Field sketch of dyke intersection on Arpatsivik. ..... 27.
5.16.... Field sketch of dyke intersection Pile Sø. ..... 28.
5.17.... Trachyte inclusions in trachyte..... 28.
5.18.... Sketch map of the district to show the relationship to the alkaline plutons ..... 29.
5.19.... View of the camptonite sill, with field sketch of the sill ..... 29.
5.20.... Profiles across the sill ..... 30.
5.21.... Small scale banding in the sill ..... 31.
5.22.... Spheroidal weathering in dolerite dyke..... 32.
5.23.... Weathering gap of dolerite dyke ..... 32.
5.24.... Bayonet injection in dolerite dyke ..... 33.
5.25.... Layering in dolerite dyke ..... 33.
5.26.... Sketch map of Mato ..... 34.
5.27.... Sketch map of Julianehaab township and adjacent areas ..... 34.
Photomicrographs and Drawings.
6.1..... Myrmekite in microcline ..... 35.
6.2..... Myrmekite with plagioclase twinning ..... 35.
6.3..... Vein perthite ..... 36.
6.4..... Quartz-microcline intergrowths ..... 36.
6.5..... Plagioclase inclusions in microcline ..... 37.
6.6..... Drawings (a), (b), (c) to show mineral relationships in granites ..... 37.
6.7..... Euhedral plagioclases with zoning ..... 38.
6.8..... Plagioclase phenocryst with zoning ..... 38.
6.9..... Drawings of plagioclases from the Porphyritic Aplitic Granite ..... 39.
6.10.... Plagioclase phenocryst with zoning ..... 39.

(list of figures, continued.) facing page

Fig. 6.11..... Alteration zones in microcline 40

6.12..... Euhedral microcline 40

6.13..... Quartz inclusions in microcline..... 41

6.14....."Herring-bone" perthite in microcline. 41

6.15..... Drawings of plagioclase - microcline relationships 42

6.16..... Photomicrograph of drawings in Fig.6.15. 42

6.17..... Contact between plagioclase and microcline. 43

6.18..... Euhedral sphene 43

7.1..... Hornblende in amphibolitic gneiss. 44

7.2..... Texture of a banded gneiss 44

7.3..... Texture of acid vein in gneiss. 45

7.4..... Contact between vein and gneiss. 45

7.5..... Plot of nZ : nY for hornblende and nZ hornblende : nZ of biotite 46

7.6..... Plot of nZ' : extinction and $2V_x$: extinction for hornblende of gneiss 47

7.7..... Plot of nZ' : position, for hornblendes from gneiss 48

7.8..... Plot of total alkalis against position and (b) plot of $\%Na_2O$: $\%K_2O$, gneiss. 49

7.9..... Plot of K_2O - Na_2O - CaO for gneiss specimens. 50

8.1..... Photomicrograph of clearing of inclusions in plagioclase about reaction rims. 51

8.2..... Apatite inclusions 51

(list of figures continued.) facing page.

Fig. 8.3..... Clinopyroxene mantling hypersthene..... 52
8.4..... Remnant hypersthene in amphibole 52
8.5.....(A) Proposed order of crystallisation for gabbroic mass and
(B) Crystallisation sequences for other basic masses. 53
8.6..... Tremolitic hornblende in amphibolite 53

9.1..... Corroded plagioclase 54
9.2..... Sheaves of biotite in amphibolitic dyke. 54
9.3..... Drawings of plagioclases with "skeleton" zoning. 55
9.4..... Photomicrograph of plagioclase showing "skeleton" zoning. 55
9.5..... Drawings of plagioclases from Kuanitic dykes. 56
9.6..... Photomicrograph of plagioclase figured in Fig. 9.5. 56
9.7..... Pseudomorph of microcline after plagioclase. 57
9.8.....'Rapakivi" feldspar in a Kuanitic dyke 57
9.9..... Classification used in naming the alkaline dykes. 58
9.10.... Sodic pyroxene rimming augite in an alkaline dyke. 58
9.11.... Plagioclase phenocryst in trachyte dyke 59
9.12.... Zoned nepheline in an alkaline dyke. 59
9.13.... Phenocryst in alkaline dyke, with growth of opaque needles. 60
9.14.... Photomicrograph of pyroxene core and amphibole mantle in the sill..... 60

(list of figures, continued.) facing page.

Fig. 9.15..... Ophitic texture in dolerite 61

9.16..... Olivine - pyroxene relationships in dolerite. 61

9.17..... Alteration of olivine in olivine dolerite. 62

9.18..... Zoned pyroxene in dolerite 62

9.19....."Skeleton" growth of ilmenite. 63

10.1..... Optical classification of the potash feldspars. 64

10.2..... Stereograms illustrating optical orientations of orthoclase and microcline. 64

10.3..... Disorder - order relationship between sanidine and microcline 65

10.5..... Intersection of the solidus and solvus in the potash feldspars 65

10.4..... Compendium of suggested phase diagrams for potash feldspars 66

10.6..... X-ray determinative curve for high temperature potash feldspars. 67

10.7..... Symmetry change between sanidine and albite and the effect of temperature. 67

10.8..... Phase diagram proposed by Laves 68A

10.9..... Various determinations of the alkali feldspar solvus 68A

10.10..... Laves phase diagram after Rao 68B

10.11..... Phase diagram of the alkali feldspars after Rao(1959) 68B

10.12..... Block diagram to show the twinning developed in microcline..... 69

10.13..... Block diagram to show the optical orientations of microcline 69

10.14..... Optic axial angle plotted against composition for microclines. 70

10.16..... Plot of composition of microclines derived by chemical and X-ray methods. 70

(list of figures, continued) facing page.

Fig. 10.15..... Determinative curve for the estimation of % Or. in the alkali feldspars. ..... 71.

10.17..... Determinative curve for the estimation of % Or in triclinic alkali feldspars, derived from Greenland material..... 72.

10.18..... X-ray diffraction chart for specimen 42896 - microcline ..... 73.

10.19.....(a) Homogenisation rates for microclines 42888P & 42896 0 to 20 hrs.

(b) As for (a) but from 0 -400 hrs..... 74.

10.20..... Homogenisation rates on various alkali feldspars, after Ernst(1960).... 75.

10.21..... Relation between rate of cooling and triclinicity. ..... 75.

10.22..... Plot of difference between, $2\theta(1\bar{3}1)$ and (131) against triclinicity. ..... 76.

10.23..... Changes in triclinicity and $2\theta(1\bar{3}0)$ - $2\theta(130)$ against time, microclines from 42888P and 42896. ..... 76.

10.24..... % Or. plotted against triclinicity, before and after homogenisation. ..... 77.

10.25.....(a): Plot of composition of 10 microclines against the difference in triclinicity before and after homogenisation.

(b): Plot of shift in triclinicity on homogenisation, against the shift in D 2θ on homogenisation..... 78

10.26.....(a): Plot of estimated temperature of crystallisation of granites, against triclinicity(natural)

(b): Plot of estimated temperature ofcrystallisation of granites against triclinicity(homogenised)..... 79.

10.27..... X-ray diffraction chart for a microcline from 23409. ..... 80.

10.28..... X-ray diffraction chart for a microcline from 23848. ..... 81.

Fig. 10.29..... Proposed solvii for ordered and disordered alkali feldspars, (Laves,1952). ..... 82.

10.31..... Diagram for the estimation of the temperature of crystallisation.(after Barth,1956) ..... 82.

10.30..... Suggested phase diagram for the system Or - Ab at normal pressure. ..... 83.

10.32..... Co-existing plagioclase-alkali feldspar phases. ..... 84.

10.33..... Estimated temperature for granites,gneisses and alkaline dykes. ..... 84.

11.1..... Modal analysis results for 40 granitic rocks,plotted on Ab - Or - Qtz. diagram 85

11.2..... Modal analysis results for 10 thin sections from specimen 42888, Ab - Or -Qtz. diag. ..... 85.

11.3..... Modal analysis results on 10 thin sections from specimen 23882, Ab - Or - Qtz.diag. ..... 86.

11.4..... Modal analysis results on G 1, granite, Ab - Or - Qtz.diag. ..... 86.

11.5..... Modal analysis results on one thin section(42888) by student operators. ..... 87.

11.6..... Modal analysis results on 42888 obtained by combined rock slab and thin section point count ..... 87.

11.7..... Modal analyses on Sanerutian and Ketilidian Granites,plotted on a Mafic - Feldspar - Qtz. diag. ..... 88.

11.8..... Plot of modal analyses for Sanerutian and Ketilidian Granites, Ab - Or - Qtz. diag. ..... 88.

13.1..... Infrared absorption spectra for G 1 granite,microcline,quartz and plagioclase. ..... 89.

List of enclosures:

Plate 1: General Geology.

Plate 2: Structure map of the area.

Plate 3: Map of the dyke and sill distribution.

All maps in the enclosure are 1 : 50,000.

The photographs in the early part of this volume illustrating field occurrences in Greenland are copyright of Grønlands Geologiske Undersøgelse, København.

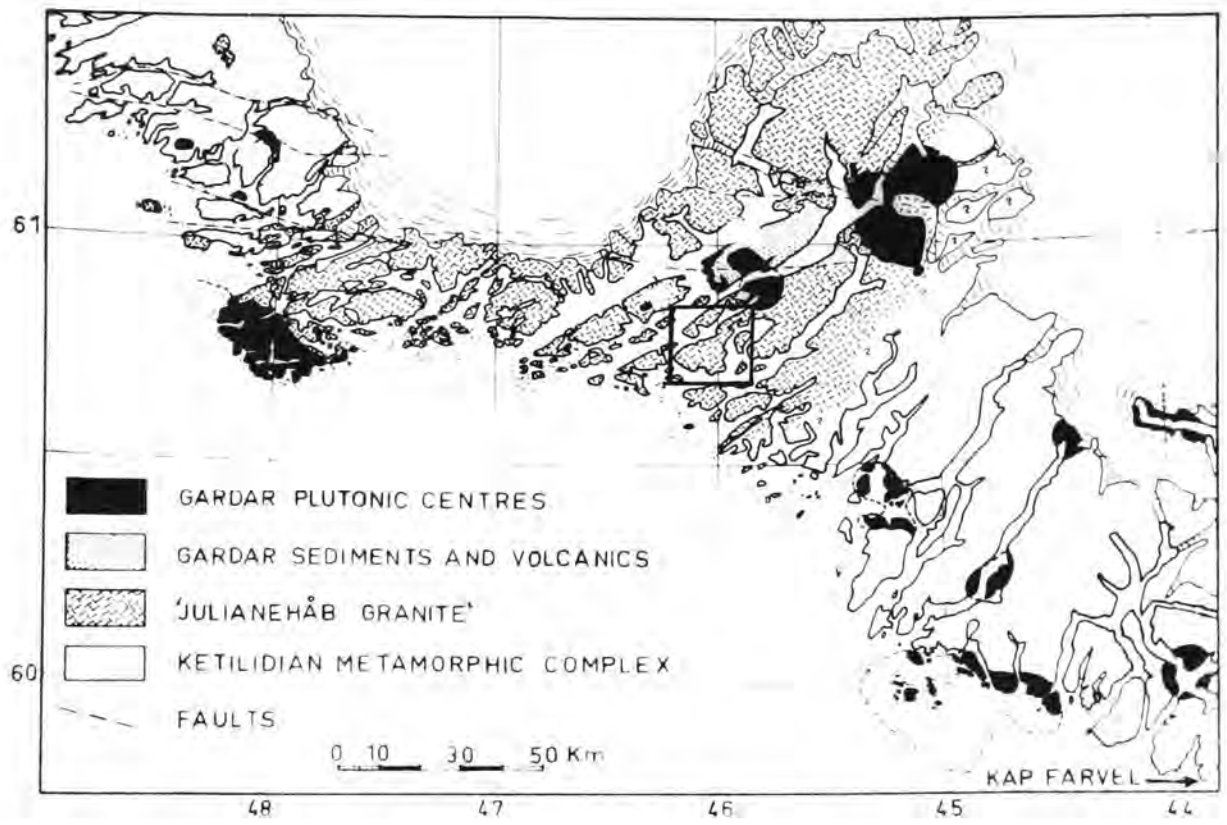
61
60
GARDAR PLUTONIC CENTRES
GARDAR SEDIMENTS AND VOLCANICS
'JULIANEHÅB GRANITE'
KETILIDIAN METAMORPHIC COMPLEX
FAULTS
0 10 30 50 Km
KAP FARVEL
48
47
46
45
44

Fig. 1.1.

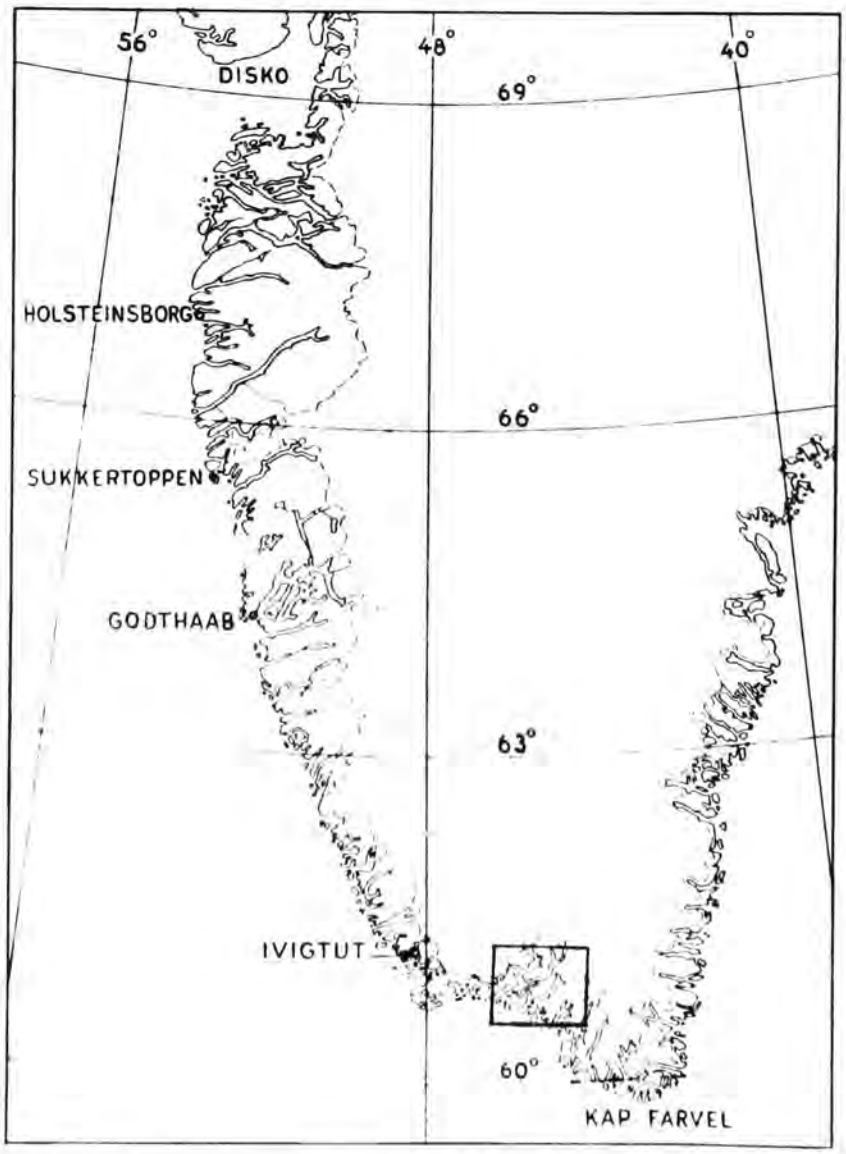
56°
DISKO
48°
40°
69°
HOLSTEINSBORG
66°
SUKKERTOPPEN
GODTHAAB
63°
IVIGTUT
60°
KAP FARVEL

Fig. 1.2.

Fig. 1.1.

General geology of the South-west part of Greenland.(after Berthelsen). The region studied is outlined.

Fig. 1.2.

The southern half of Greenland,showing the major settlements and the position of the area studied.

Fig. 1.3.

A locality map of the Julianehaab District. The names in block letters indicate regions and those in small letters, specific localities. (Most of the names used are approved by the Geodetic Institute, Copenhagen.)

LOCALITY MAP OF THE JULIANEHÅB DISTRICT.

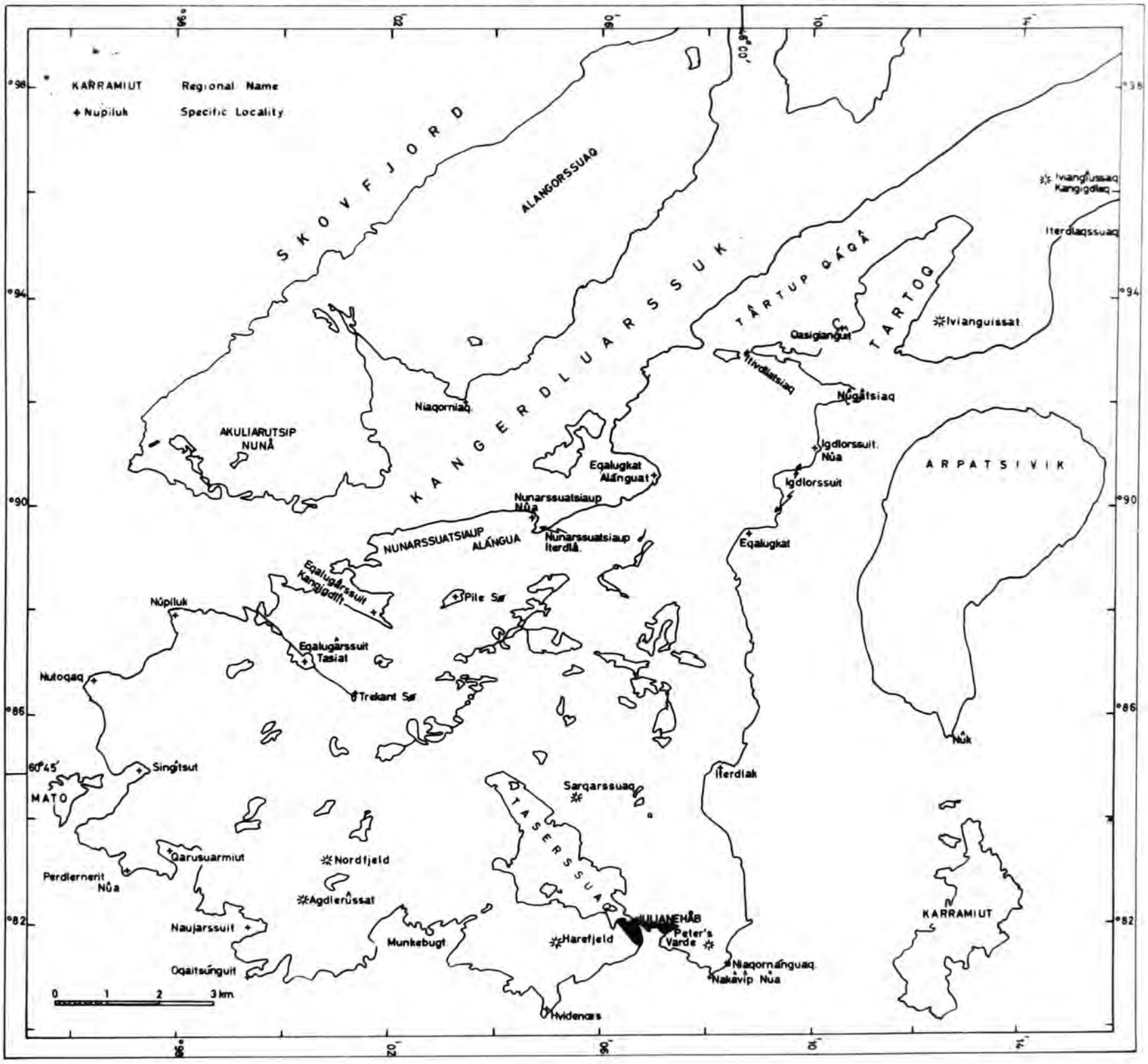

Fig. 1.3.

Fig. 2.1.

Fig. 2.2.

Fig. 2.1.

Veins of Sanerutian Granite cutting a Porphyritic Ketilidian Granite. North of Eqalugkat Alanguat, (10/066920).

Fig.2.2.

Block of porphyritic older granite within the Sanerutian Granite. North-east coast of Arpatsivik. (10/148900).

Fig. 2.3.

Fig. 2.4.

Fig. 2.3.

Banding in the Sanerutian Granite, northern end of Karrarmiut. (10/133833).

Fig. 2.4.

Junction of the Sanerutian Granite with a fine-grained dioritic gneiss. Near Eqalugkat (10/082889) Note the inclined contact with the aplitic vein along it. Diffuse veins of diorite cut the gneiss.

Fig. 2.5.

Fig. 2.6.

Fig. 2.5.

Contact of the Sanerutian Granite and a Porphyritic Ketilidian Granite,west coast of Tartoq. Note the aplitic vein along the junction and the patch of Porphyritic Granite within the younger granite.(just above hammer head.)

Fig. 2.6.

Aligned xenolithic material within the Big Feldspar Phenocryst Granite, south coast of the Julianehaab Peninsula.(Photo from colour.)

Fig. 2.7.

Fault breccia in a Porphyritic Granite, with associated quartz veins. East coast of Arpatsivik.

Fig. 2.7.

Fig. 3. 1.

Fig. 3. 2.

Fig. 3.1.

A view looking east toward Trekant Sø over the prominent feature made by the vein gneiss band(in the foreground). Erosion gaps of alkaline dykes can be seen in the facing slopes of the hill in the background.

Fig. 3.2.

Good development of almost vertical veins of acid material within the gneiss band. South-west of Trekant Sø (10/003860).

Fig. 3.3.

Fig. 3.4.

Fig. 3.3.

Banding in the amphibolitic gneiss, southern tip of Mato. (00/959840).

Fig. 3.4.

Wedge of amphibolitic gneiss in contact with the acid gneiss. Note the folding pattern, the amphibolitic type occurring in a fold-core and the absence of acid vein material in the basic rock.

Fig. 3.5.

Fig. 3.6.

Fig. 3.5.

Wedges of thin stringers of acid gneiss within the amphibolitic gneiss, southern tip of Mato. Note the tight folding in the acid gneiss.

Fig. 3.6.

Folded and faulted amphibolitic gneiss, southern tip of Mato. Note the banding is developed within the more leucocratic horizons also.

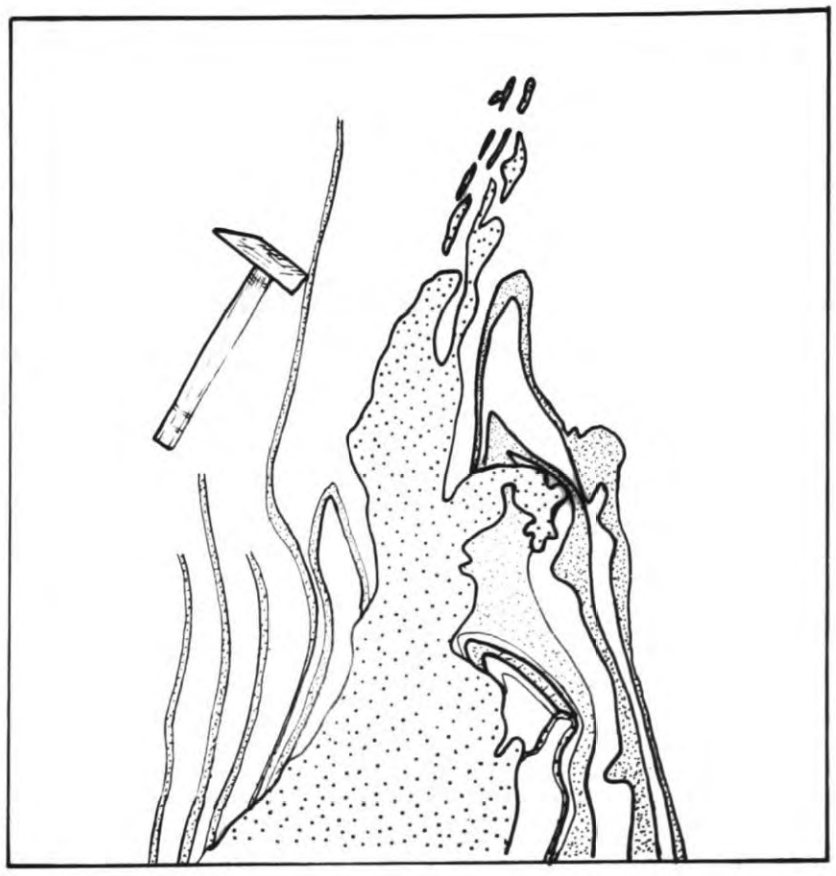

Fig. 3.7.

Fig. 3.8.

Fig. 3.7.

Folding of the axial planes of vertical isoclinal folds within the amphibolitic gneiss, Mato. Acid bands within the gneiss are ornamented(sketch from photograph.)

Fig. 3.8.

Banded amphibolitic gneiss with broken segments of an aplitic vein cutting through it. Mato.

Fig. 3.9.

Fig. 3.10.

Fig. 3.9.

Rounded, partially digested block of gneiss, within a Porphyritic Granite, northern margin of the gneiss band, Mato.

Fig. 3.10.

Migmatitic contact between granite and gneiss, Mato.

Fig. 3.11.

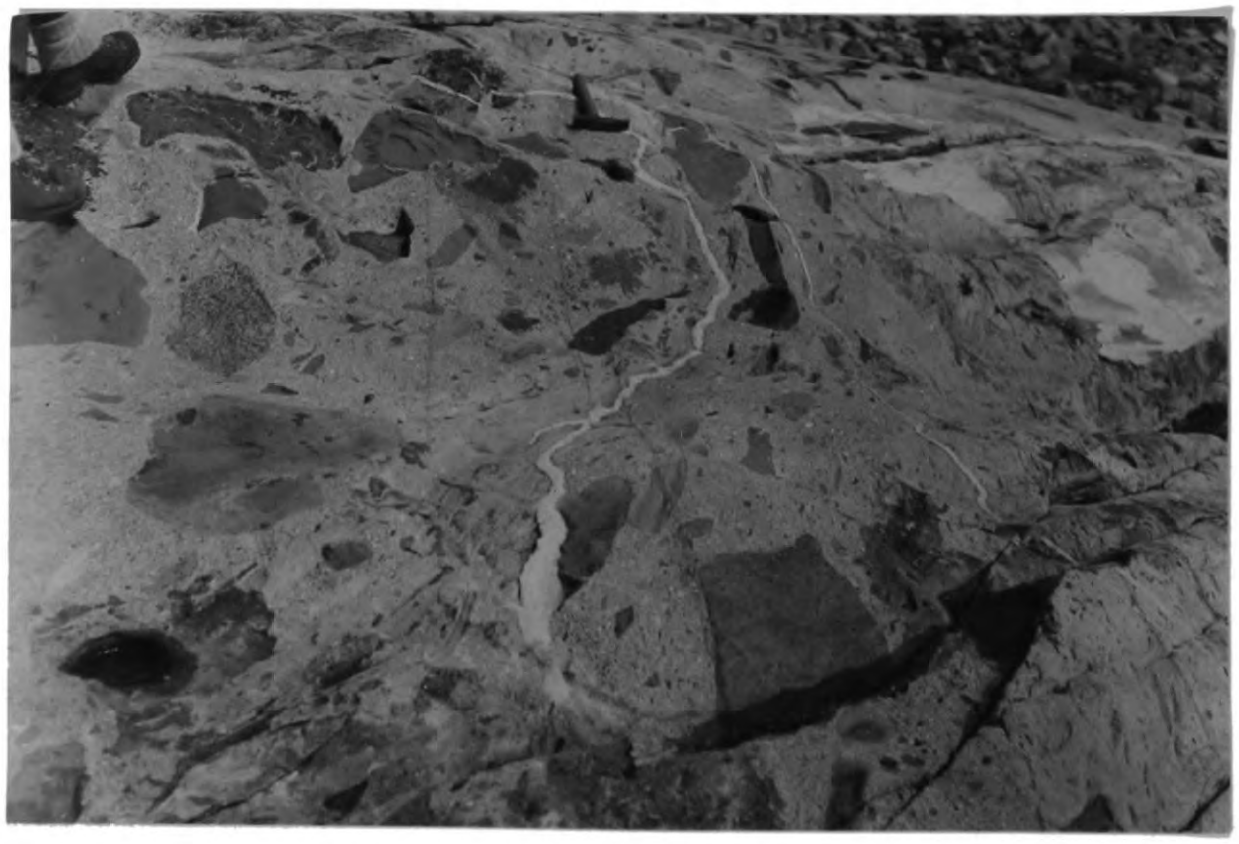

Fig. 3.12.

Fig. 3.11.

Acid veins, ptygmatically folded, cutting the gneiss band, north shore of Singitsut. (00/970849).

Fig. 3.12.

Central part of the breccia zone, Perdlernerit Nua. (00/970830).

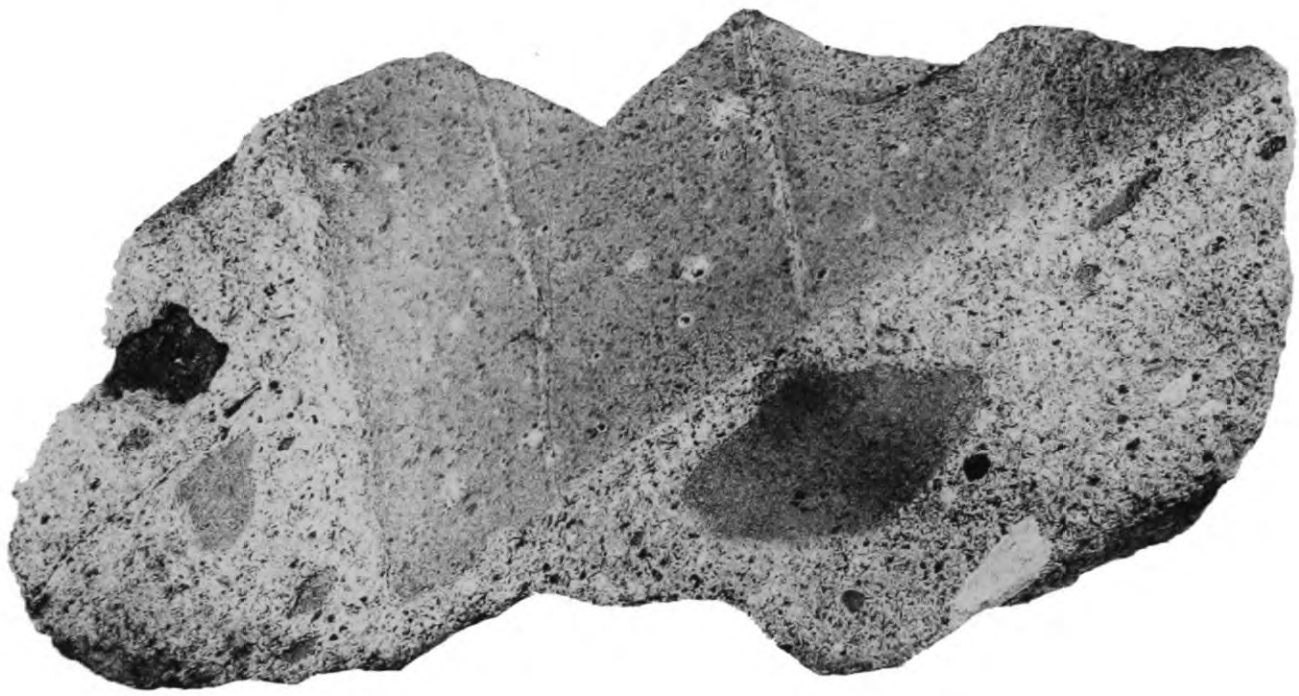

Fig. 3.13.

Fig. 3.14 .

Fig. 3.13.

Block of granite collected from the central part of the breccia zone(see Fig. 3.12.). The specimen is just less than a metre in length. A fragment of amphibolite occurs on the left and a piece of leucocratic gneiss on the bottom right. The other blocks are mainly diorites and dioritic gneisses.

Fig. 3.14.

Northern margin of the breccia zone. The granite containing the small angular assorted fragments(on the left of the photograph) passes sharply into a granite with comminuted xenolithic fragments. (Phtot from colour).

Fig. 3.15.

Fig. 3.17.

Fig. 3.15.

View looking south over the gabbro knolls, in the eastern lakes region. (10/065863). The white weathering granite can be seen in the background in contact with amphibolite. (Photo from colour).

Fig. 3.17.

Contact between a dioritic amphibolite and a Porphyritic Granite, at the eastern margin of the central lakes region (10/058870).

Fig. 3.16.

Sketch map of the gabbro-norite-amphibolite mass, showing the distribution of the dominant igneous rock types within the amphibolites (stippled). The contact with the surrounding granite is also shown.

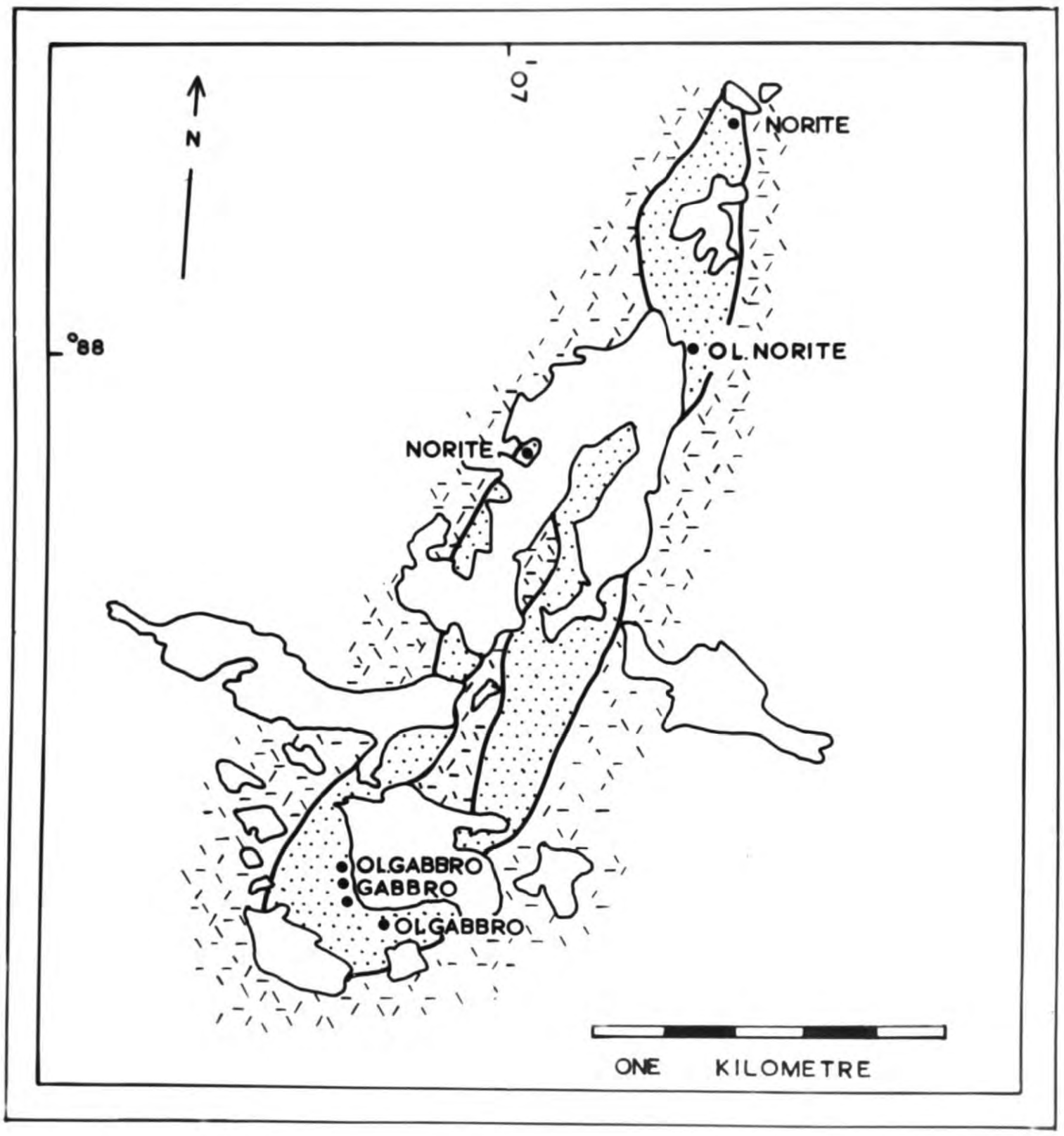
N
07
88
NORITE
OL. NORITE
NORITE
OL GABBRO
GABBRO
OL GABBRO
ONE KILOMETRE

Fig. 3.18.

Fig. 3.19

Fig. 3.18.

Injection contact between granite and dioritic amphibolite, east coast of Arpatsivik. (10/130870) (c.f. Fig. 3.17.).

Fig. 3.19.

Blocks of dioritic amphibolite and fine grained gneiss within "basified" granite" southern margin of dioritic amphibolite mass. (10/055863).

Fig. 3.20.

Fig. 3.21.

Fig. 3.20.

Contact of a dioritic amphibolite and the Sanerutian Granite on Karramiut(10/127802). Note the brecciated fragments of fine grained gneiss, accumulating against the amphibolite and the faint parallel schlerion within that rock.

Fig. 3.21.

Schlerion within the dioritic amphibolite, Karrarmiut.

Fig. 3.22.

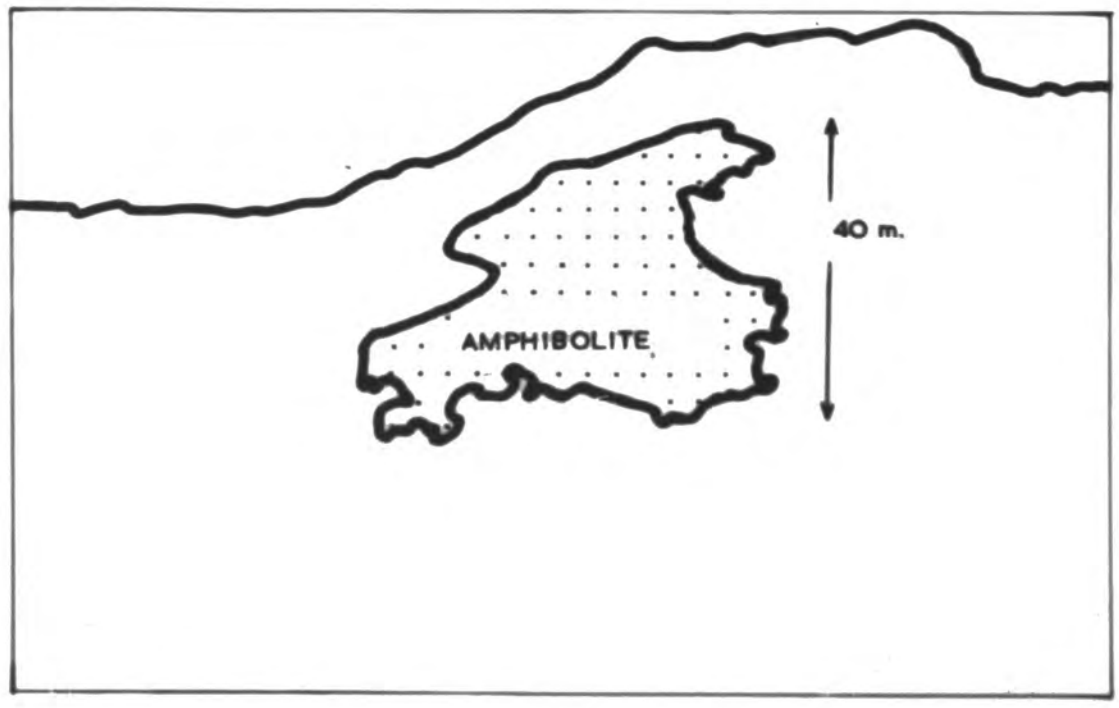

Fig. 3.23.

Fig. 3.22.

"Raft" of amphibolite in the Sanerutian Granite, Karrarmiut(10/125813).

Fig. 3.23.

Sketch to show the disposition of the amphibolite in the cliff face.

Fig. 3.24.

Fig. 5.1.

Fig. 3.24.

Aerial view of the northern part of Karrarmiut, (10/133835), to show the large scale penetration of acid veins of Sanerutian age, into dioritic amphibolite.

Fig. 5.1.

Distorted and broken amphibolitised dykes (Kuanitic dykes), within the Big Feldspar Phenocryst Granite. Coastal section, south east part of the Julianehaab Peninsula.

Fig. 5.2.

Fig. 5.3.

Fig. 5.2.

Kuanitic dyke, within a Porphyritic Granite and cutting xenoliths within the granite, Iterdlak.

Fig. 5.3.

Blocks of Porphyritic Granite within a Kuanitic dyke. Note the fine grained nature of the dyke adjacent to the blocks and also the flow structure following the contours of the blocks.
Hvidenaes, (10/050807).

Fig. 5.4.

Fig. 5.5.

Fig. 5.4.

Granite block within a Kuanitic dyke(whole exposure not shown on the photograph), with a quartz vein cutting through the granite. Note the abrupt termination of the vein against the dyke. Just north of Iterdlak.

Fig. 5.5.

Granite block within a Kuanitic dyke with a small vein of the dyke penetrating the granite.(same locality as Fig. 5.4.)

Fig. 5.6.

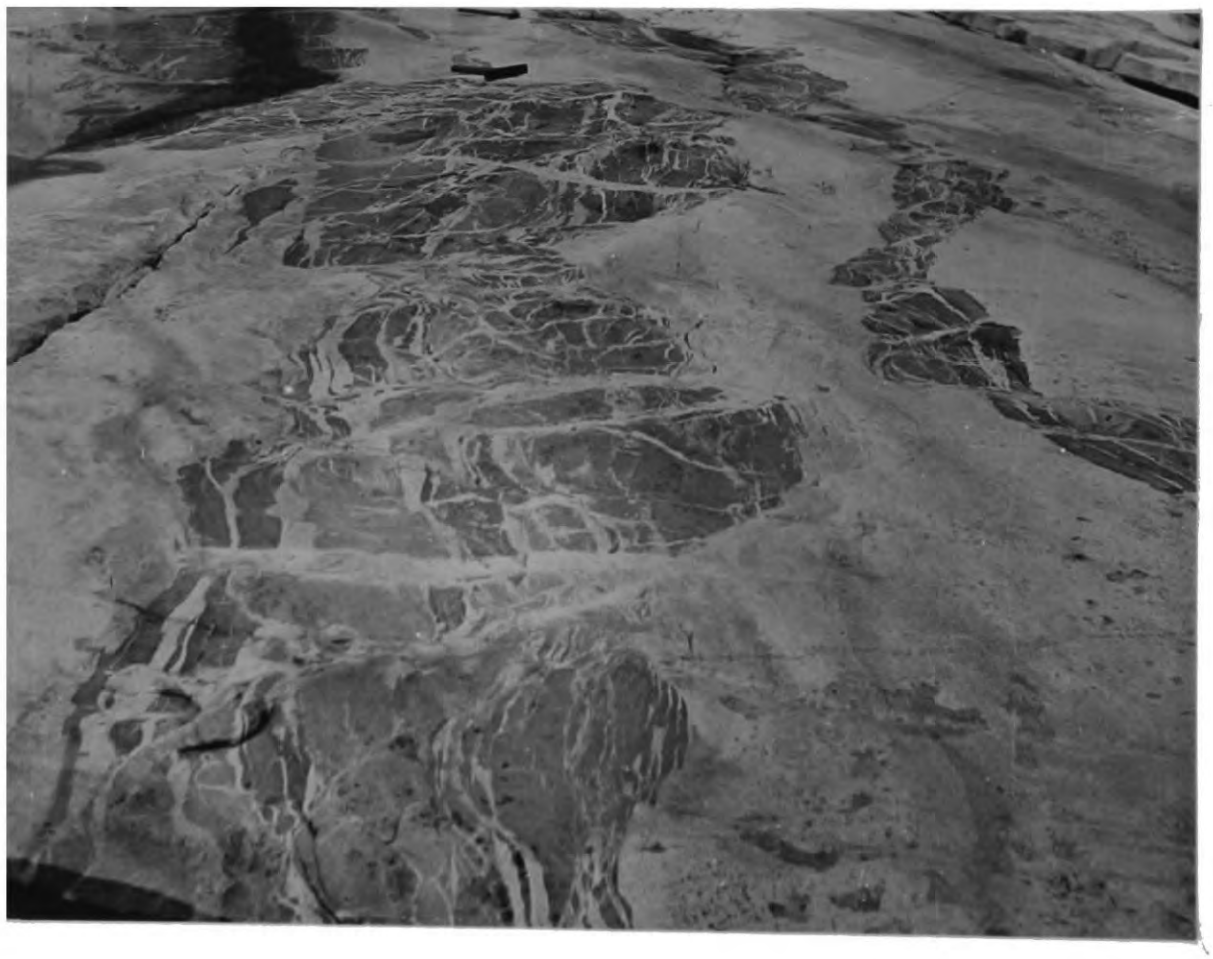

Fig. 5.7.

Fig. 5.6.

Kuanitic dyke within the Ketilidian Granite, north of Iterdlak.

Fig. 5.7.

Kuanitic dykes within the Sanerutian Granite, east coast of Arpatsivik. (Compare this locality with that figured in Fig. 5.1.)

Fig. 5.8.

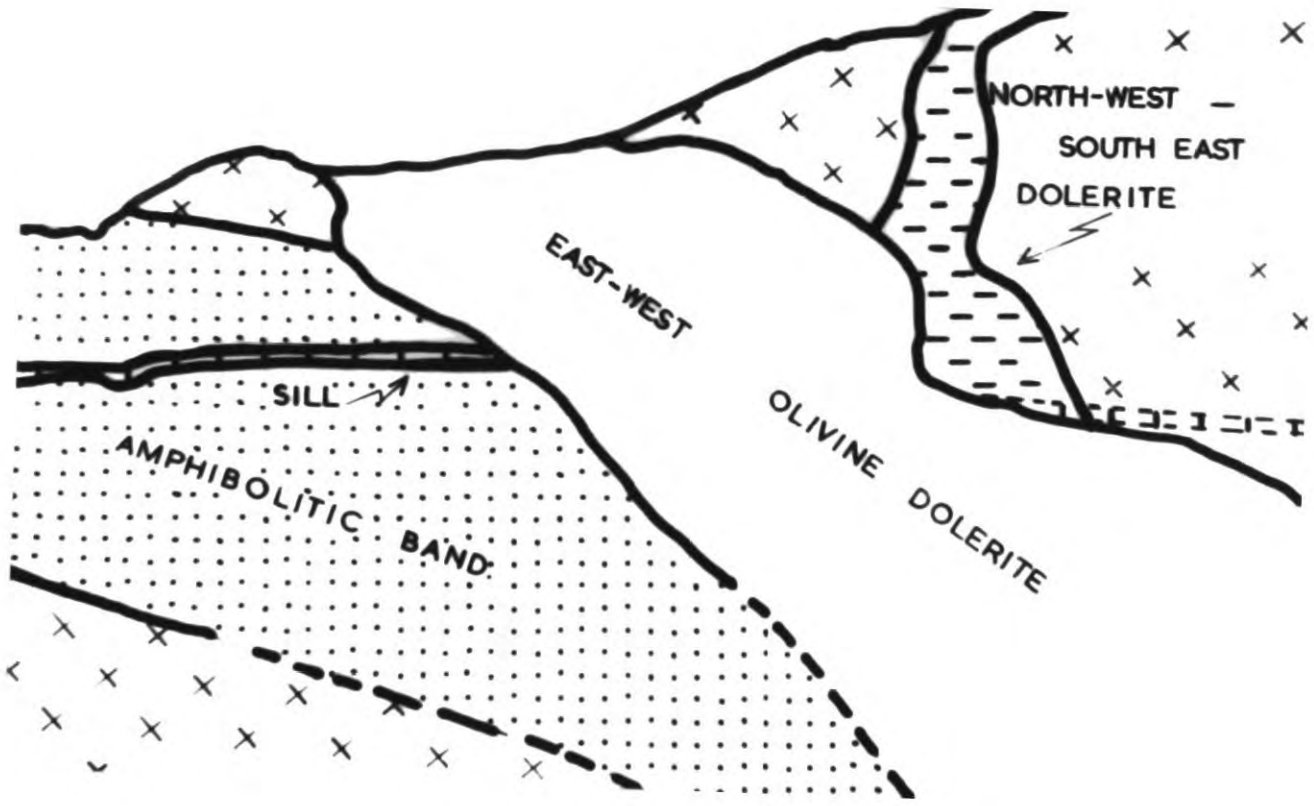
NORTH-WEST –
SOUTH EAST
DOLERITE
EAST-WEST
SILL
AMPHIBOLITIC BAND
OLIVINE DOLERITE

Fig. 5.9.

Fig. 5.8.

Intersection of dolerite dykes with the lamprophyric sill and the amphibolitic band, north-east of Munkebugt.

Fig. 5.9.

Sketch of the locality figured in Fig. 5.8.

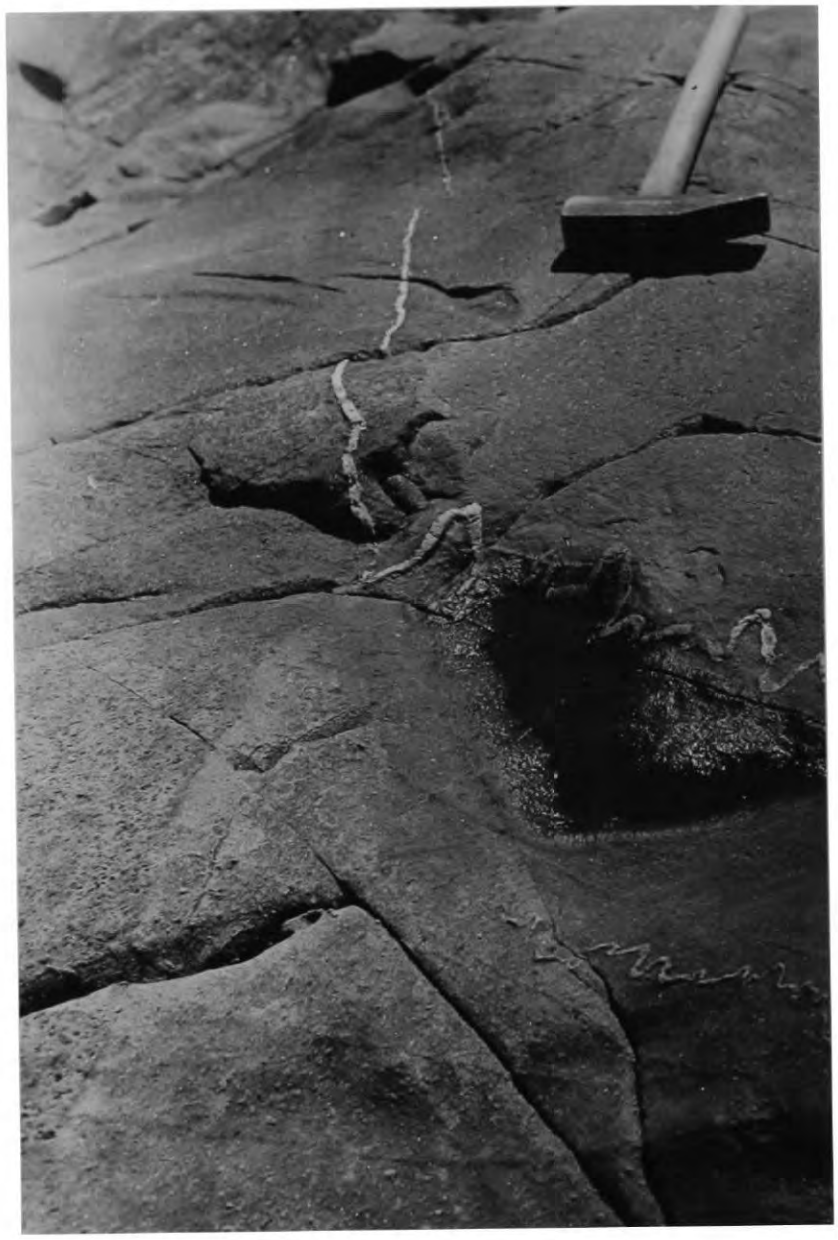

Fig. 5.10.

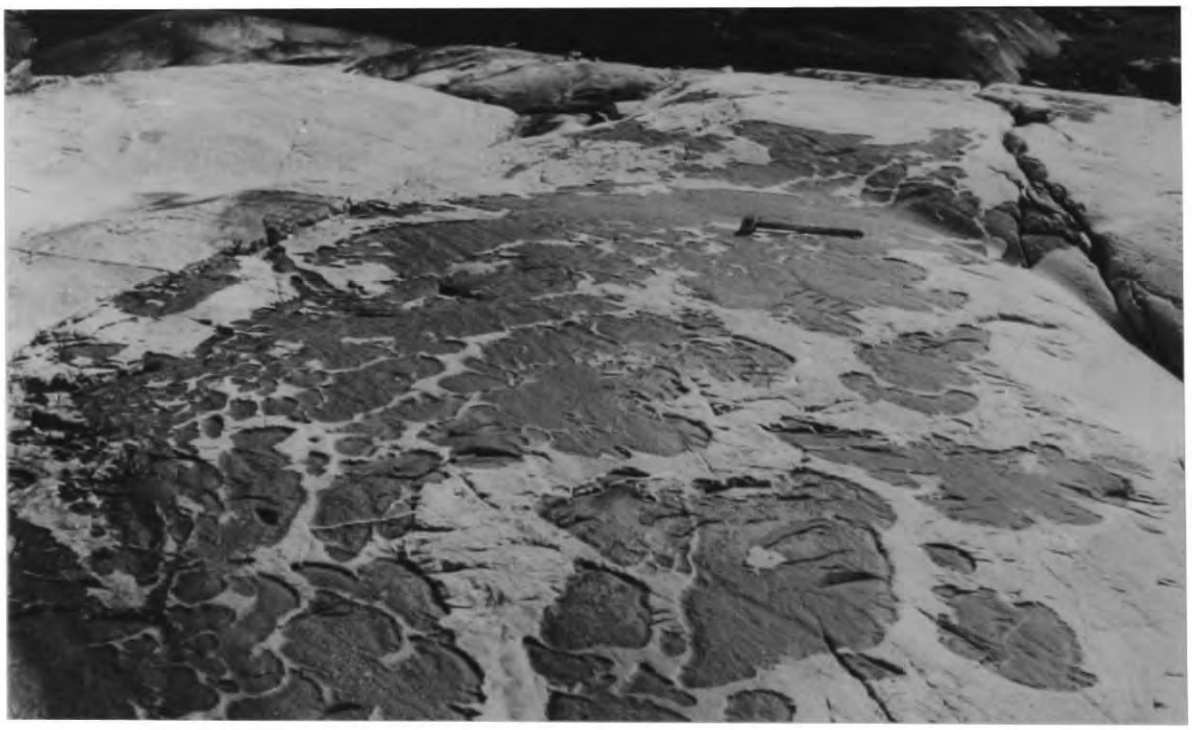

Fig. 5.11.

Fig. 5.10.

Junction between two Kuanitic dykes, (the contact is parallel to the shaft of the hammer), the younger dyke is on the right of the photograph. The acid vein, cutting both dykes is fairly straight in the older but shows ptygmatic folding in the younger, north of Iterdlak.

Fig. 5.11.

Pseudo-agmatites, exhibiting the rounded surfaces (cauliflower structures) of the basic rock, which is lying in the Sanerutian Granite. Note the dyke-like form of the body. South-east part of Karrarmiut. (Photo. from colour).

Fig. 5.12.

POTASH FELDSPAR ALBITE	PLAGIOCLASE An_{10-50}	PLAGIOCLASE An_{10-50}
SYENITE	MONZONITE	DIORITE
(AUGITE SYENITE PORPHYRY) MICROSYENITE (NEPHELINE PORPHYRY)	MICROMONZONITE	MICRODIORITE
(HEDRUMITE.) POTASSIC SODIC TRACHYTE	(MONZONITE PORPHYRY) TRACHYANDESITE	ANDESITE → TRACHYBASALT

Fig. 5.13 .

Fig. 5.12.

Pseudo-agmatites on the north-east coast of Karrarmiut These are more massive than those illustrated in Fig. 5.11.

Fig. 5.13.

Classification used in naming the alkali dykes. Names in brackets are those used by Ussing(1912) and have been placed alongside their compositional equivalents,as used by the present writer. The undersaturated types have not been differentiated,so as not to complicate the system of classification. (Compiled mainly after Johannsen and Hatch and Wells)

Fig. 5.14.

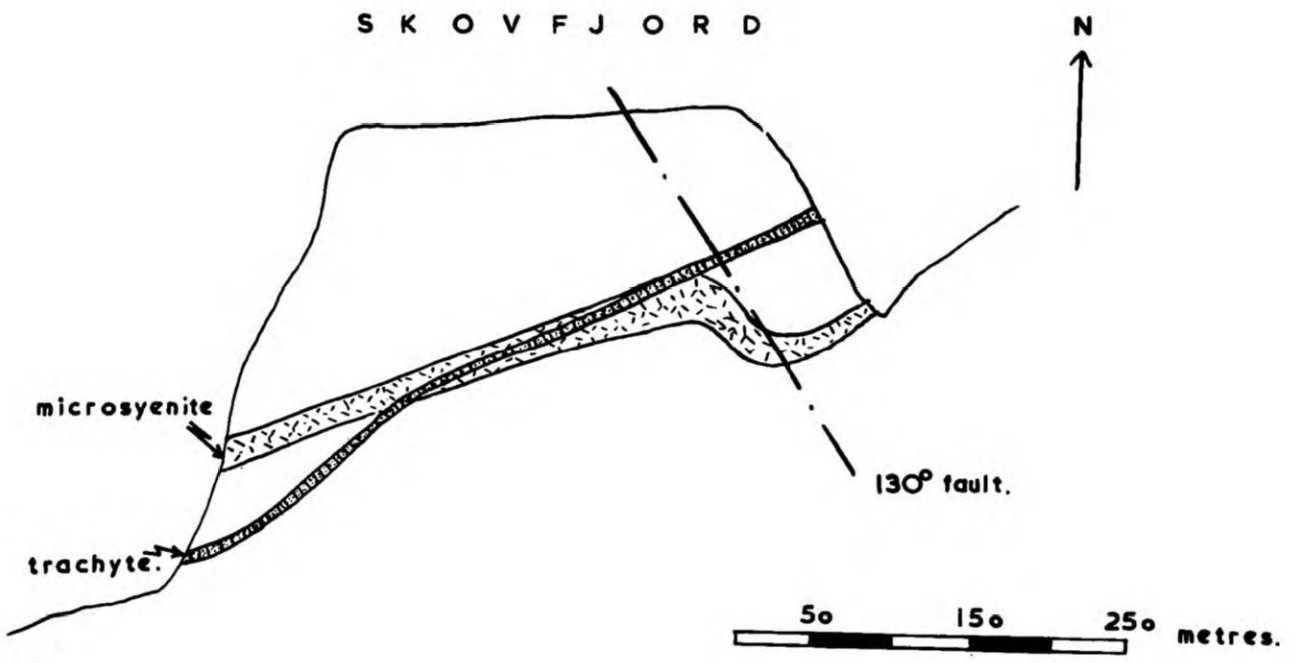

Fig. 5.15.

Fig. 5.14.

Nepheline microsyenite dyke. Both nepheline and alkali feldspar phenocrysts are developed. North-east coast of Eqalugkat Alanguat;)

Fig. 5.15.

Field sketch of a trahcyte-microsyenite dyke intersection, south coast of Skovfjord.(10/008948).

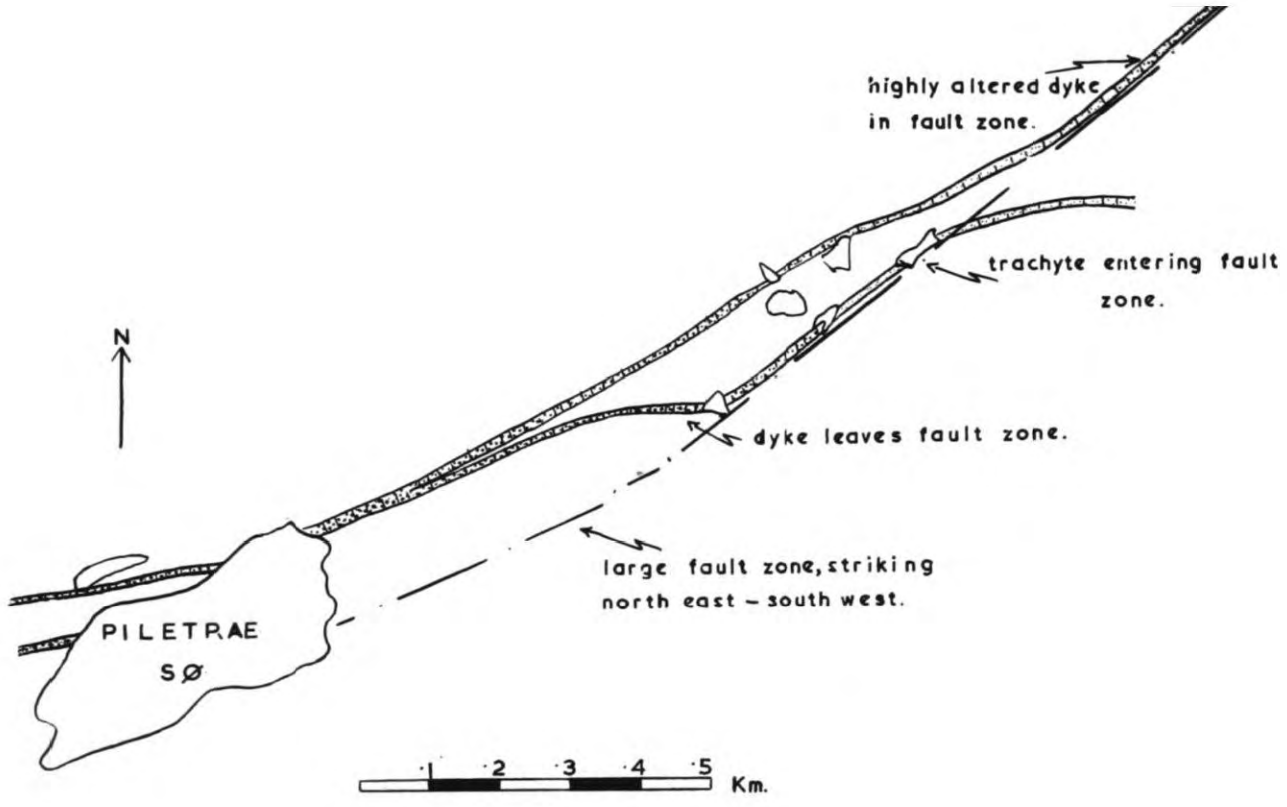

Fig. 5.16.

Fig. 5.17.

Fig. 5.16.

Field sketch of the Piletrae Sø (= Pile Sø) region, (10/030885), to show the relationship of the alkaline dykes to the fault zones.

Fig. 5.17.

Chilled trachyte inclusions within a trachyte dyke, Eqalugkat, (10/086895).

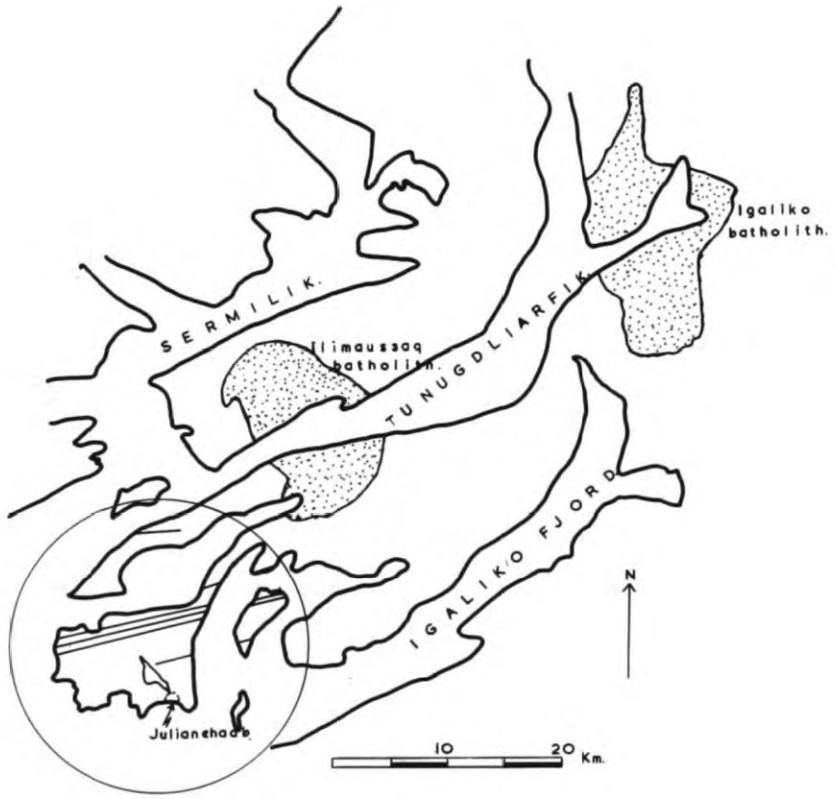

Fig. 5.18.

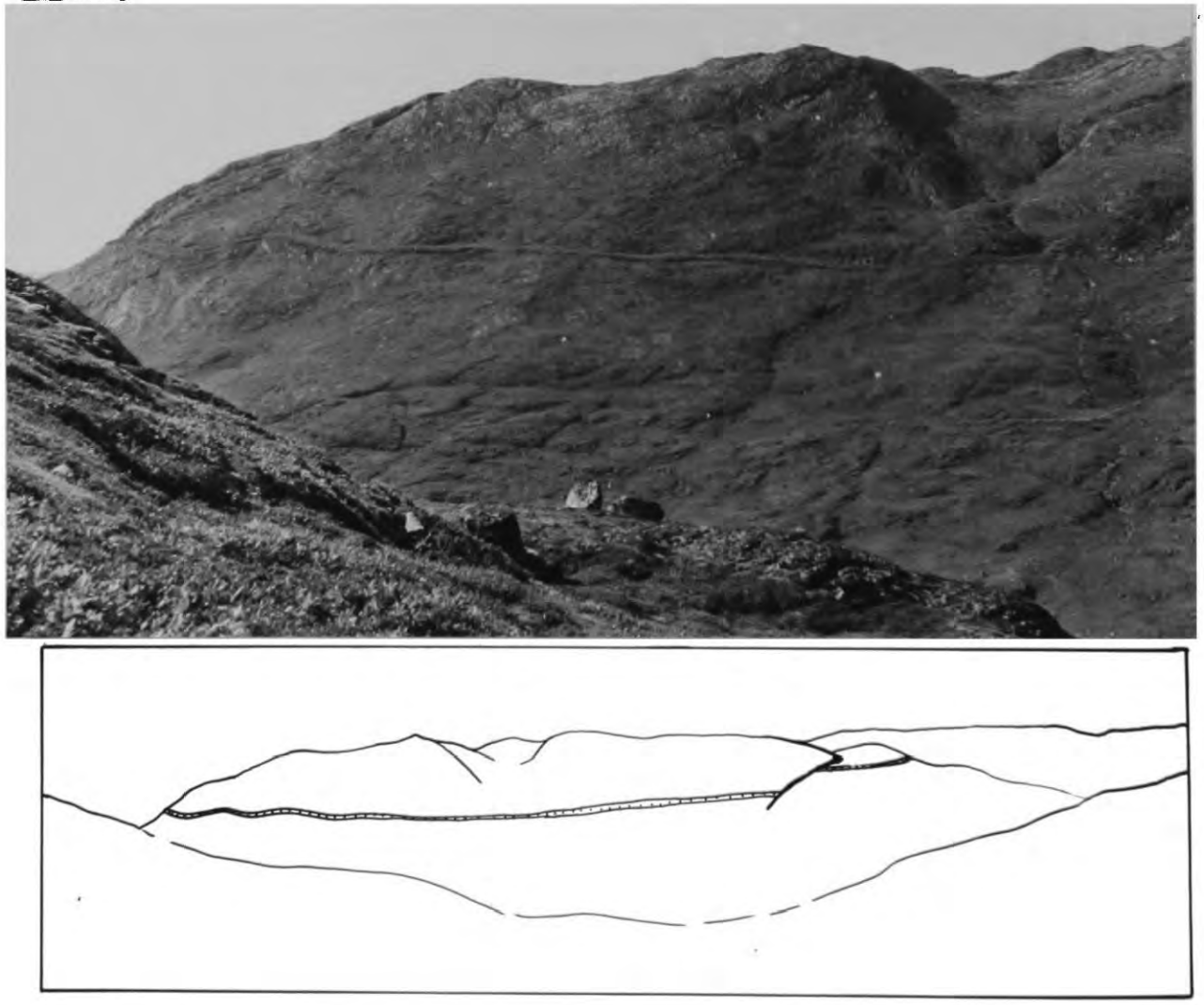

Fig. 5.19.

Fig. 5.18.

Sketch map of the Julianehaab Peninsula and the surrounding districts, to show the relationship of the alkaline dykes (shown as thin straight lines) to the Igaliko and Ilimaussaq batholiths.

Fig. 5.19.

View of the hill slopes on the western side of Taserssuaq, (from Sarqarssuaq) showing the sill at about 180 metres. The sketch below, shows the full development of the sill in these slopes, as well as the relationship of the intrusion to the low angled fault (extreme right of the diagram).

N.NW

S.SE.

Sarqarssuaq.

N

S

N.NW.

S.SE.

Munke Bugt.

W

E

Sarqarssuaq.

Taserssuaq.

0 600

0 300

SCALE IN METRES.

VERTICAL

HORIZONTAL

Fig. 5.20.

Profiles across the sill.

a: East of Tasrssuaq.

b: High ground west of Taserssuaq.

c: West of Taserssuaq, from about (10/010855) in the north, to Munkebugt, in the south.

d: E - W section across Taserssuaq.

Fig. 5.21.

Fig. 5.21.

Small scale banding in the sill, south of Nunarssuatsiaup Iterdla, about (10/060890).

Fig. 5.22.

Fig. 5/23.

Fig. 5.22.

Spheroidal weathering of an olivine dolerite dyke, (typical "brown" dyke using the terminology of Wegmann). In part, the dyke is reduced to a sandy gravel.

Fig. 5.23.

Large weathering gap of an olivine dolerite dyke, (starting at the bottom right of the photograph and moving toward the lake in the central part of the illustration). The large lake is Taserssuaq and the township of Julianehaab can be seen to the right of it, situated between the lake and the fjord.

Fig. 5.24.

Fig. 5.25.

Fig. 5.24.

Bayonet injection of a thin dolerite dyke, north of Iterdlak, c.f. Fig. 5.6.

Fig. 5.25.

Small scale layering in an olivine dolerite dyke, south end of Karrarmiut.

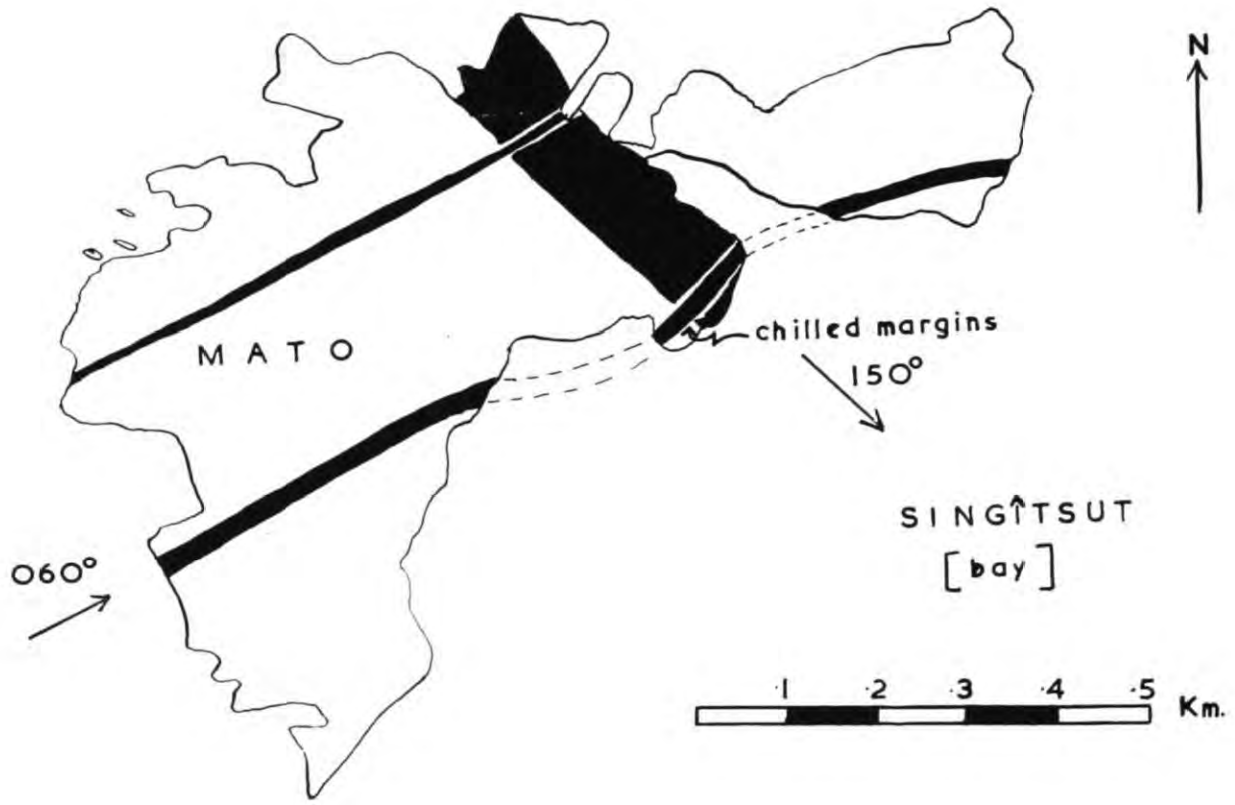

Fig. 5.26.

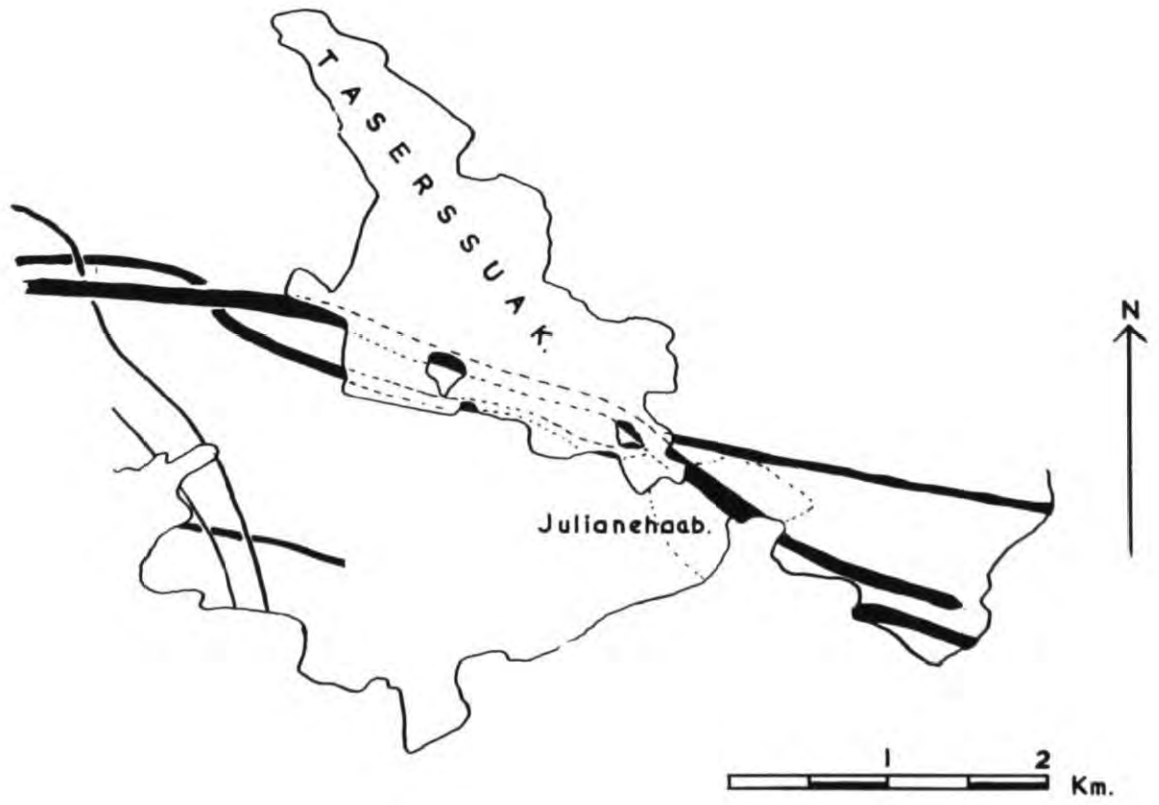

Fig. 5.27.

Fig. 5.26.

Sketch map of the island of Mato, to show the relationship of several dolerite dykes.

Fig. 5.27.

Sketch map of the area around Taserssuaq and Julianehaab, to show the age relationships of some of the dolerite dykes. (Note the rapid termination of the large W.N.W. -E.S.E. dyke on the east coast.

Fig. 6.1.

Fig. 6.2.

Fig. 6.1.

Mymekite development in microcline(specimen 43069), which shows two types of perthite, the coarse vein perthite and the finer which may be string or film perthite. Crossed nicols x40.

Fig. 6.2.

Myrmekite development with plagioclase twinning in the replacement plagioclase. Specimen 42972, crossed nicols x 40.

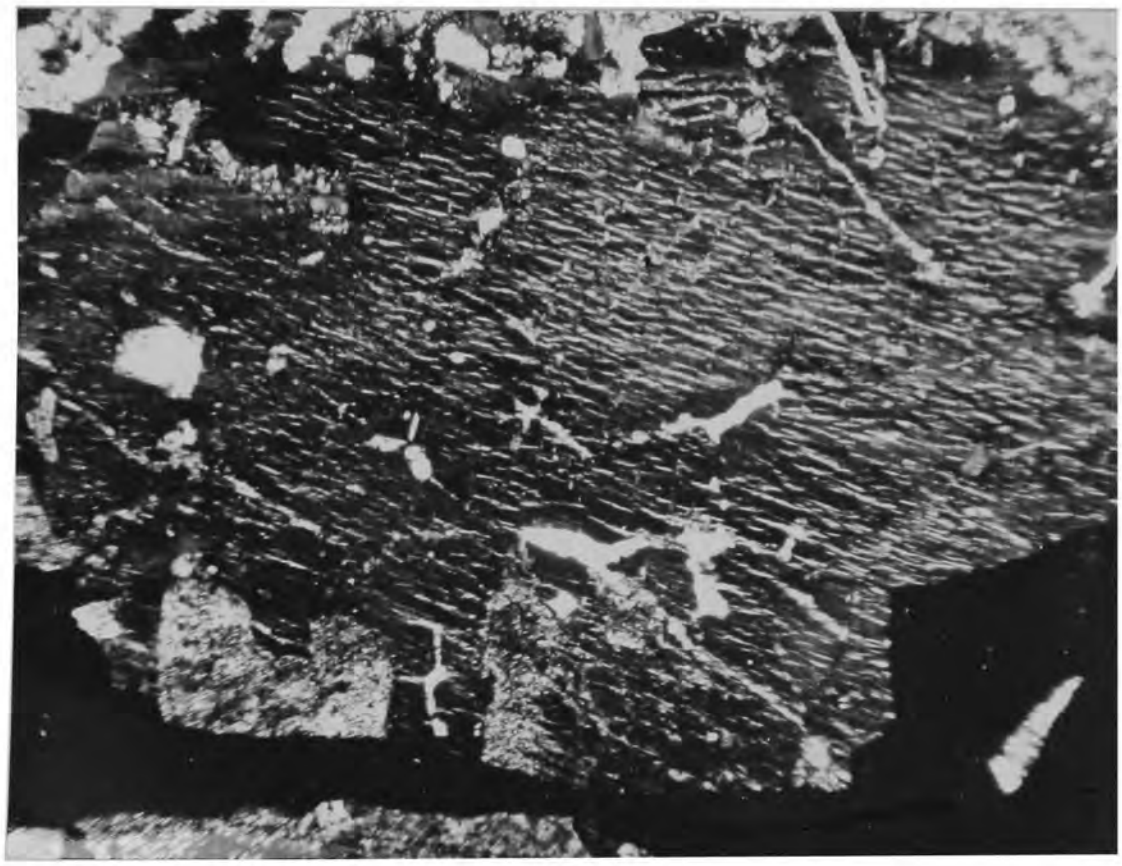

Fig. 6.3.

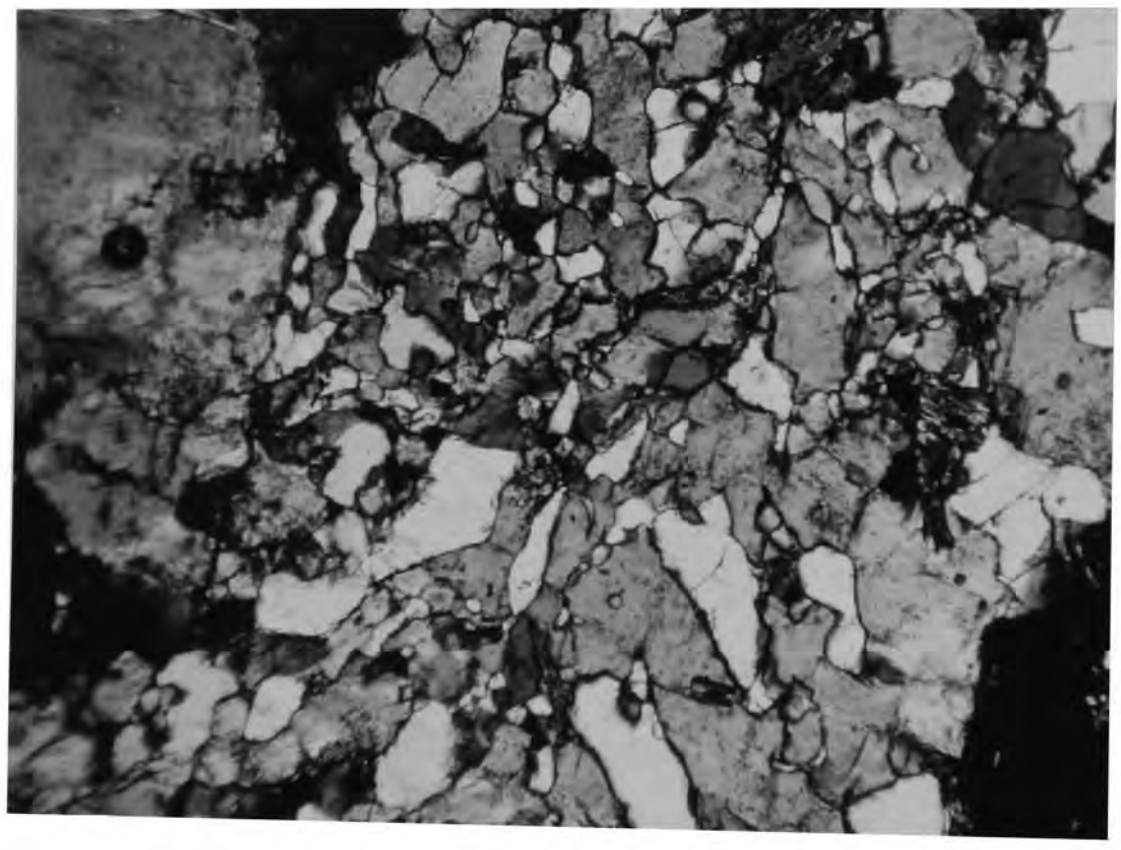

Fig. 6.4.

Fig. 6.3.

Vein perthite in microcline, specimen 42888.
Crossed nicols x 40.

Fig. 6.4.

Intergrowth of quartz and microcline(the twinning of microcline cannot be seen in this position). Specimen 42888,crossed nicols x 80.

Fig. 6.5.

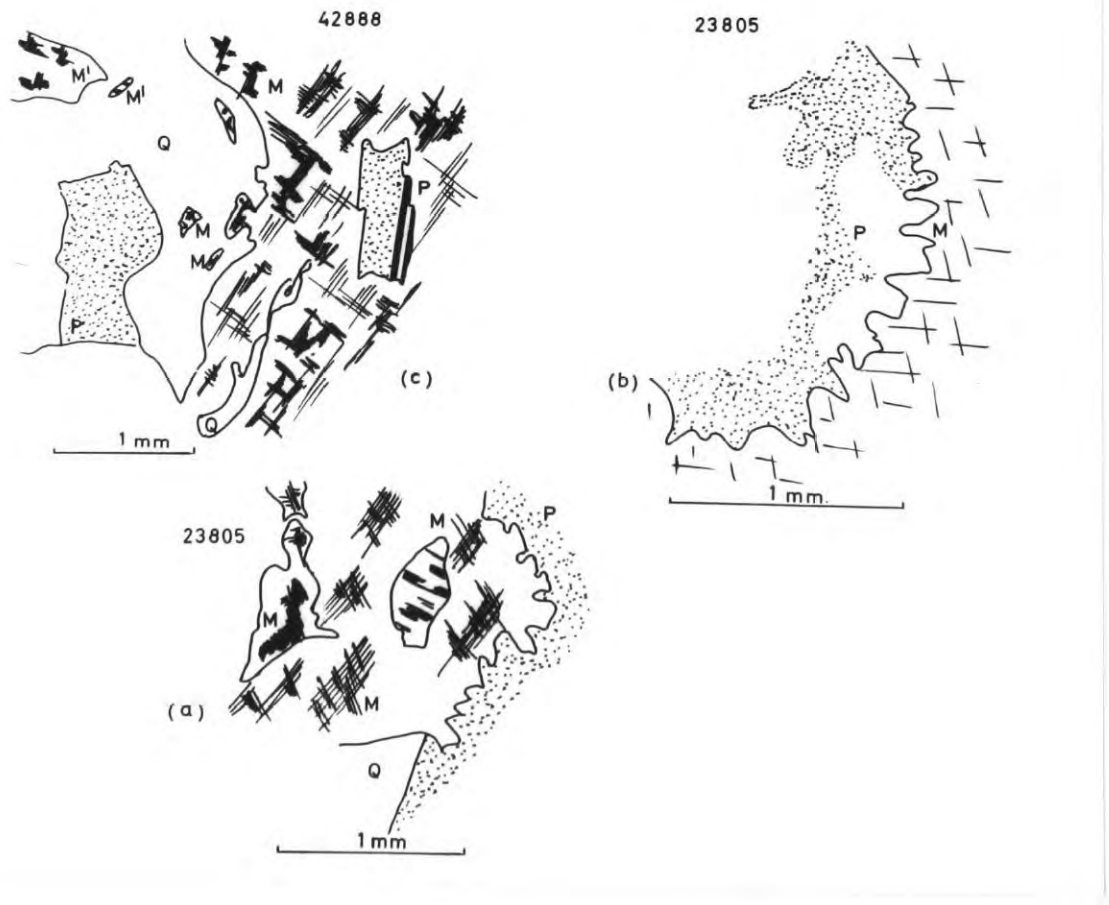

Fig. 6.6.

Fig. 6.5.

Plagioclase inclusions in microcline, with an albitic rim formed around most of the inclusions. Specimen 42861, crossed nicols x 90.

Fig. 6.6.

Drawings to show the mineral relationships in the granites.

(a): Microcline phenocrysts (porphyroblasts) against a plagioclase grain, with an irregular margin developed. Within the microcline are smaller grains of the same mineral but in different orientations.

(b): Contact of a microcline and a plagioclase with an irregular boundary.

(c): Quartz in contact with two microclines (M and M') Microcline inclusions within the quartz are in optical continuity with the nearest large potash feldspar;

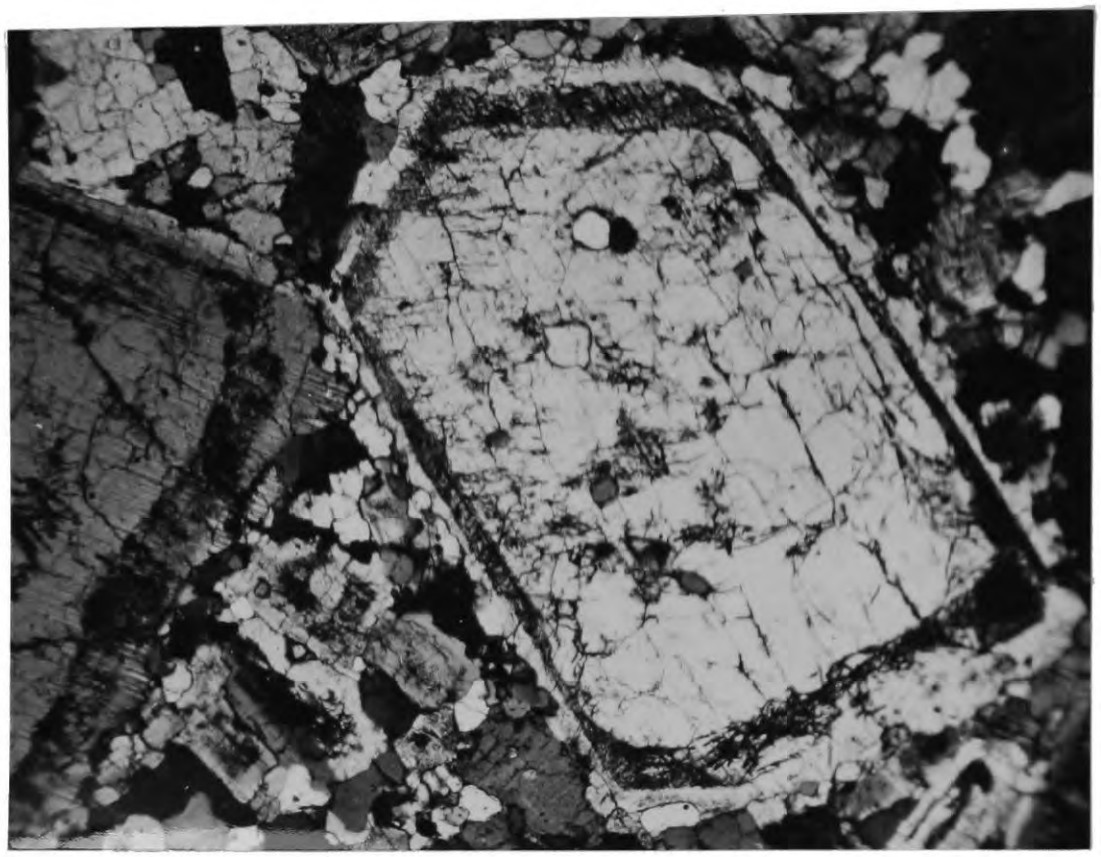

Fig. 6.7.

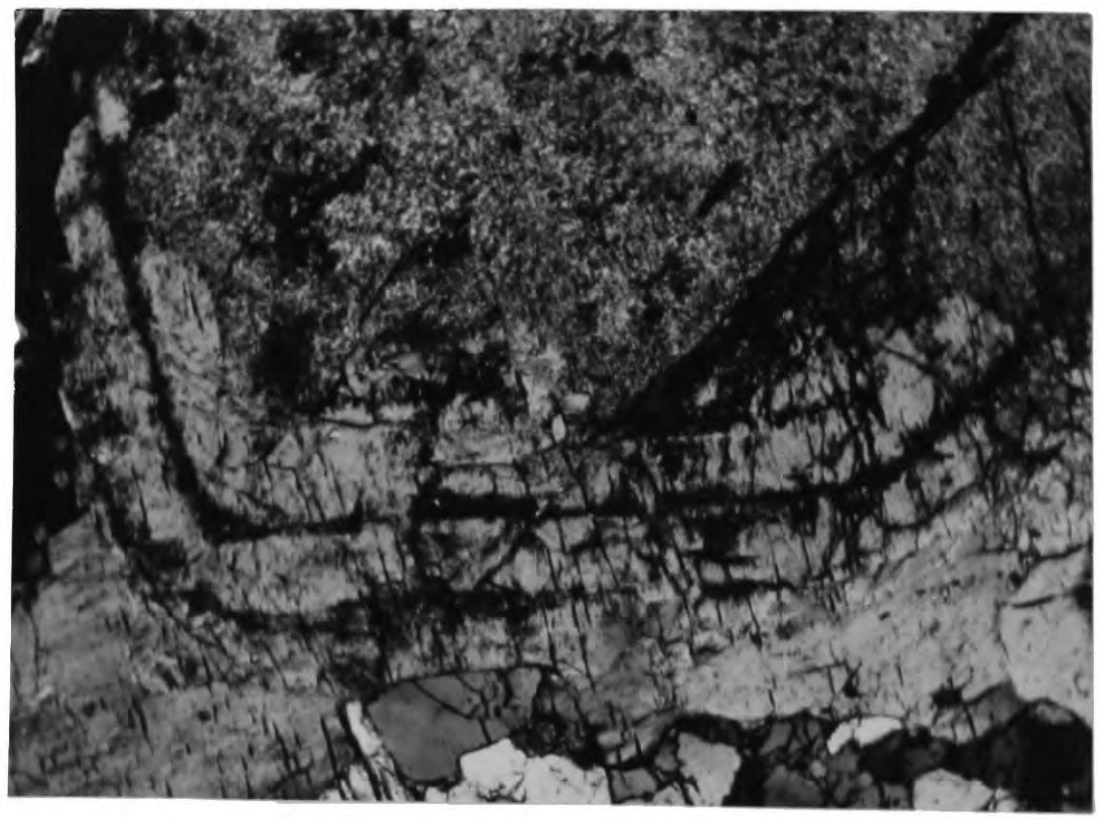

Fig. 6.8.

Fig. 6.7.

Euhedral plagioclase phenocrysts with conformable zones of alteration. Porphyritic Aplitic Granite, specimen 42062, crossed nicols x 40.

Fig. 6.8.

Part of a plagioclase phenocryst(see Fig. 6.9 a) with two or perhaps three concentric alteration zones Specimen 43041, Porphyritic Aplitic Granite, crossed nicols x 60.

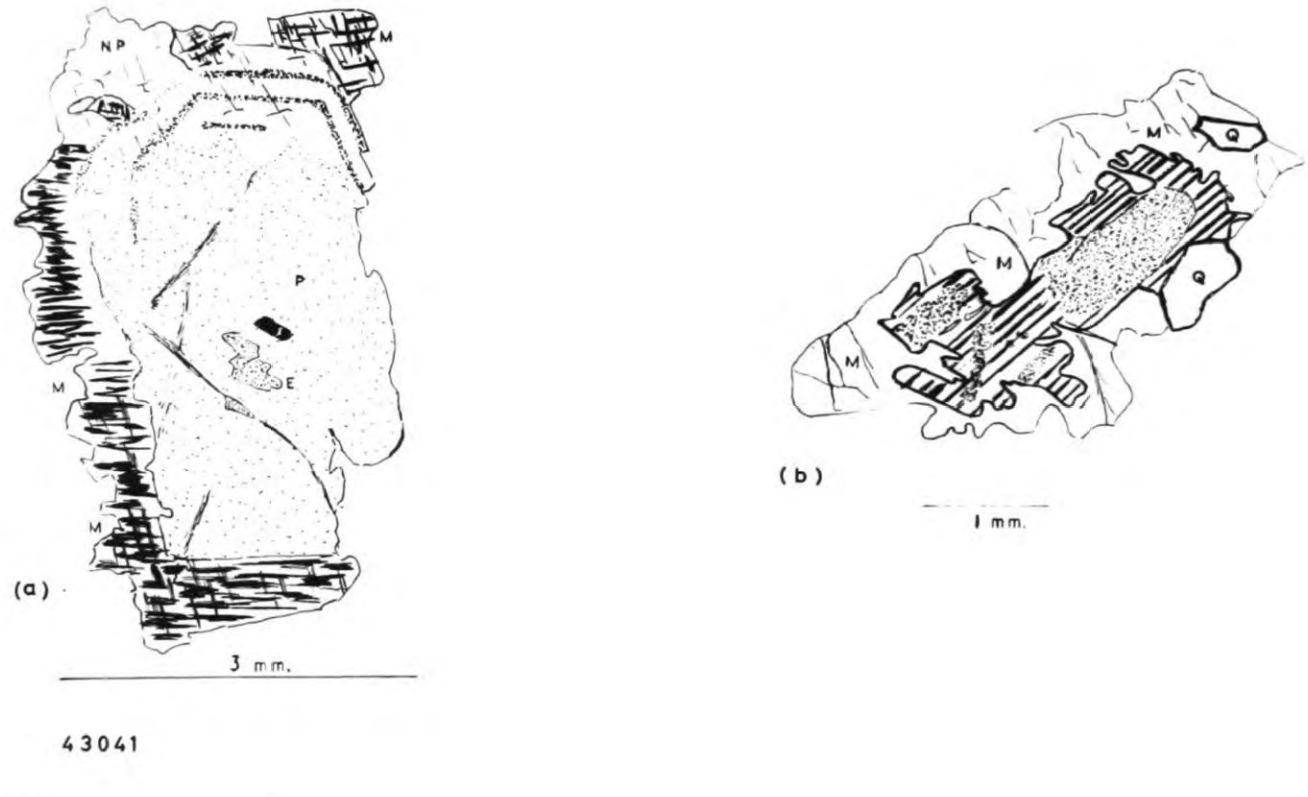

Fig. 6.9.

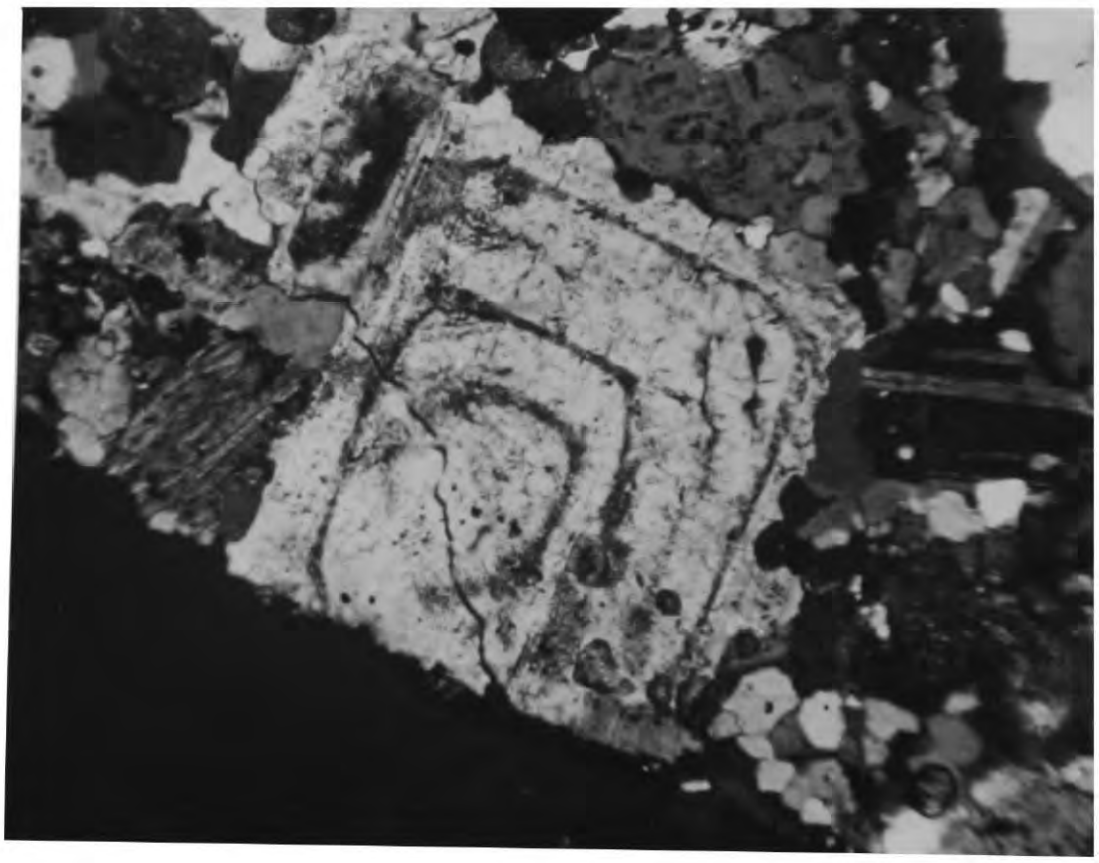

Fig. 6.10.

Fig. 6.9.

(a): Drawing of a plagioclase with a mantle of microcline and albitic feldspar(N.P.) The conformity of the alteration bands to the shape of the grain is brought out by the drawing, c.f. Fig. 6.8.

(b): Drawing of a plagioclase grain with a microcline mantle. The irregular shape of the plagioclase core is typical.

Fig. 6.10.

Plagioclase phenocryst with at least three conformable zones of alteration. Porphyritic Aplitic Granite, 43062, crossed nicols x 40.

Fig. 6.11.

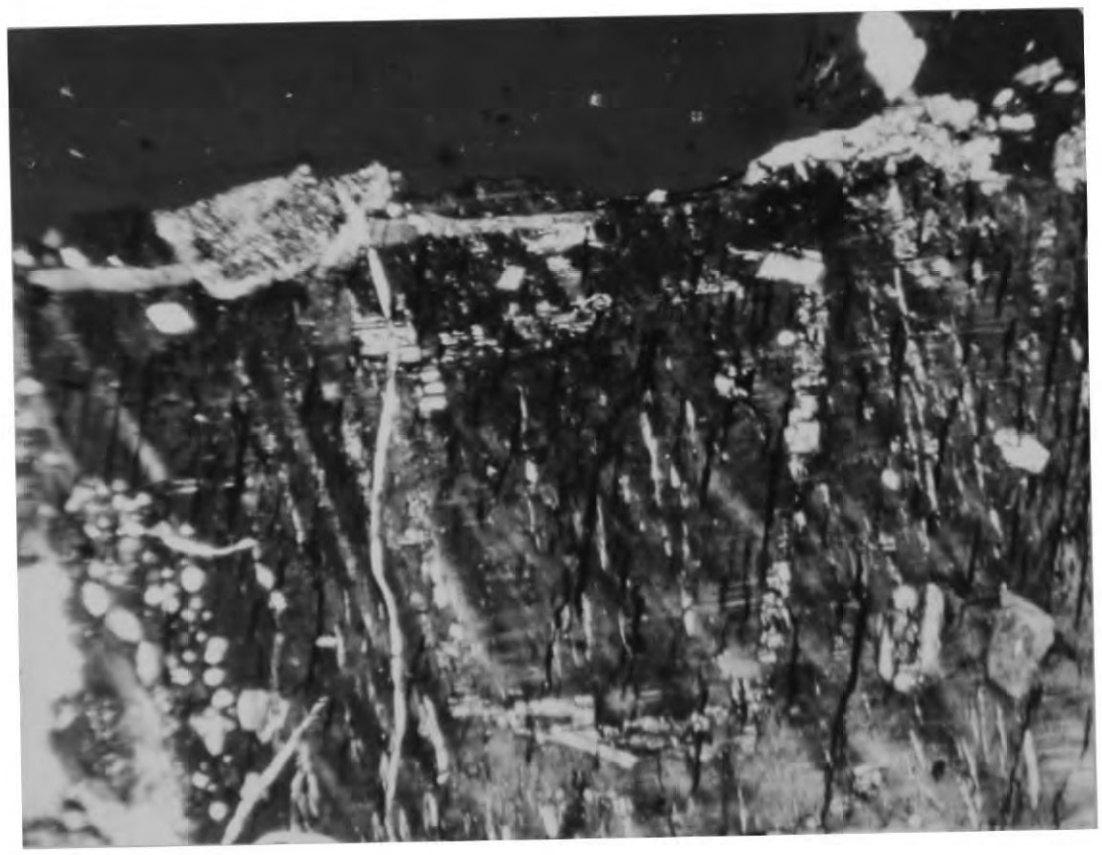

Fig. 6.12.

Fig. 6.11.

Euhedral microcline with concentric zones of alteration. Crossed nicols x 60.

Fig. 6.12.

Euhedral microcline with concentric zones of alteration. Crossed nicols x 50.

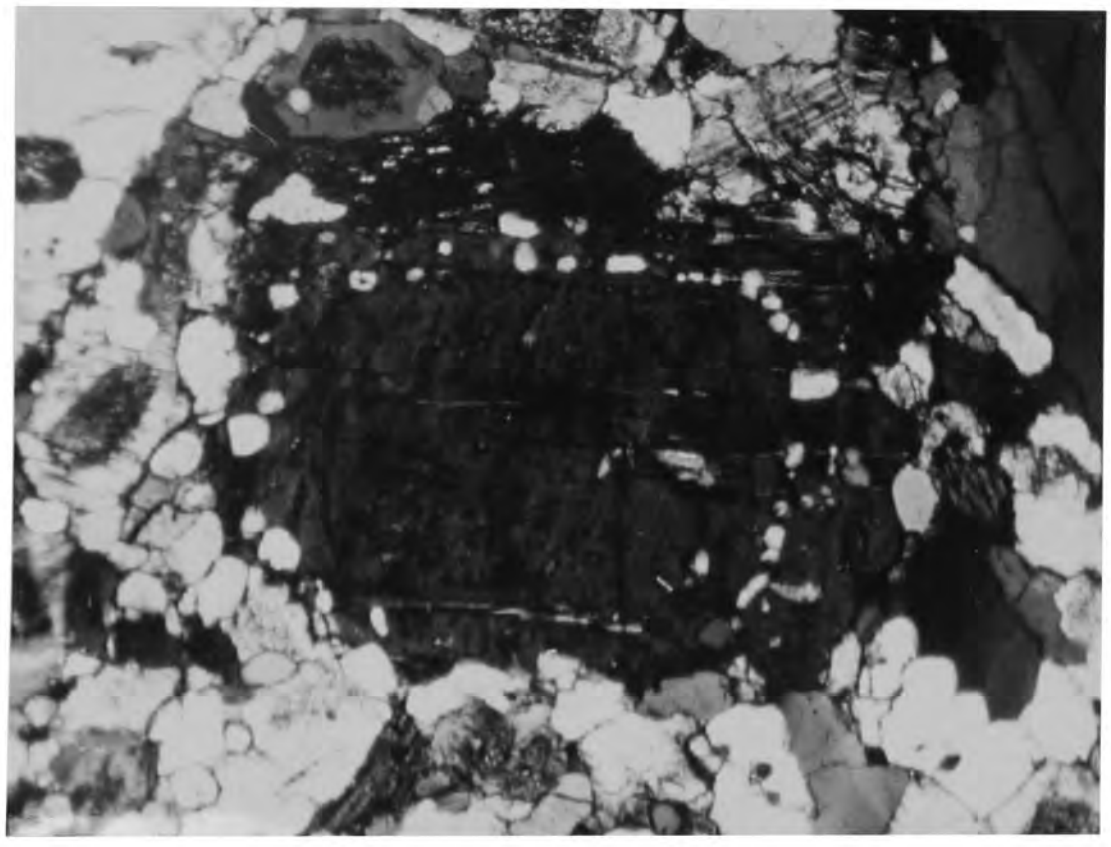

Fig. 6.13.

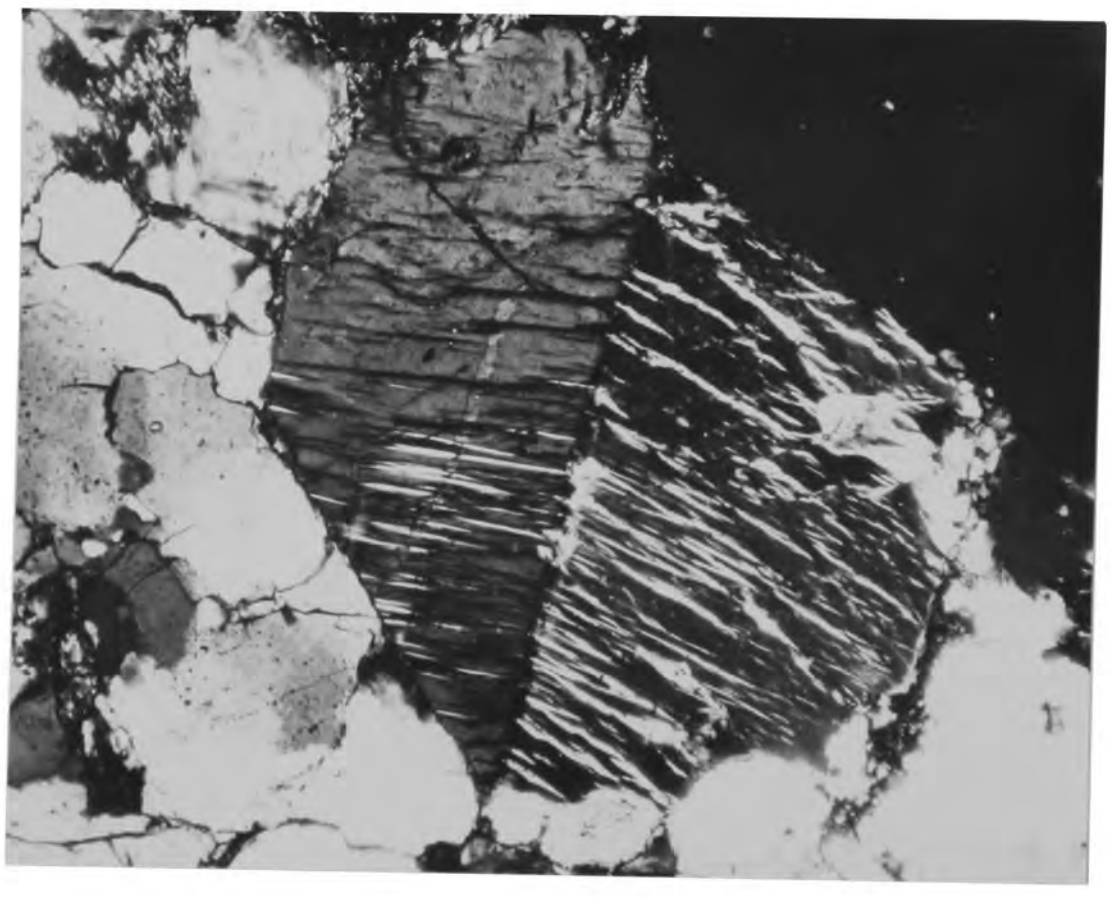

Fig. 6.14.

Fig. 6.13.

Microcline phenocryst with a zone of quartz inclusions conformable to the grain boundaries. Porphyritic Aplitic Granite, 43062. Crossed nicols x 50.

Fig. 6.14.

Twinned microcline phenocryst with "herring-bone" effect produced by perthite lamellae. Specimen 43041, crossed nicols x 75.

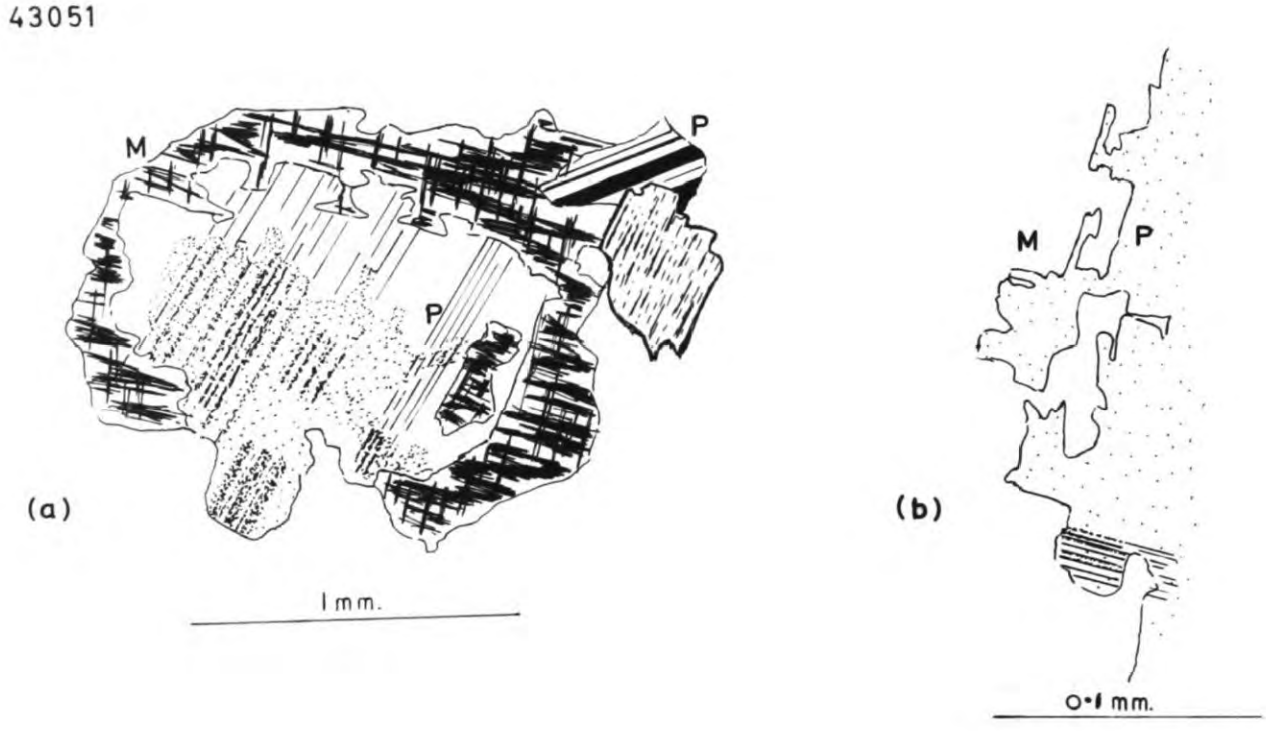

Fig. 6.15.

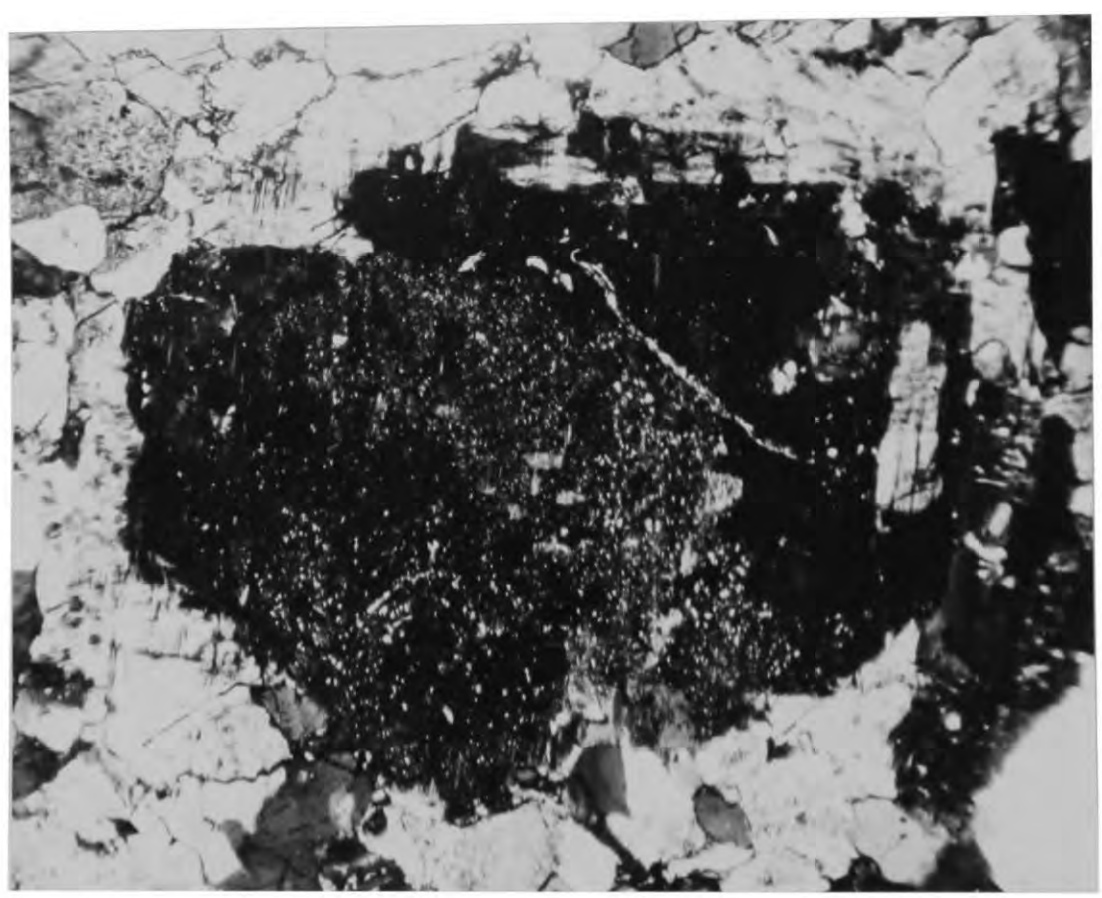

Fig. 6.16.

Fig. 6.15.

Drawings of plagioclase-microcline relationships; specimen 43051.

(a): Plagioclase grain mantled by microcline(M).

(b): Detail of the contact between the two minerals drawn from the same grain.

Fig. 6.16.

Photomicrograph of the grain figured in Fig. 6.15. Crossed nicols x 40.

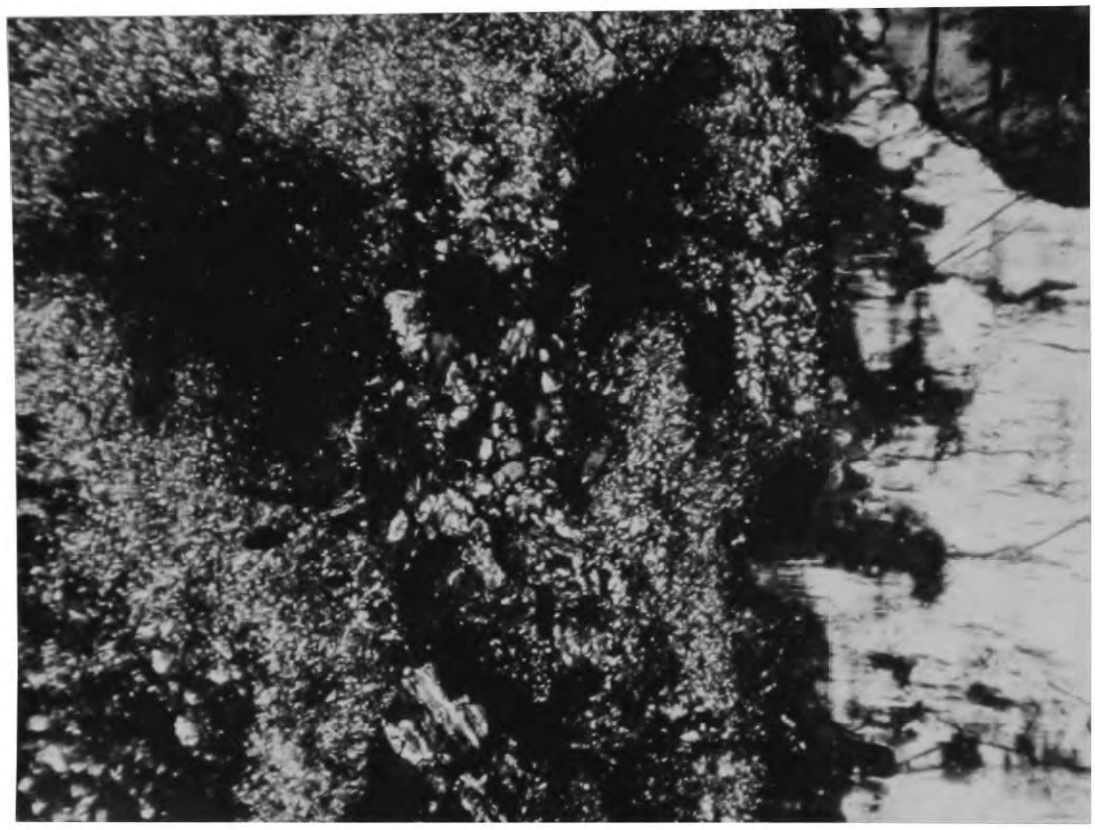

Fig. 6.17.

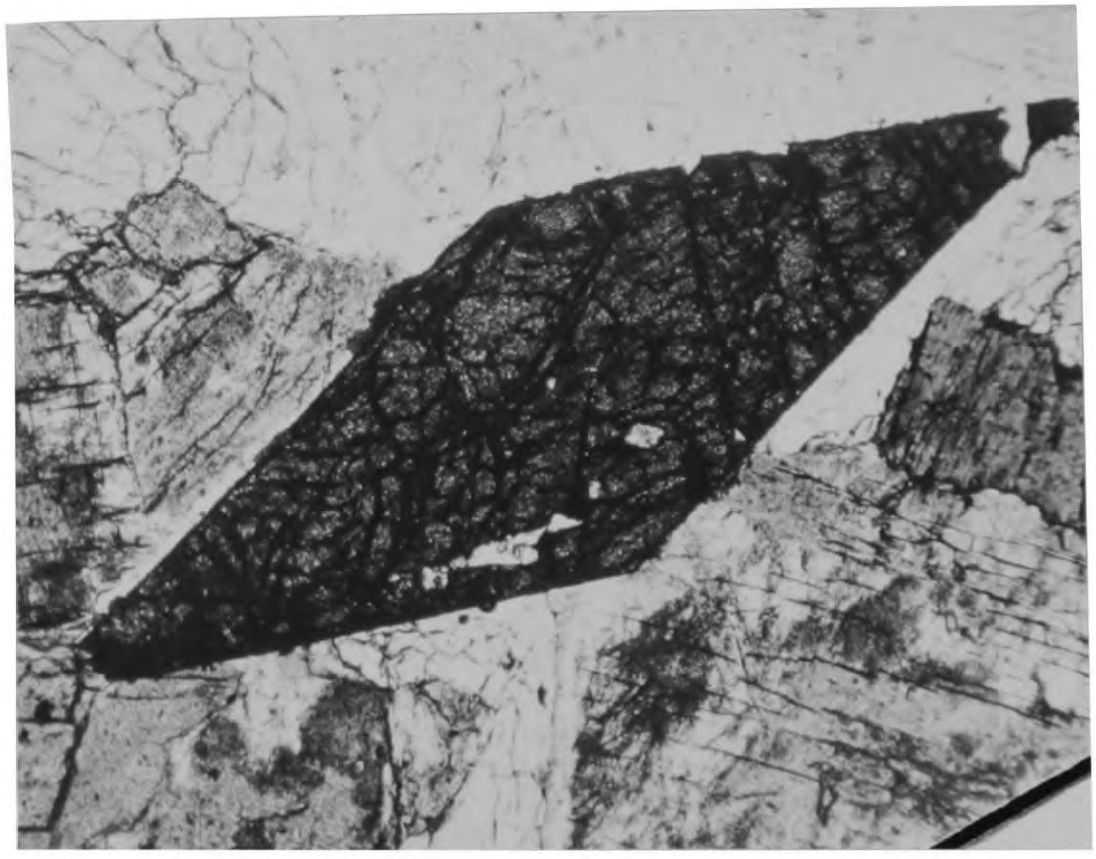

Fig. 6.18.

Fig. 6.17.

Photomicrograph of the contact between the plagioclase core and microcline mantle of a composite grain. Specimen 43041. Epidote granules can be seen within the plagioclase, which is at extinction.
Crossed nicols x 200.

Fig. 6.18.

Typical sphene(titanite) developed in the Euhedral Phenocryst Granite, specimen 43064.
Plane polarised light x 50.

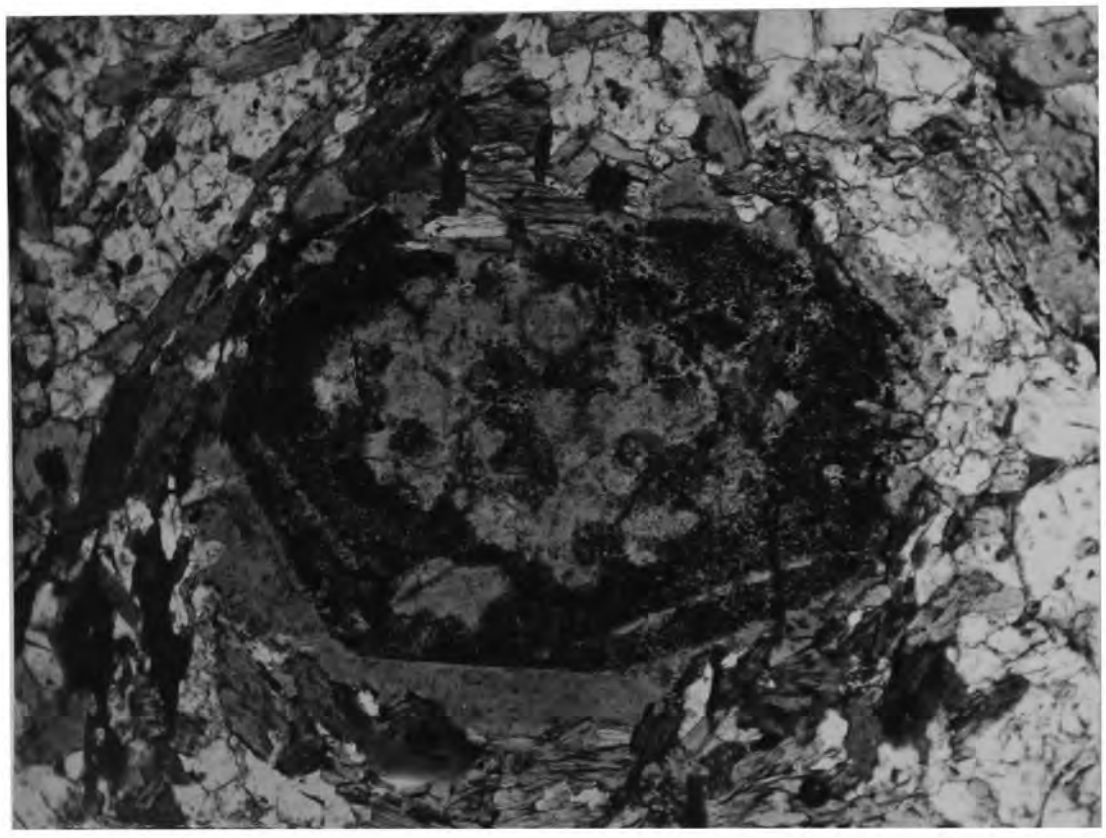

Fig. 7.1.

Fig. 7.2.

Fig. 7.1.

Hornblende in the amphibolitic facies of the gneiss band. Magnetite(?) granules in euhedral from lie within the grain. The general texture of the biotites is parallel to the length of the hornblende, but the figure shows some which are wrapped around the larger grain.
Specimen 43004, plane polarised light x 45.

Fig. 7.2.

Photomicrograph showing the general texture of the banded amphibolitic gneiss. Specimen 43087 x 40.

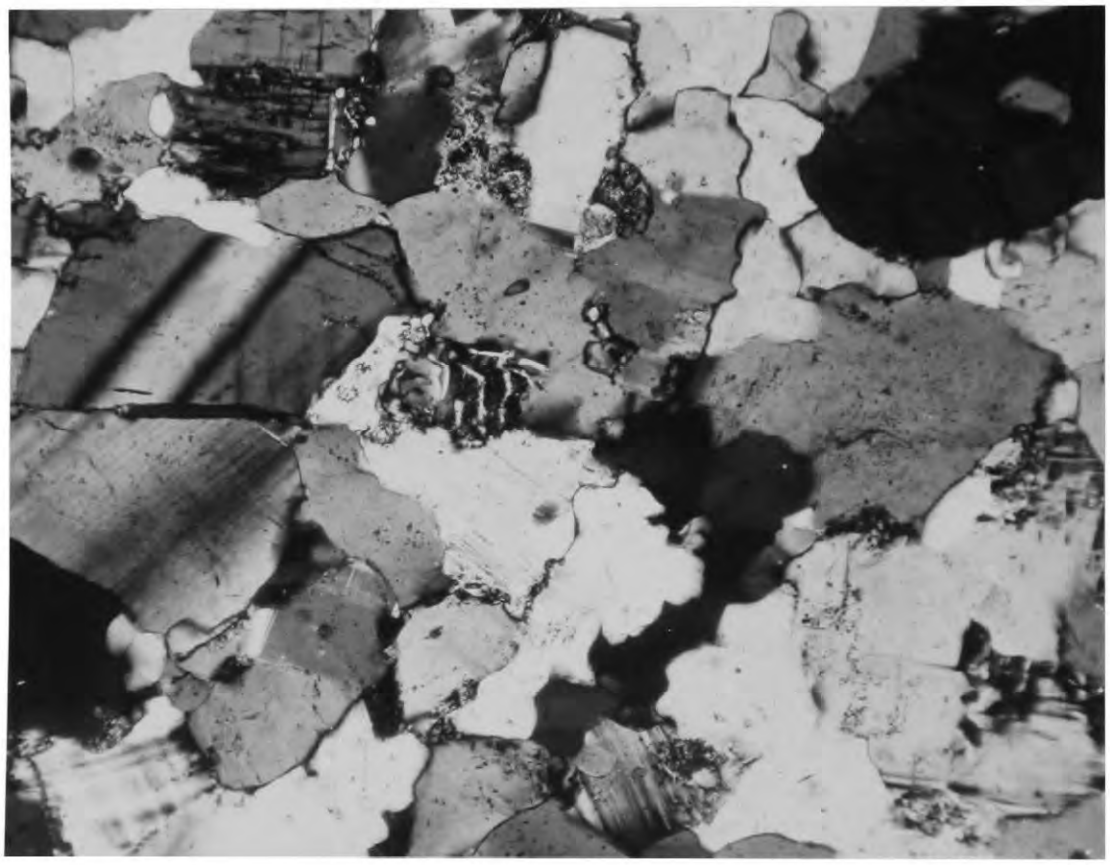

Fig. 7.3.

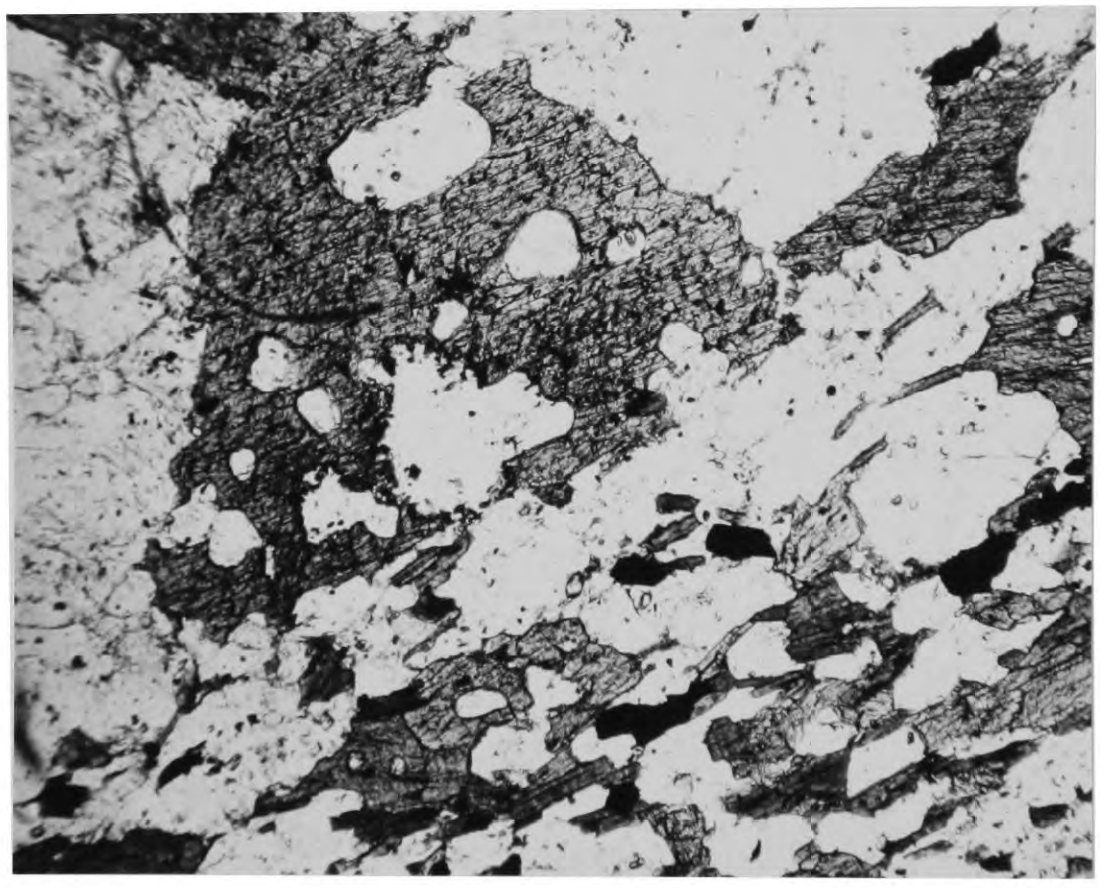

Fig. 7.4.

Fig. 7.3.

General texture of an acid vein within the gneiss band. Specimen 23497, crossed nicols about x 40.

Fig. 7.4.

Photomicrograph showing the contact of a vein against gneiss. Note the development of a larger amphibole in the vein. Specimen 43001, plane polarised light x 50.

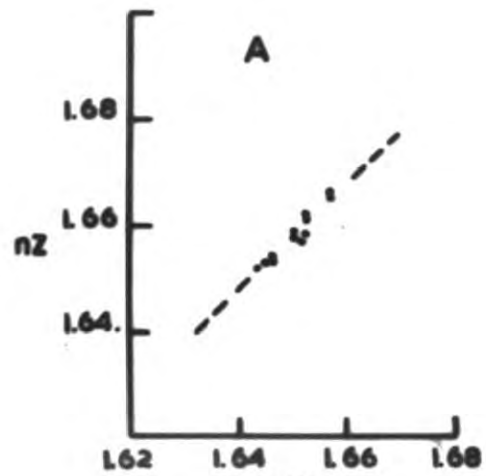
A
1.68
1.66
nZ
1.64
1.62
1.64
1.66
1.68
nY

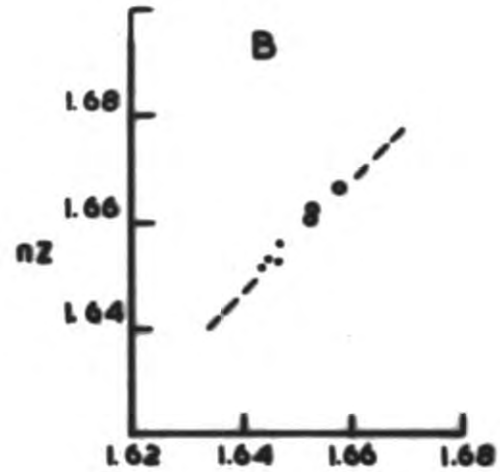
B
1.68
1.66
nZ
1.64
1.62
1.64
1.66
1.68
nY.

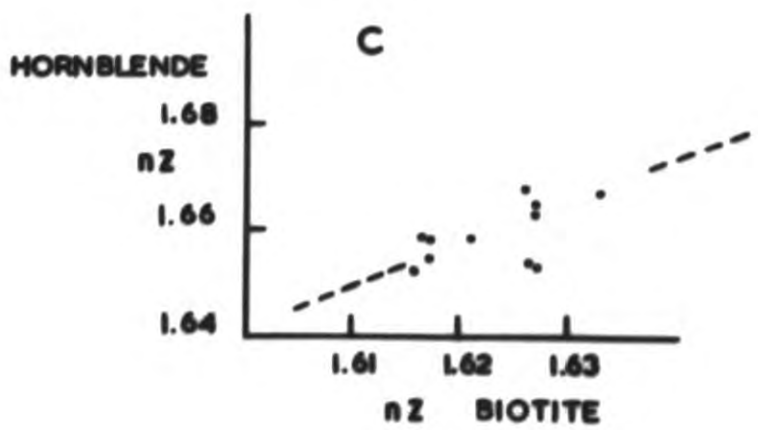
C
HORNBLENDE
1.68
nZ
1.66
1.64
1.61
1.62
1.63
nZ BIOTITE

Fig. 7.5.

Optical data on amphiboles and biotites from the gneiss band.

A: Plot of nZ' against nY for all amphiboles measured.

B: Plot of nZ' against nY for measurements quoted in the text. Solid dots are amphiobles from the amphibolitic gneiss.

C: Plot of nZ' amphibole against nZ' biotite.

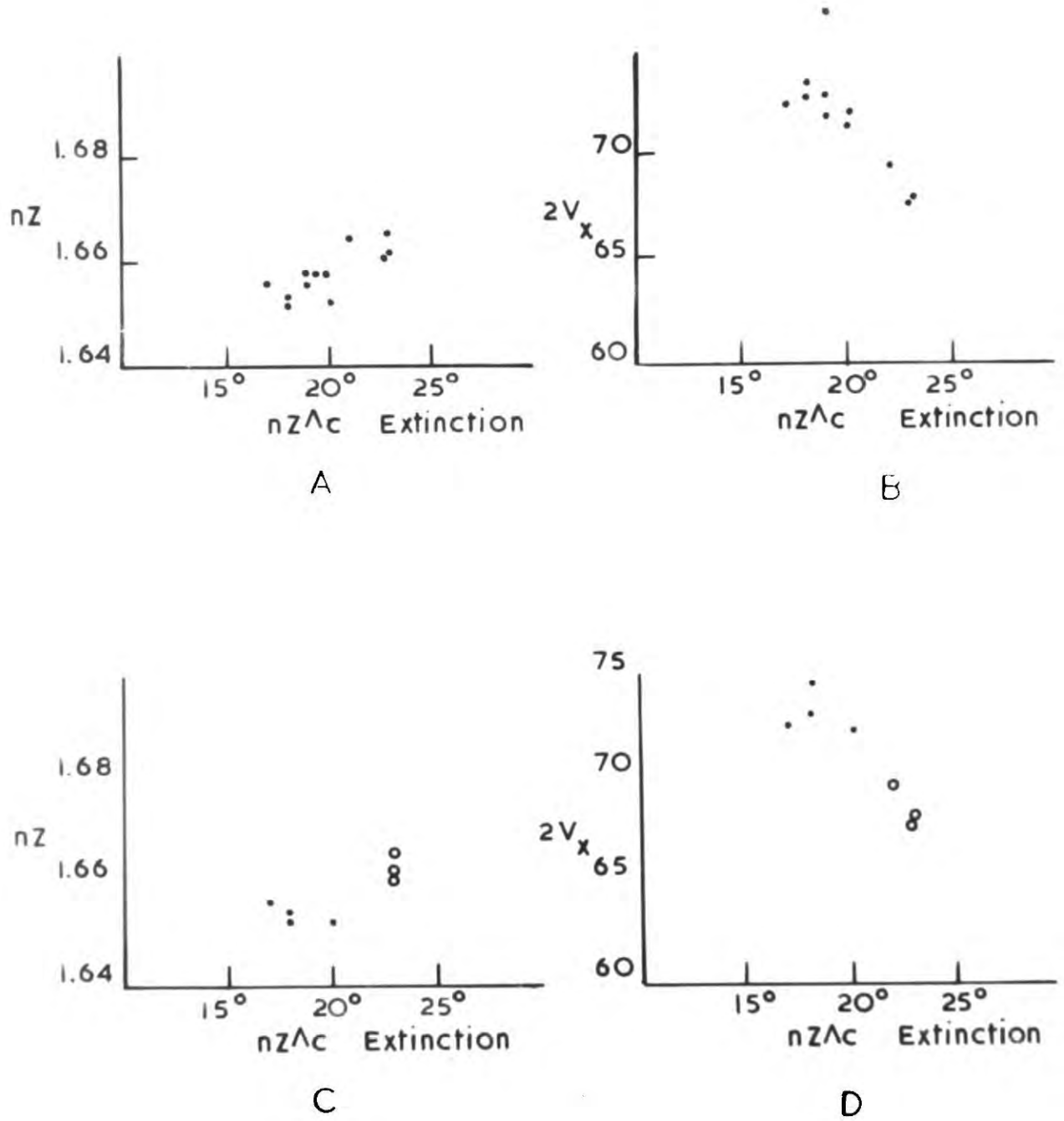
1.68
nZ
1.66
1.64
15°
20°
25°
nZ^c Extinction
A
70
2V_x
65
60
15°
20°
25°
nZ^c Extinction
B
1.68
nZ
1.66
1.64
15°
20°
25°
nZ^c Extinction
C
70
2V_x
65
60
15°
20°
25°
nZ^c Extinction
D

Fig. 7.6.

47

Fig. 7.6.

Optical data on amphiboles from the gneiss band.

A: Plot of nZ' against extinction.

B: Plot of extinction against optic axial angle. For all amphiboles measured from the gneiss.

C: Plot of nZ' agaisnt extinction.

D: Plot of extinction against optic axial angle. Solid dots are amphiboles from amphibolitic gneiss and open circles are specimens from more leucocratic gneiss which are quoted in the text.

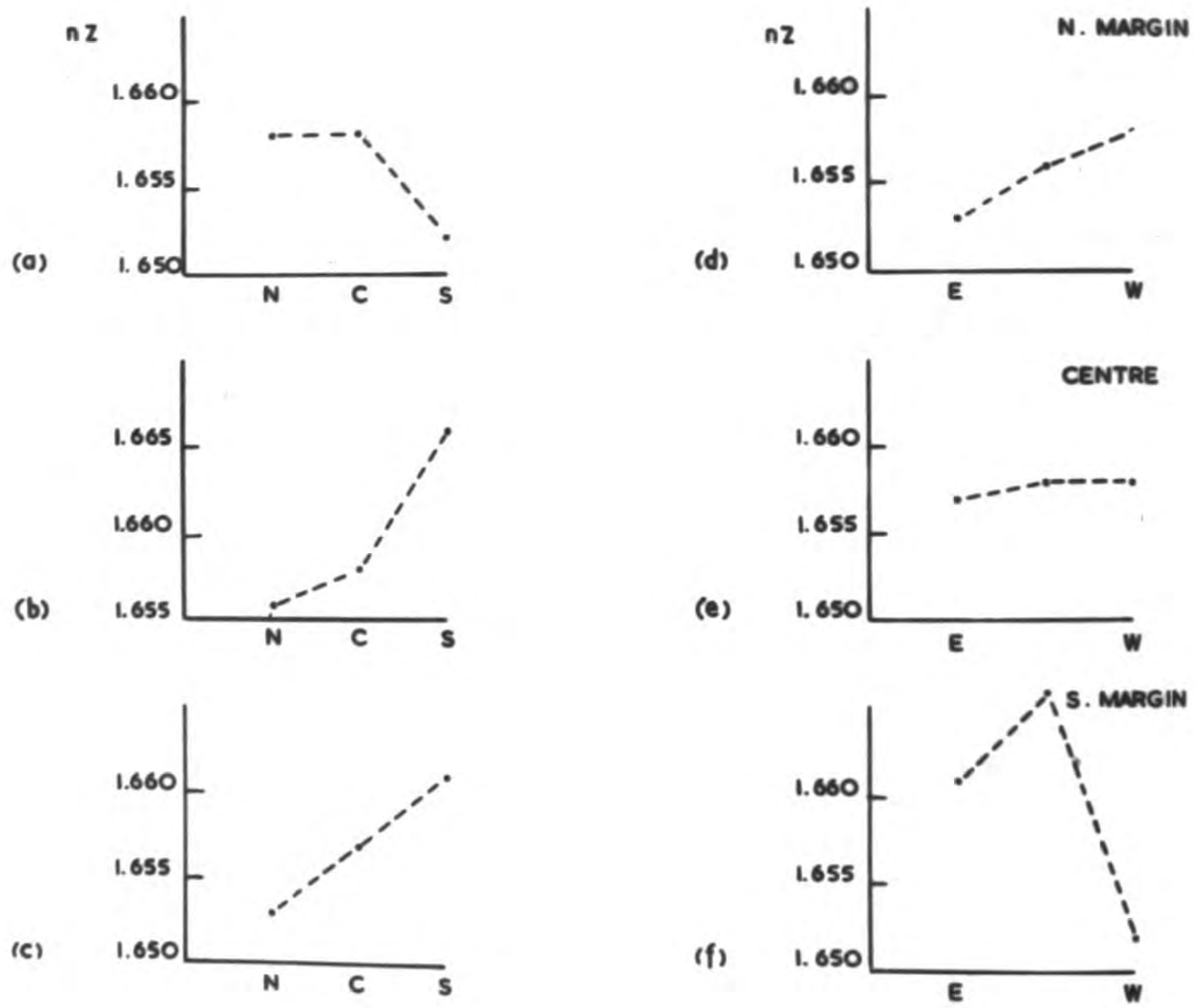
nZ
1.660
1.655
1.650
(a)
N
C
S
(b)
1.665
1.660
1.655
(c)
N. MARGIN
(d)
E
W
CENTRE
(e)
S. MARGIN
(f)

Fig. 7.7.

48.

Fig. 7.7.

Plot of nZ' for amphiboles from the gneiss band, relative to their position in the band.

(a): Specimen 43021, 43022 and 43023(north, centre and south respectively).

(b): Specimen 43027, 43028 and 43029.

(c): Specimen 43004, 43002 and 43001.

Fig. (d - f) are plots of nZ' from the northern margin along the length of the band(d) from the centre(e) and from the southern margin(f).

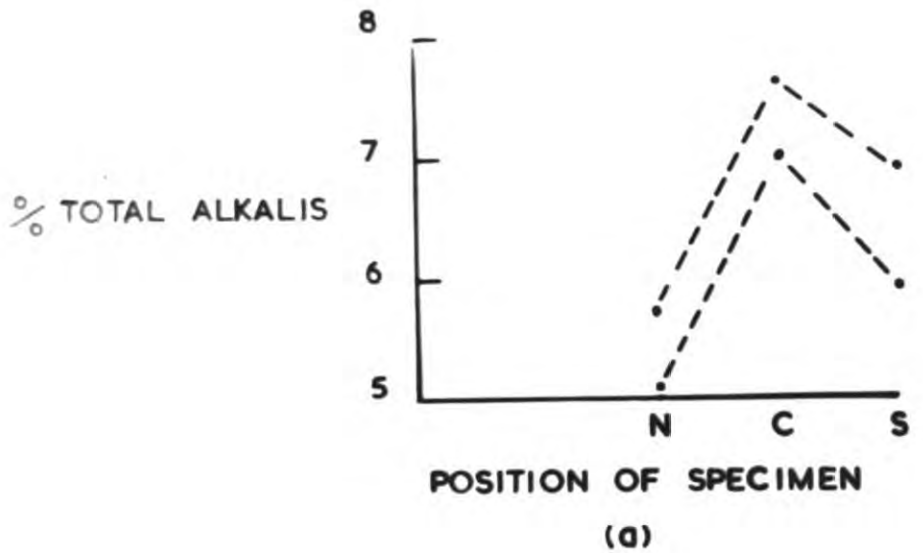
% TOTAL ALKALIS
8
7
6
5
N
C
S
POSITION OF SPECIMEN

(a)

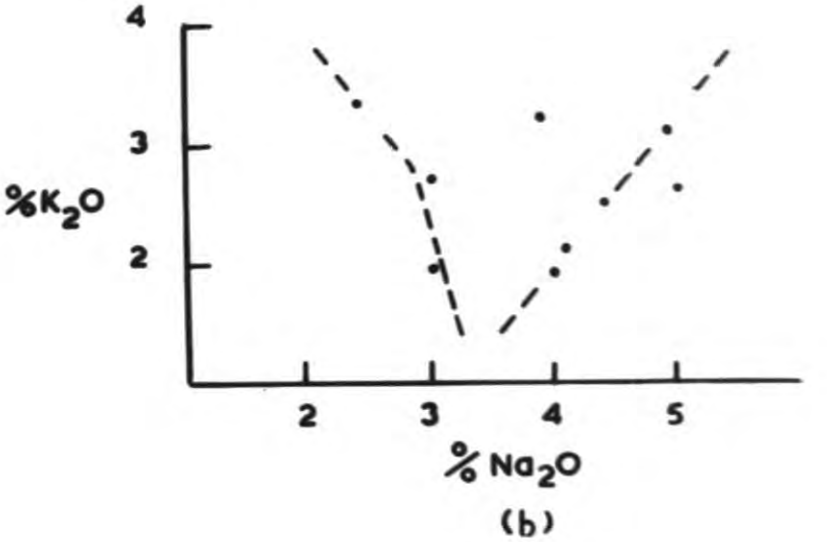
%K2O
4
3
2
2
3
4
5
% Na2O

(b)

Fig. 7.8.

(a): plot of the total alkalis against the position of the gneiss specimen across the strike(from the north and south margins and centre.)

(b): plot of % Na_2O against % K_2O. (Note the separation of the amphibolitic gneiss hornblendes from the remainder of the specimens. The isolated point mid-way between the two dotted lines, is a sample from an acid vein within the gneiss band.

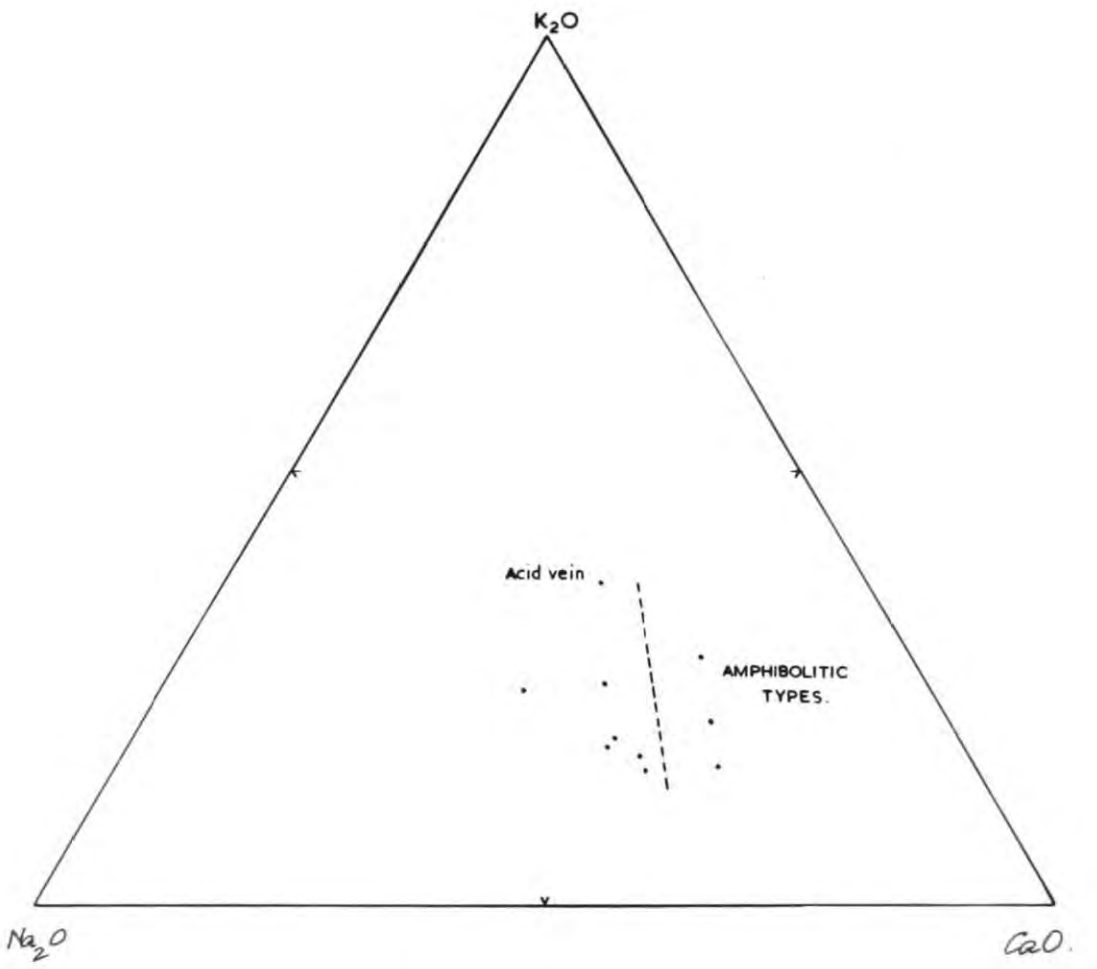

Fig. 7.9.

Fig. 7.9.

Plot of K_2O - Na_2O - CaO for gneiss band specimens.

Fig. 3.1.

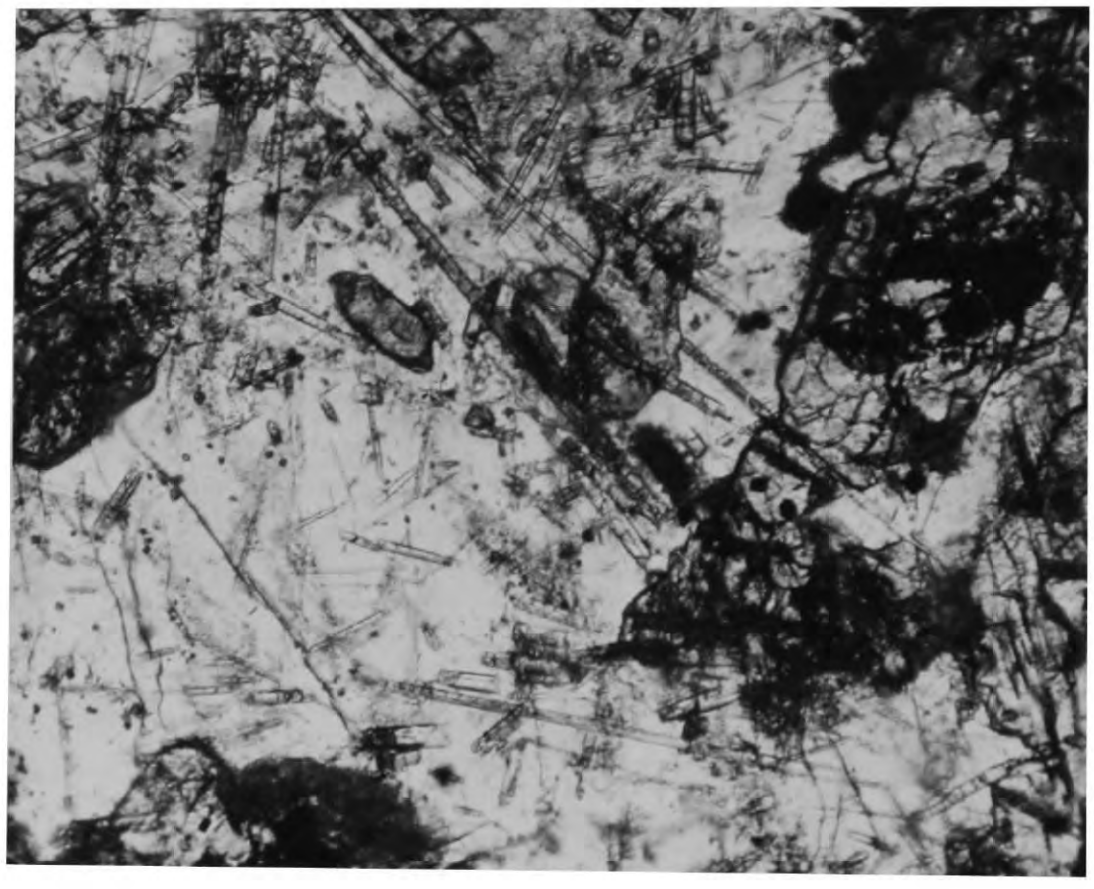

Fig. 8.2.

Fig. 8.1.

Photomicrograph to show the clearing of the opaque inclusions about the reaction, olivine gabbro. Specimen 23373, plane polarised light x 50.

Fig. 8.2.

Apatite inclusions within the plagioclase, olivine gabbro, specimen 23373. Plane polarised light x 200.

Fig. 8.3.

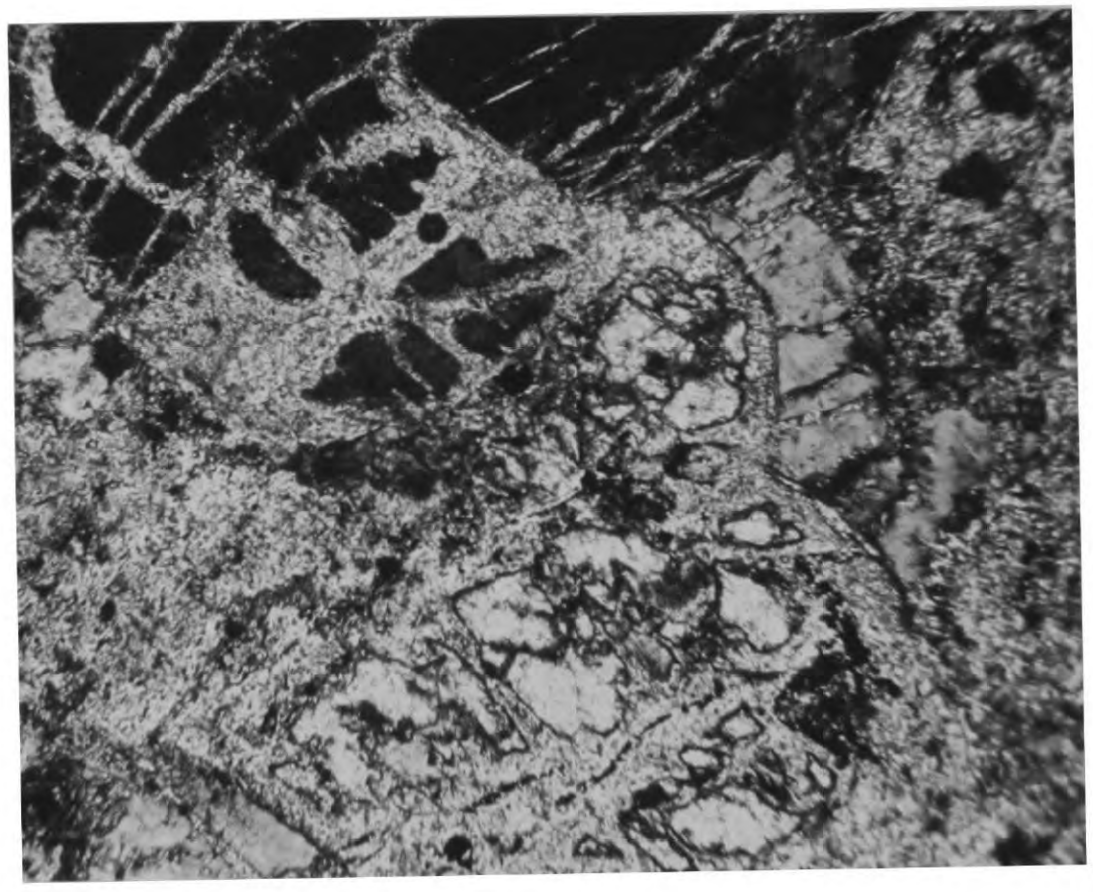

Fig. 8.4.

Fig. 8.3.

Mantle of clinopyroxene grains about a hypersthene. Norite, specimen 23834, crossed nicols x 50.

Fig. 8.4.

Small patch of hypersthene left in the amphibole pseudomorph after hypersthene. Note the veins of uralitic amphibole penetrate into the adjacent plagioclase(in extinction). Norite, specimen 42960. Crossed nicols x 100.

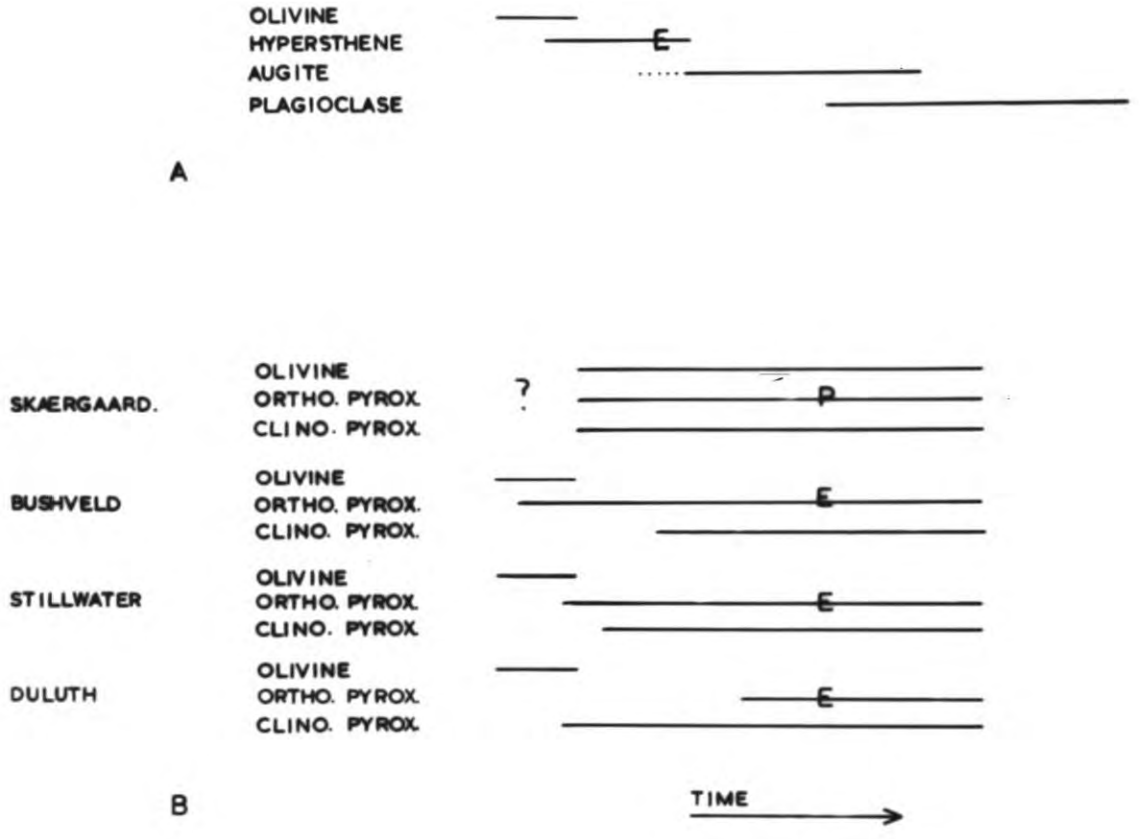
OLIVINE
HYPERSTHENE
AUGITE
PLAGIOCLASE
A
SKAERGAARD.
OLIVINE
ORTHO. PYROX.
CLINO. PYROX.
?
P
BUSHVELD
OLIVINE
ORTHO. PYROX.
CLINO. PYROX.
E
STILLWATER
OLIVINE
ORTHO. PYROX.
CLINO. PYROX.
E
DULUTH
OLIVINE
ORTHO. PYROX.
CLINO. PYROX.
E
B
TIME

Fig. 8.5.

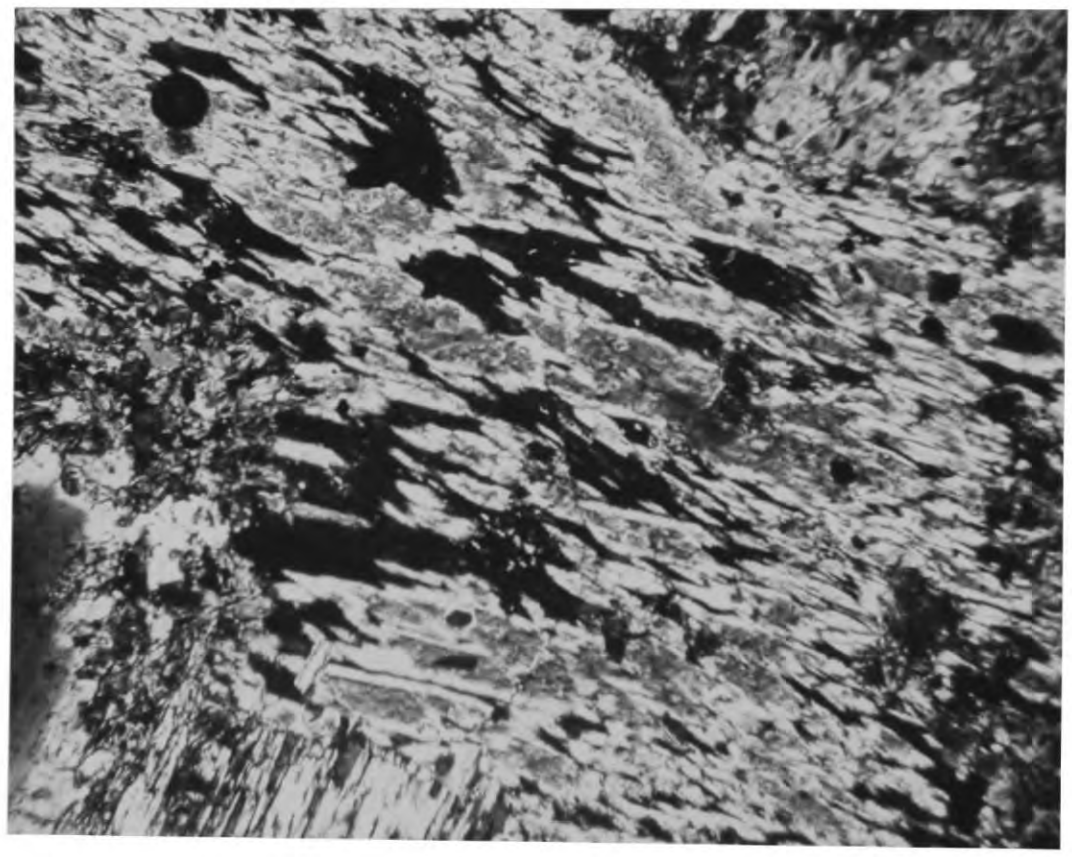

Fig. 8.6.

Fig. 8.5.

A: Proposed order of crystallisation for the gabbro-norite mass on the Julianehaab Peninsula.

B: Proposed crystallisation sequences for other masses, (mainly after Wager and Deer, 1939: Hall 1932: and Hess 1941).

Abb. E = clinopyroxene exsolving from orthopyroxene
P = pigeonitic clinopyroxene exsolving from orthopyroxene.

Fig. 8.6.

Photomicrograph to show the unusual extinction of tremolitic amphiboles, developed within the amphibolites around the gabbro-norite mass. Specimen 23833, crossed nivols x 80.

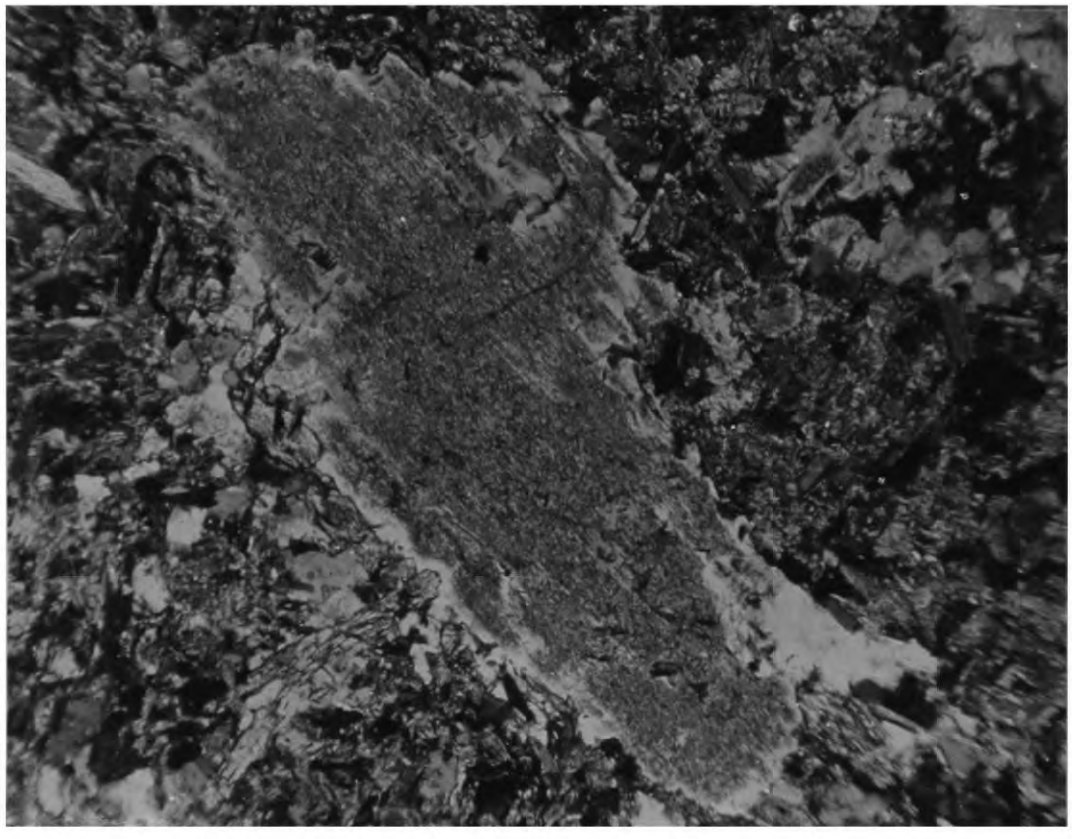

Fig. 9.1.

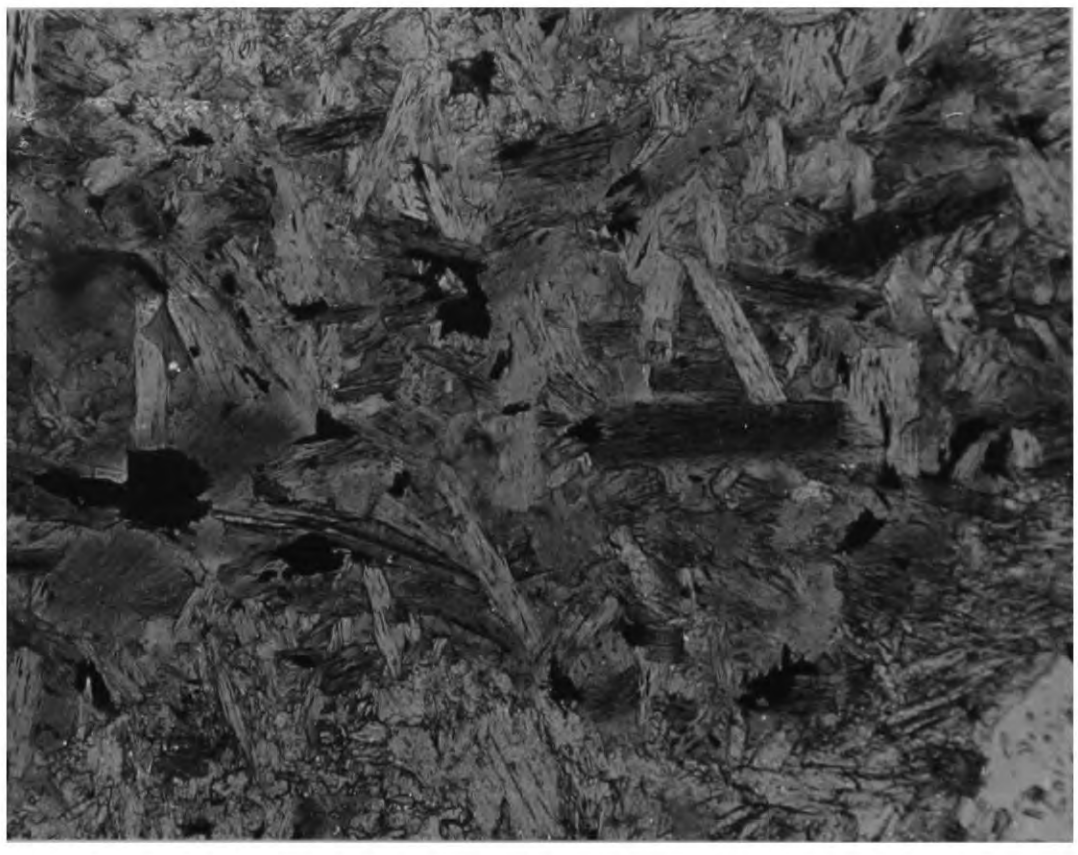

Fig. 9.2.

Fig. 9.1.

Corroded plagioclase phenocryst in dyke-like amphibolitic horizon, of Kuanitic(?) age. Specimen 23337,crossed nicols x 40.

Fig. 9.2.

Sheaves of interlocking biotite,developed in the amphibolitic bands. Specimen 23337, plane polarised light x 80.

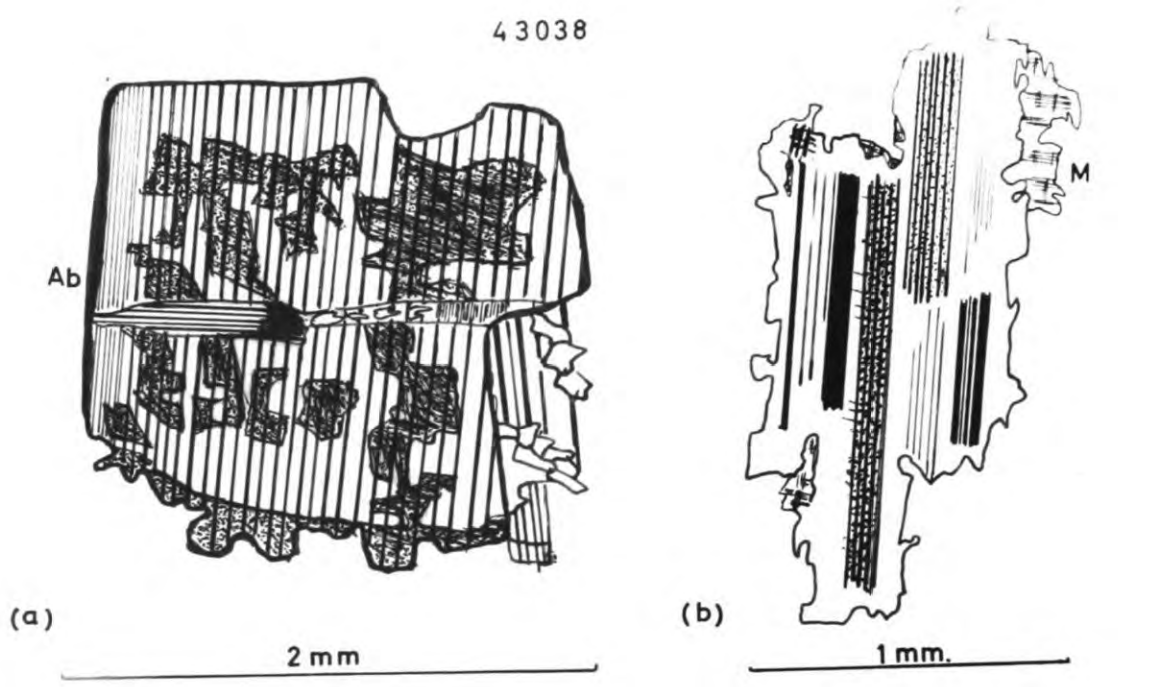

Fig. 9.3.

Fig. 9.4.

Fig. 9.3.

Drawings of plagioclase in specimen 43038.

(a): Plagioclase with "skeleton" zoning and figured below. Note the fracture across the grain, infilled with plagioclase of a different orientation and the sealing off of the fracture by later albite deposited around the margin of the grain.

(b): Corroded plagioclase. The twinning ceases before the margin, which is later, albitic plagioclase. Note also the microcline infilling the pits in the grain.

Fig. 9.4.

Part of the plagioclase figured in Fig. 9.3(a). The plagioclase infilling the fracture is indistinct but the associated quartz can be clearly seen. Crossed nicols x 40.

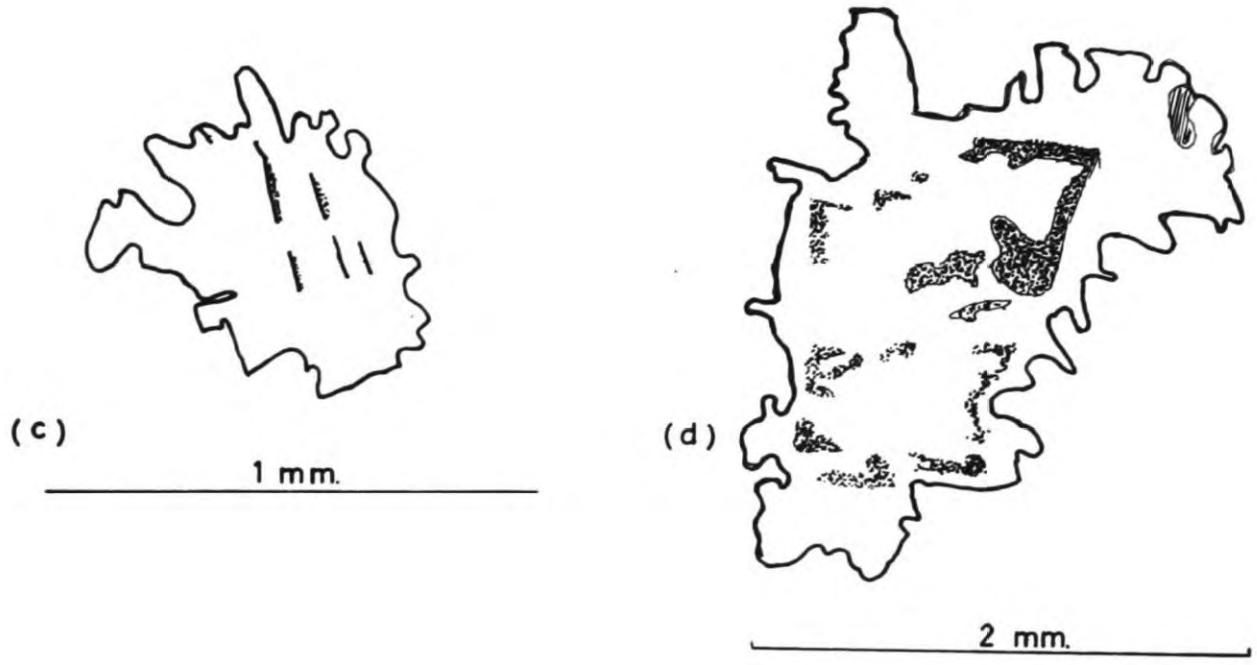

Fig. 9.5.

Fig. 9.6.

Fig. 9.5.

Drawings of plagioclase grains in specimen 43038 (Kuanitic dyke).

(c): Small grain showing corroded margins.

(d): Skeleton zoning in a plagioclase grain with corroded margins.

Fig. 9.6.

Photomicrograph of the plagioclase shown in Fig. 9.5.(d), at a slightly different orientation Crossed nicols x 35.

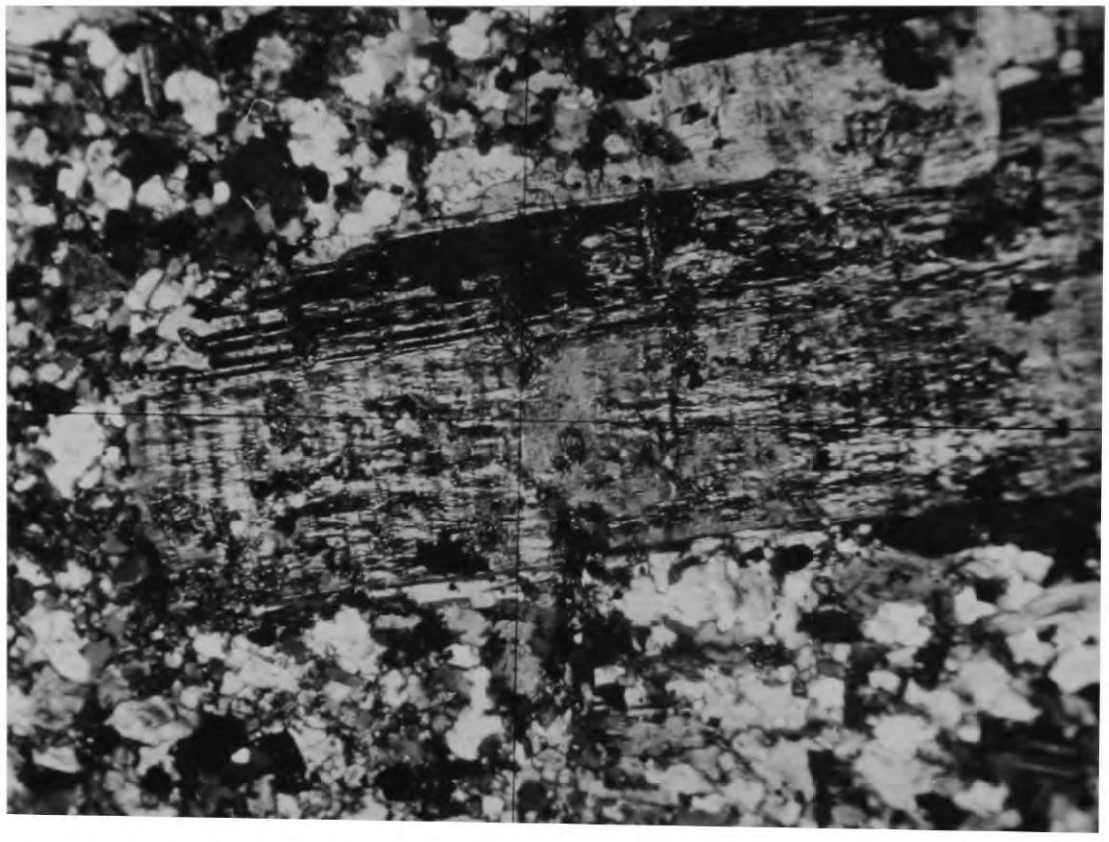

Fig. 9.7.

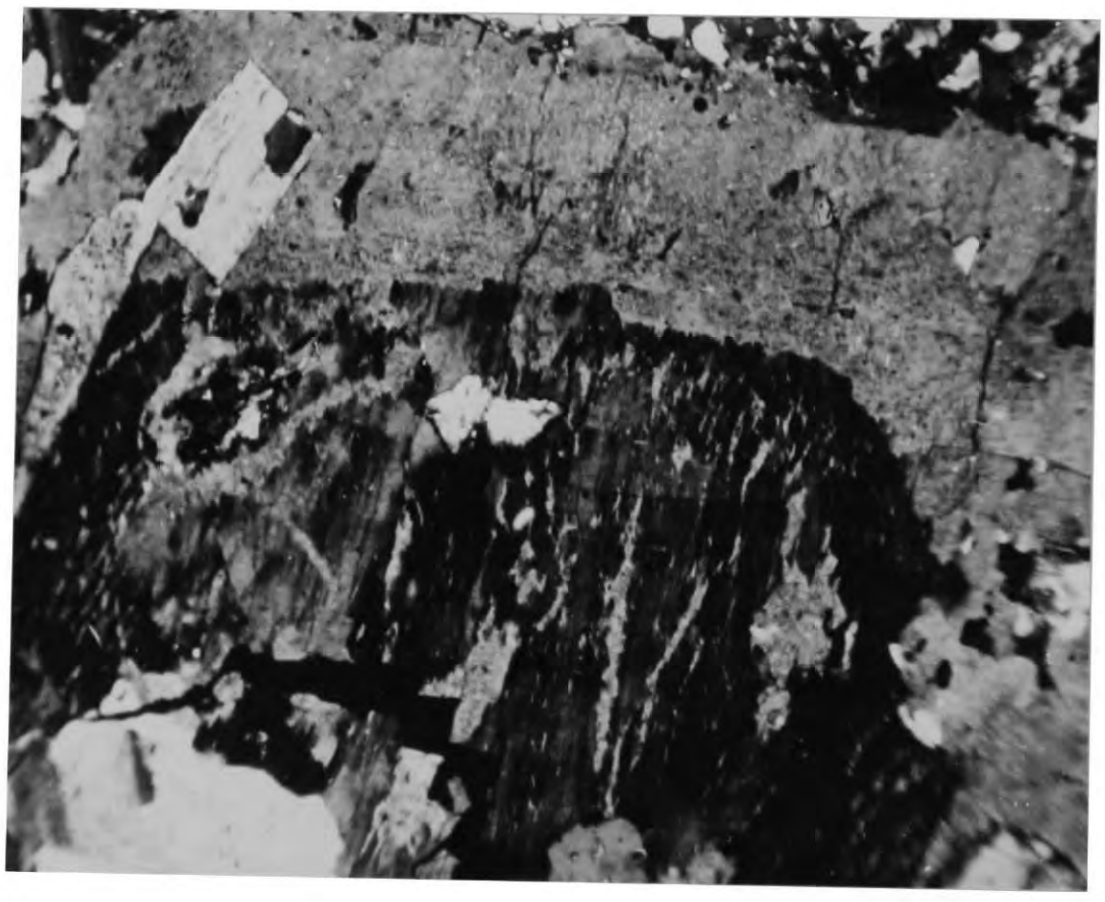

Fig. 9.8.

Fig. 9.7.

Pseudomorph of microcline after plagioclase. In the upper left of the photograph, microcline can be seen between the albite twins of the plagioclase. Note the disintegration of the albite lamellae in the upper right of the photograph. Specimen 42851, crossed nicols x 35.

Fig. 9.8.

Rapakivi feldspar with a perthitic microcline core and an albite mantle. The whole grain has euhedral outlines. The perthite lamellae are in the same optical orientation as the albite mantle. Small quartz blebs can be seen in the albite(upper centre of the photograph) Specimen 23376, crossed nicols x 30.

POTASH FELDSPAR ALBITE	PLAGIOCLASE. An_{10-50}	PLAGIOCLASE An_{10-50}
SYENITE	MONZONITE	DIORITE
(AUGITE SYENITE PORPHYRY) MICROSYENITE (NEPHELINE PORPHYRY)	MICROMONZONITE	MICRODIORITE
(HEDRUMITE.) POTASSIC SODIC TRACHYTE	(MONZONITE PORPHYRY) TRACHYANDESITE	ANDESITE → TRACHYBASALT

Fig. 9.9.

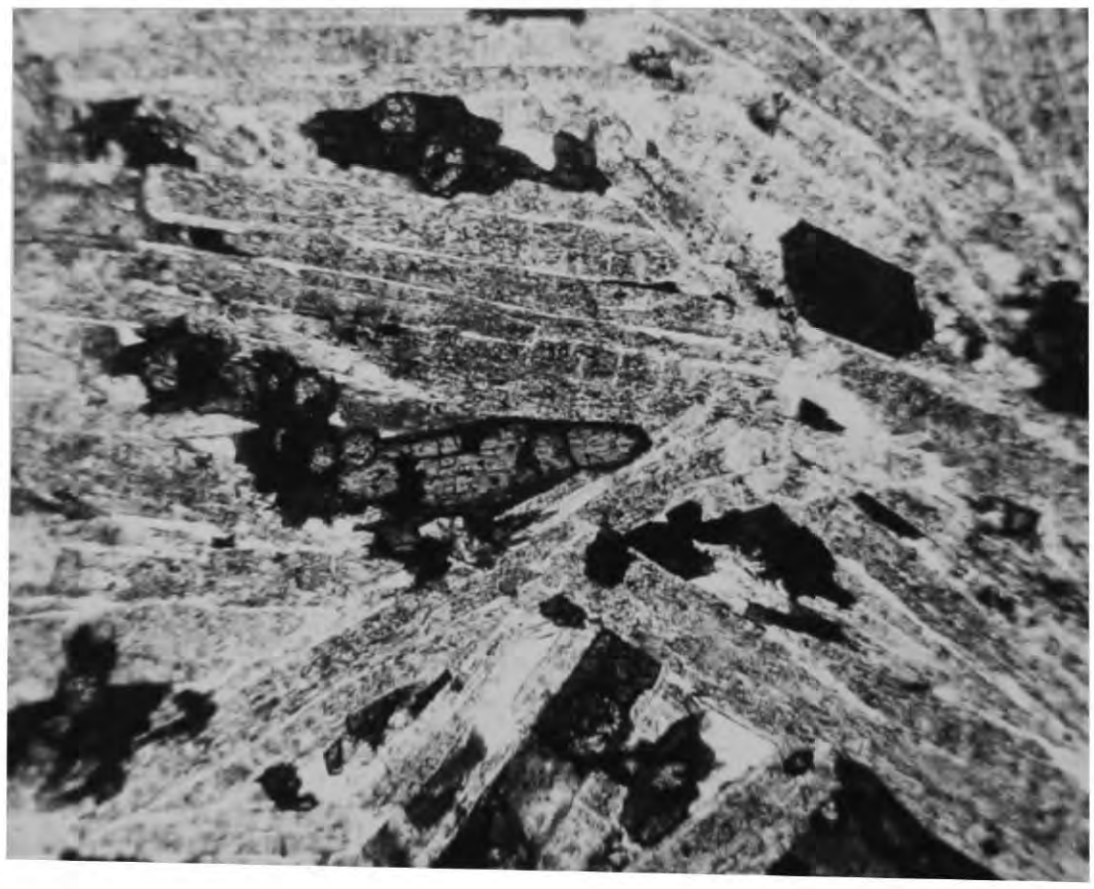

Fig. 9.10.

Fig. 9.9.

Classification used in naming the alkali dykes(repeat of Fig. 5.13. - see this diagram for further description)

Fig. 9.10.

Photomicrograph to show the general trachytic texture developed within some alkaline dykes and also the rim of sodic pyroxene around the augitic pyroxene a feature typical of these dykes. Specimen 23496, ordinary light x 200.

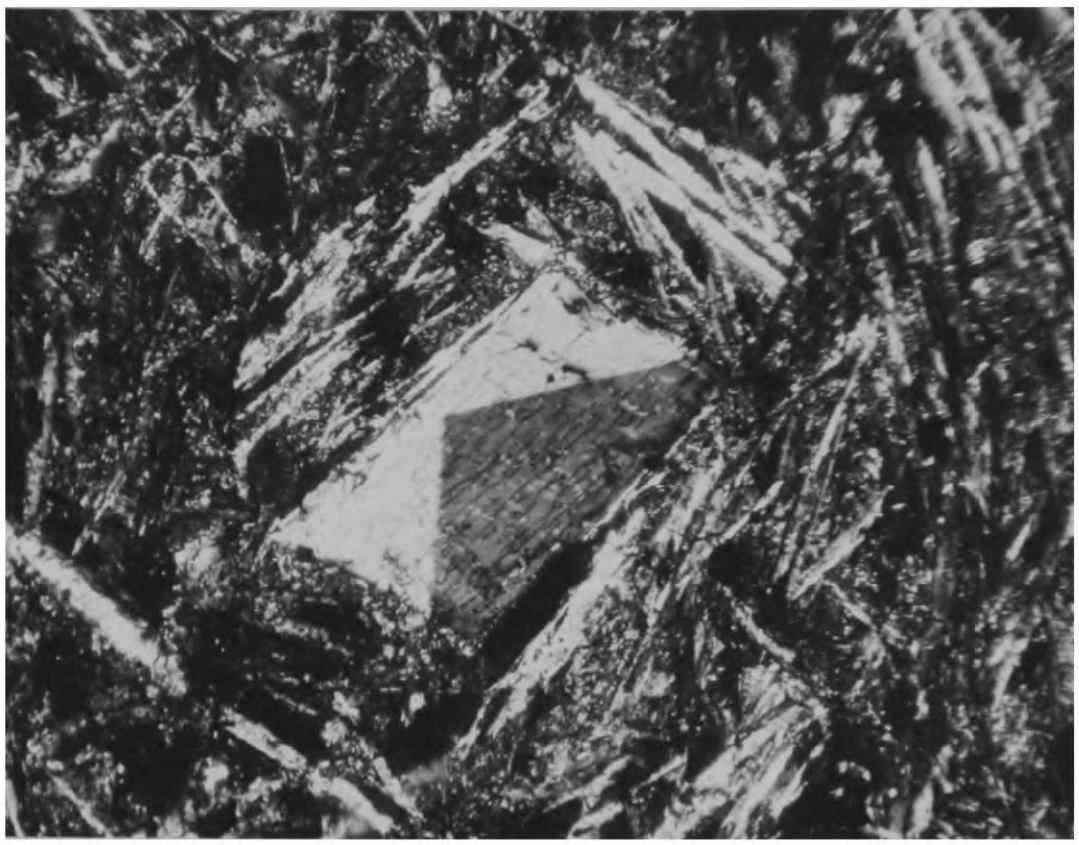

Fig. 9.11.

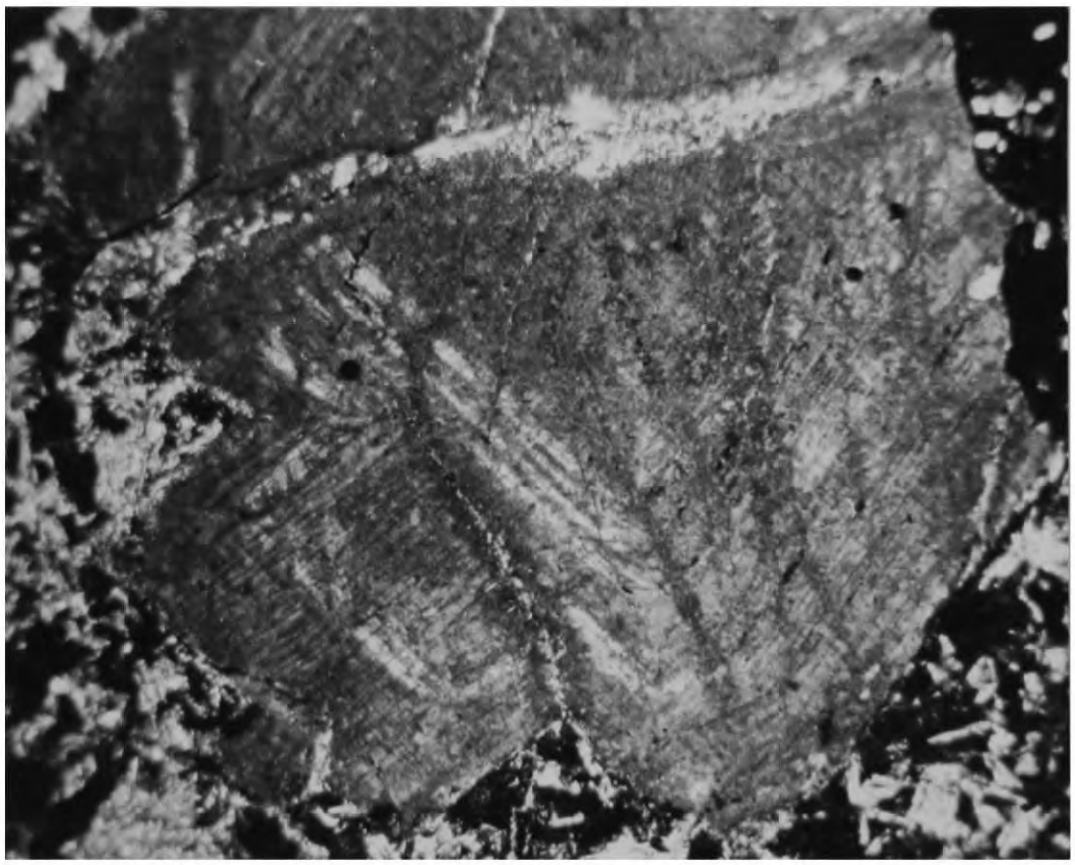

Fig. 9.12.

Fig. 9.11.

Plagioclase phenocryst in trachyte dyke.
Specimen 43039, crossed nicols x 125.

Fig. 9.12.

Zoned nepheline phenocrysts in nepheline microsyenite, specimen 43045, plane polarised light, x 50.

Fig. 9.13.

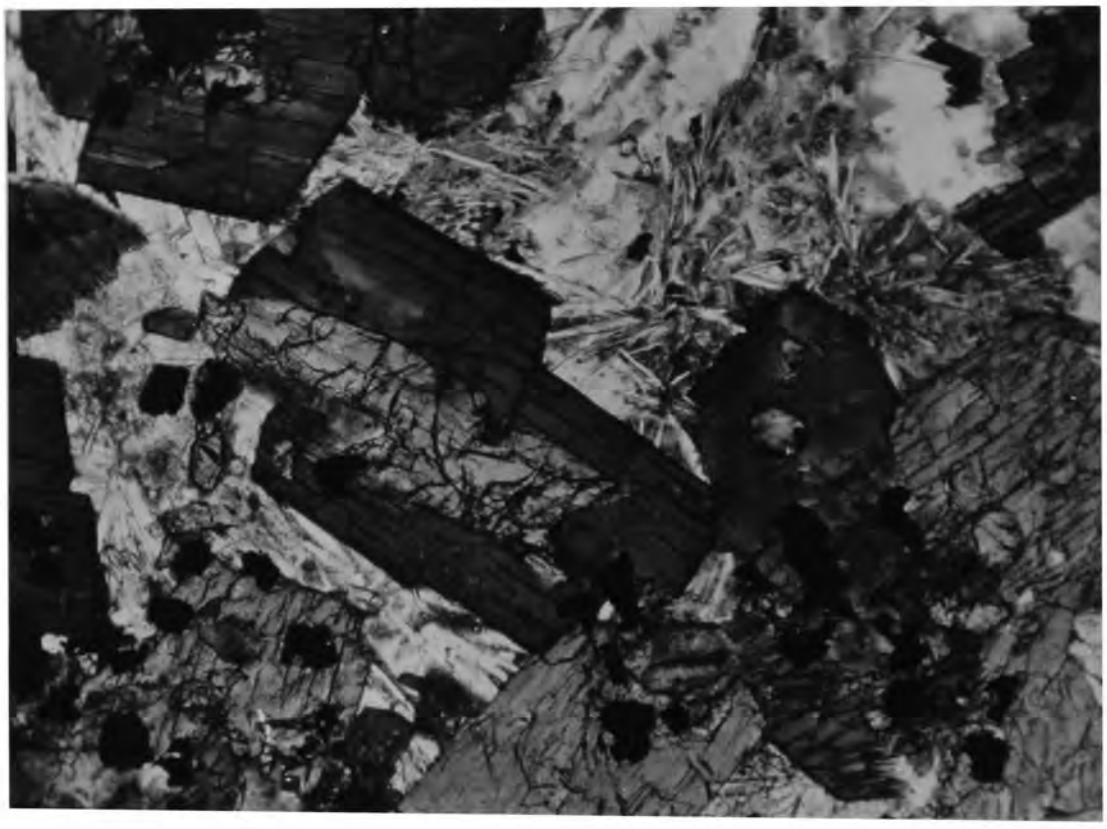

Fig. 9.14.

Fig. 9.13.

Photomicrograph to show the development of opaque needles at right angles to the phenocryst on a porphyritic trachyandesite dyke, specimen 23409. Plane polarised light x 70.

Fig. 9.14.

General texture of a camptonite sill(specimen 23804). The photograph shows an unusually large pyroxene core mantled by a barkevikitic amphibole. Plaen polarised light. x 120.

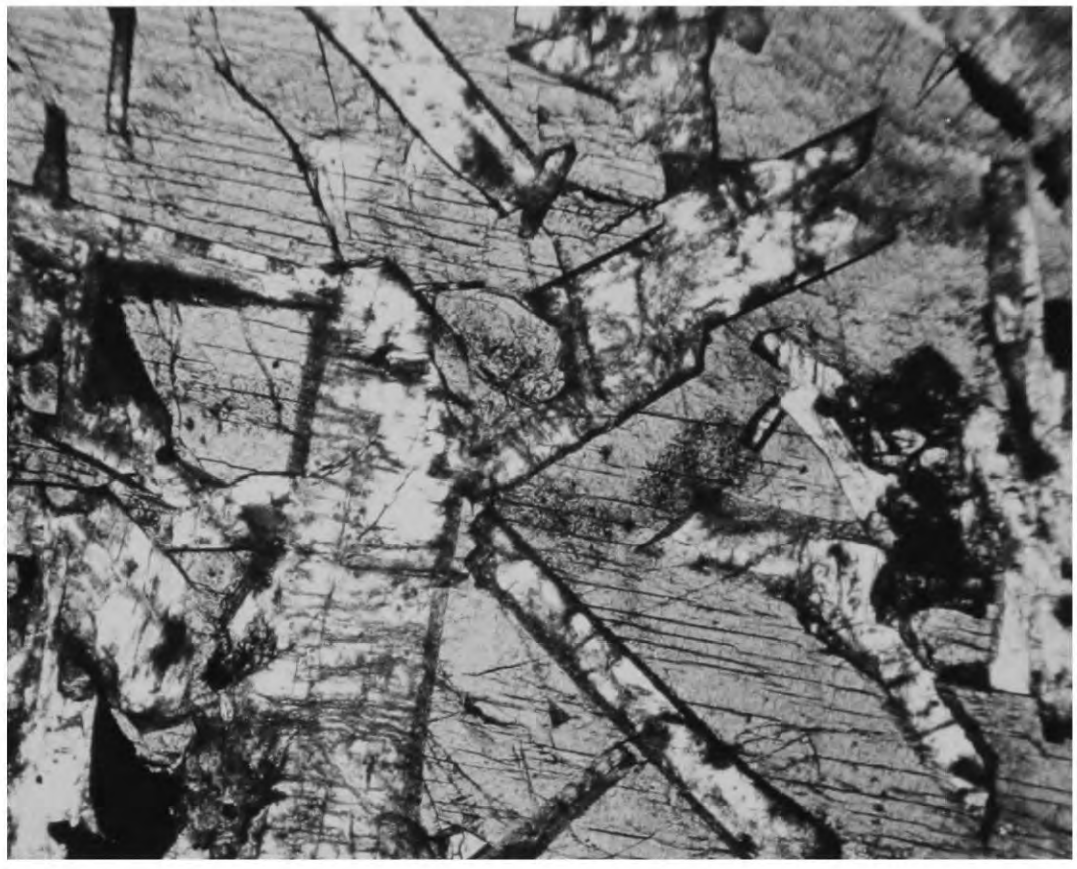

Fig. 9.15.

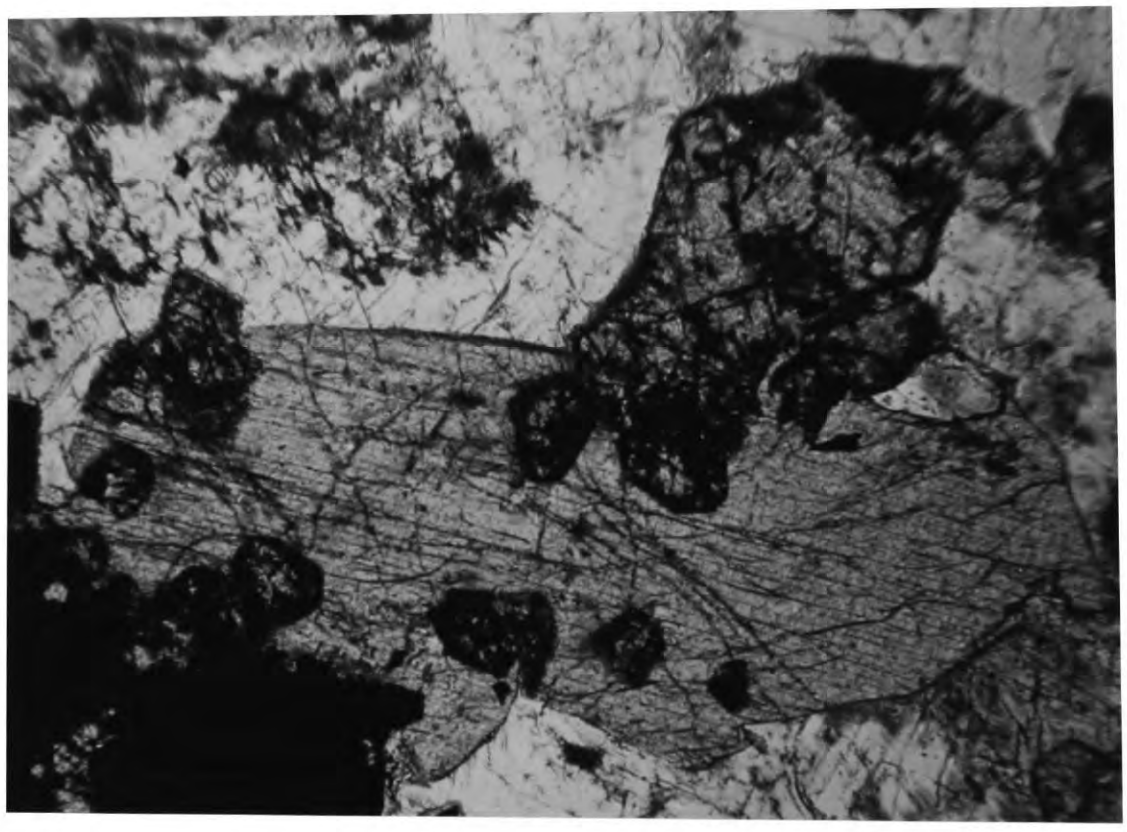

Fig. 9.16.

Fig. 9.15.

Typical ophitic texture developed within the olivine dolerite dykes. Specimen 23333, plane polarised light x 40.

Fig. 9.16.

Photomicrograph to show the inclusions of olivine (showing abundant exsolved magnetite) within the later pyroxene. Plane polarised light x 40.

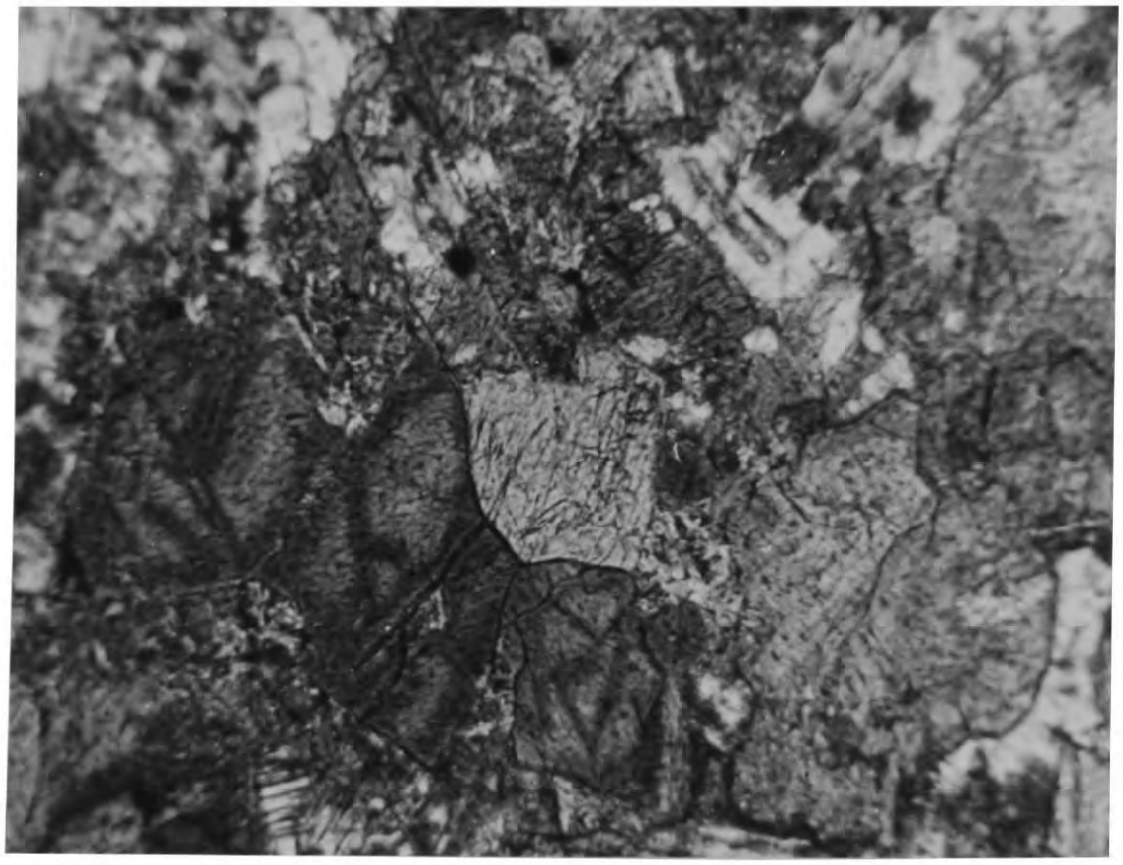

Fig. 9.17.

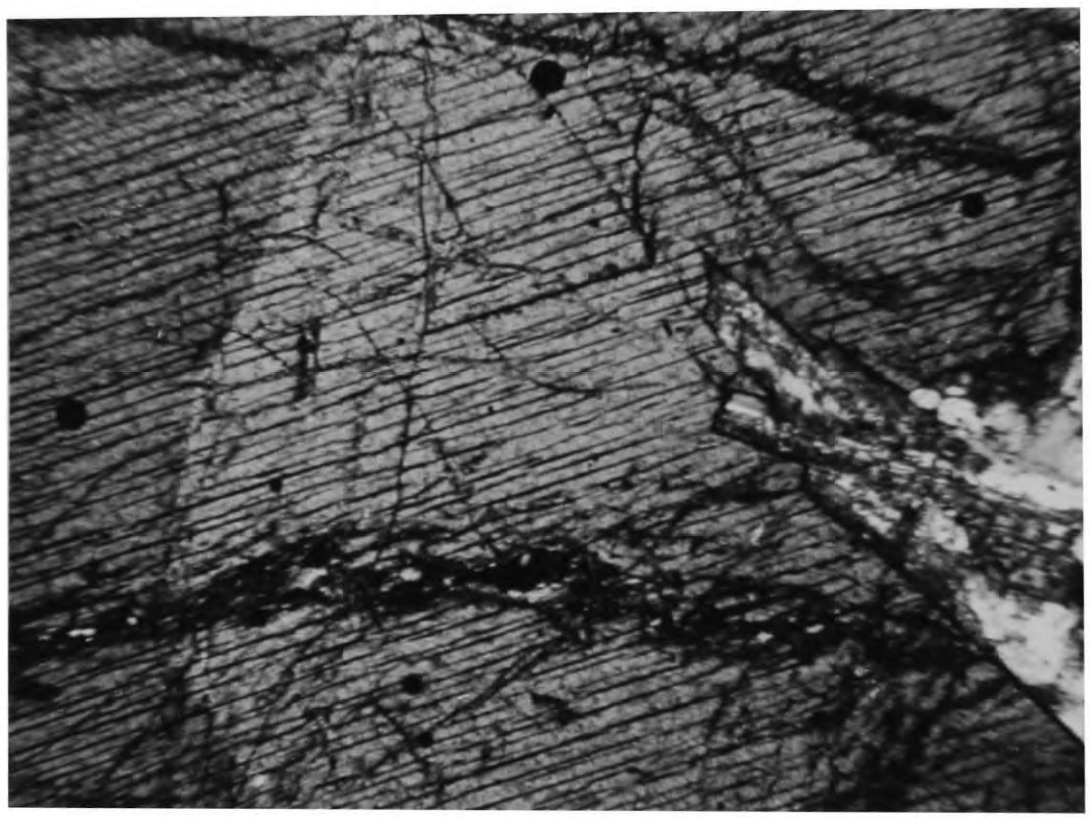

Fig. 9.18.

Fig. 9.17.

Alteration products of olivine in a dolerite dyke, specimen 23310. Plane polarised light x 50.

Fig. 9.18.

Large plate of pyroxene showing a sharp junction between two zones. Specimen 23893, dolerite dyke, crossed nicols x 40.

Fig. 9.19.

Grain of ilmenite showing a type of skeleton growth. Olivine dolerite, plane polarised light x 35.

Fig. 9.19.

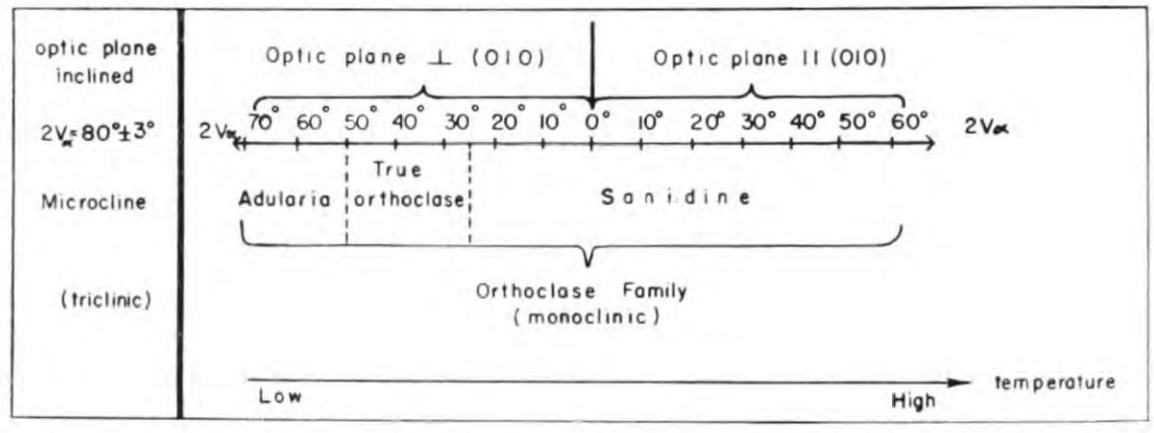

Fig. 10.1.

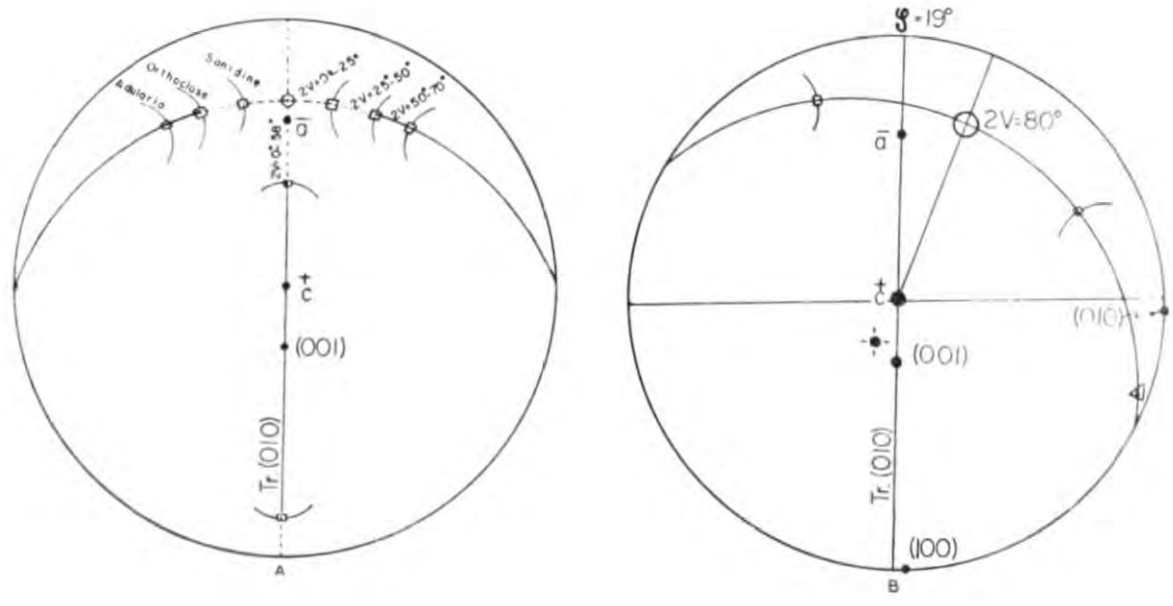

Fig. 10.2.

Fig. 10.1.

Polymorphic forms of potash, showing optical classification. (after Spencer 1937 and Chaisson 1950.)

Fig. 10.2.

Stereograms illustrating the optical orientations of the orthoclase family (A) and microcline (B). Also shown is the orientation of high sanidine. In monoclinic crystals, $\propto$ axis emerges on the (010) cleavage trace and in triclinic microcline (maximum microcline) this axis is 19^{o} away from the cleavage trace. Thus a series of stereograms between sanidine and max. microcline would show the progressive shift of this axis (after Chaisson 1950).

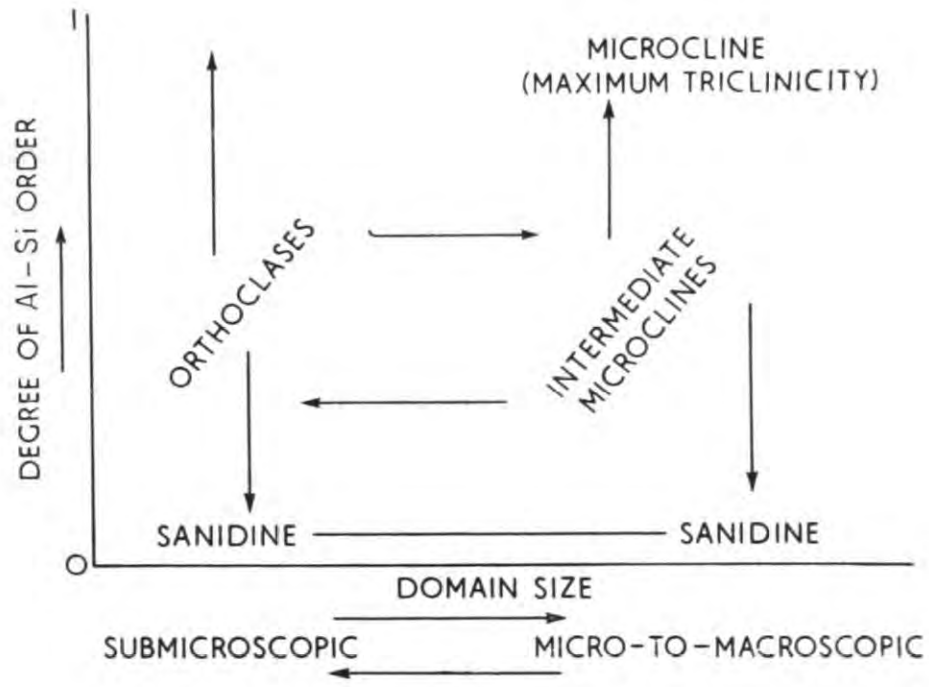

Fig. 10.3.

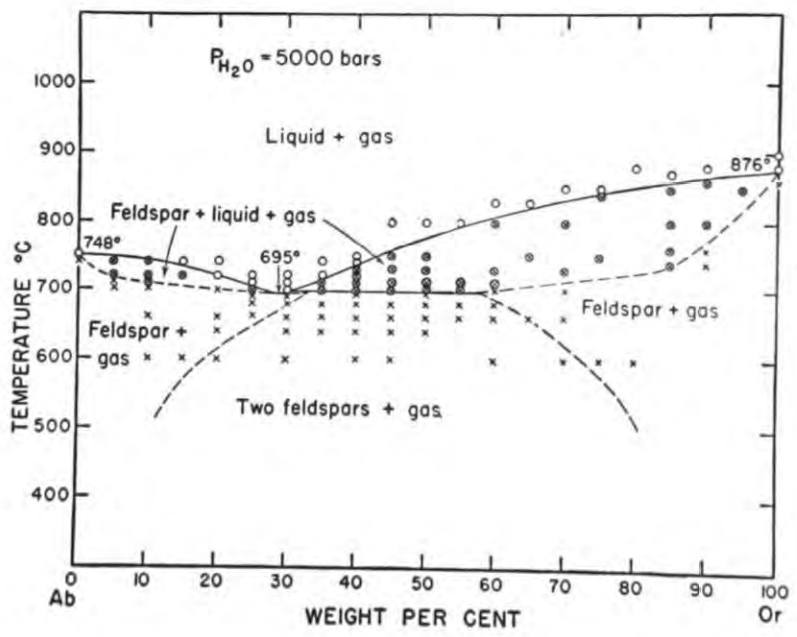

Fig. 10.5.

Fig. 10.3.

Diagram to show the intermediate stages between sanidine(disordered) and microcline(odered), (after Goldsmith and Laves 1954a).

Fig. 10.5.

Diagram to show the intersection of the feldspar solidus with the solvus(after Yoder et.al 1957). This shows that at 5,000 bars it is possible to have two alkali feldspars crystallisaing similtaneously.

Fig. 10.4.

Compendium of phase diagrams, (after Laves 1952)

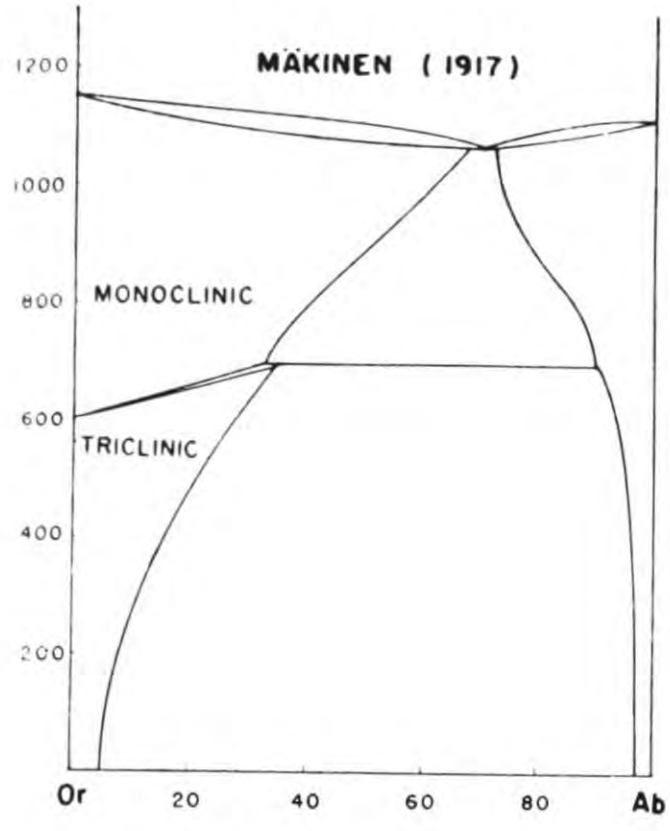
MÄKINEN (1917)
1200
1000
800
600
400
200
MONOCLINIC
TRICLINIC
Or
20
40
60
80
Ab

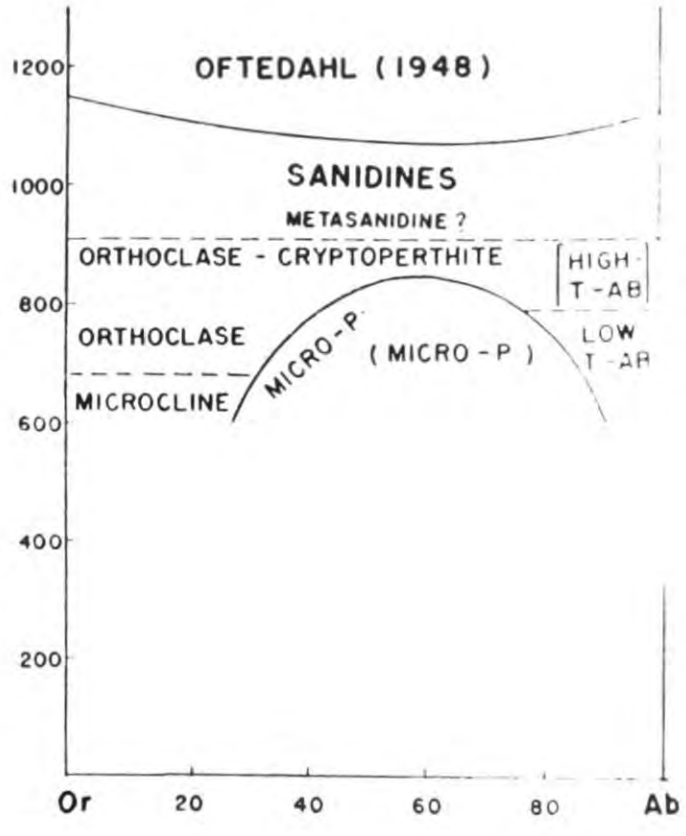
OFTEDAHL (1948)
1200
1000
800
600
400
200
SANIDINES
METASANIDINE ?
ORTHOCLASE - CRYPTOPERTHITE
HIGH T-AB
ORTHOCLASE
MICRO-P
(MICRO-P)
LOW T-AB
MICROCLINE
Or
20
40
60
80
Ab

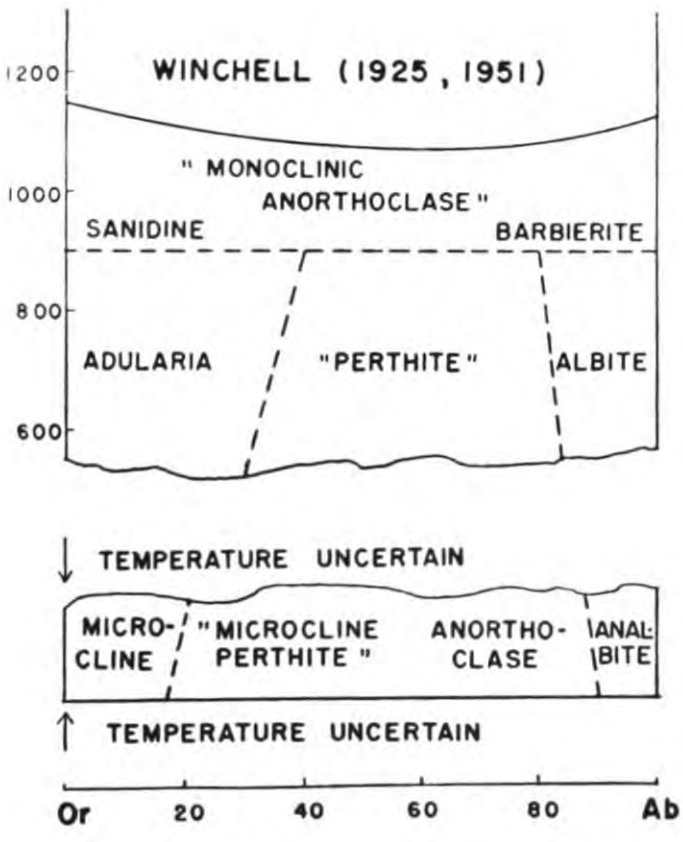
WINCHELL (1925, 1951)
1200
1000
800
600
" MONOCLINIC ANORTHOCLASE "
SANIDINE
BARBIERITE
ADULARIA
"PERTHITE"
ALBITE
TEMPERATURE UNCERTAIN
MICRO-CLINE
"MICROCLINE PERTHITE"
ANORTHO-CLASE
ANAL-BITE
TEMPERATURE UNCERTAIN
Or
20
40
60
80
Ab

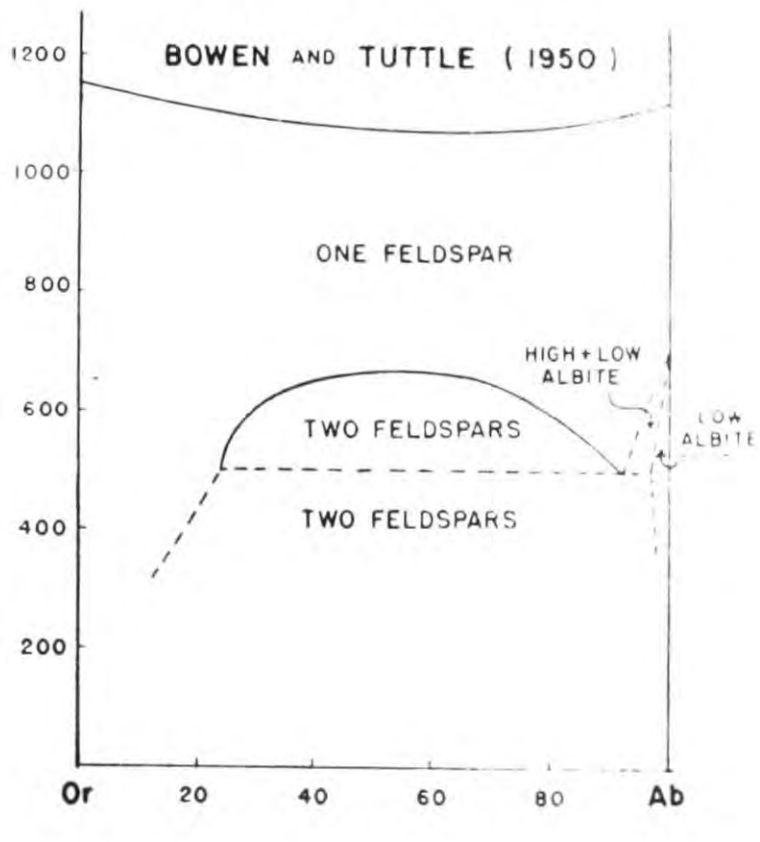
BOWEN AND TUTTLE (1950)
1200
1000
800
600
400
200
ONE FELDSPAR
HIGH + LOW ALBITE
TWO FELDSPARS
LOW ALBITE
TWO FELDSPARS
Or
20
40
60
80
Ab

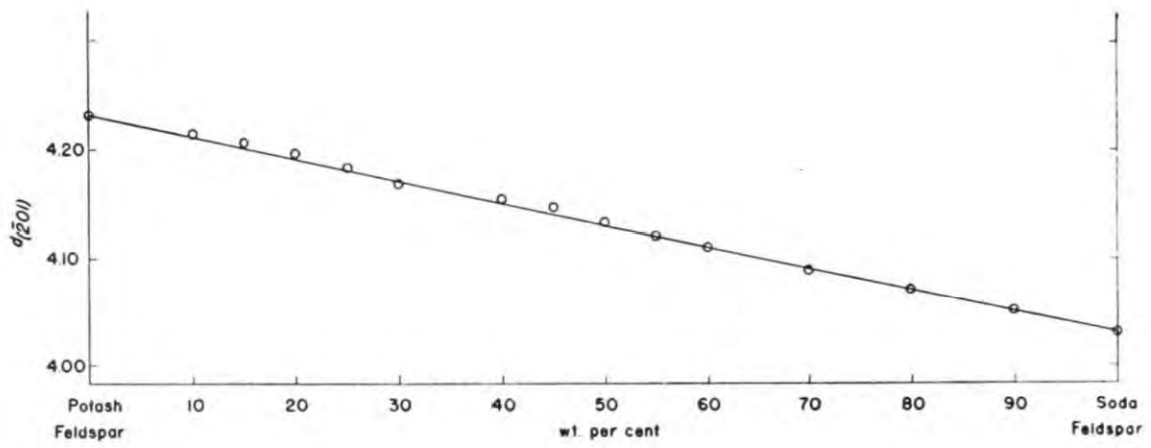

Fig. 10.6.

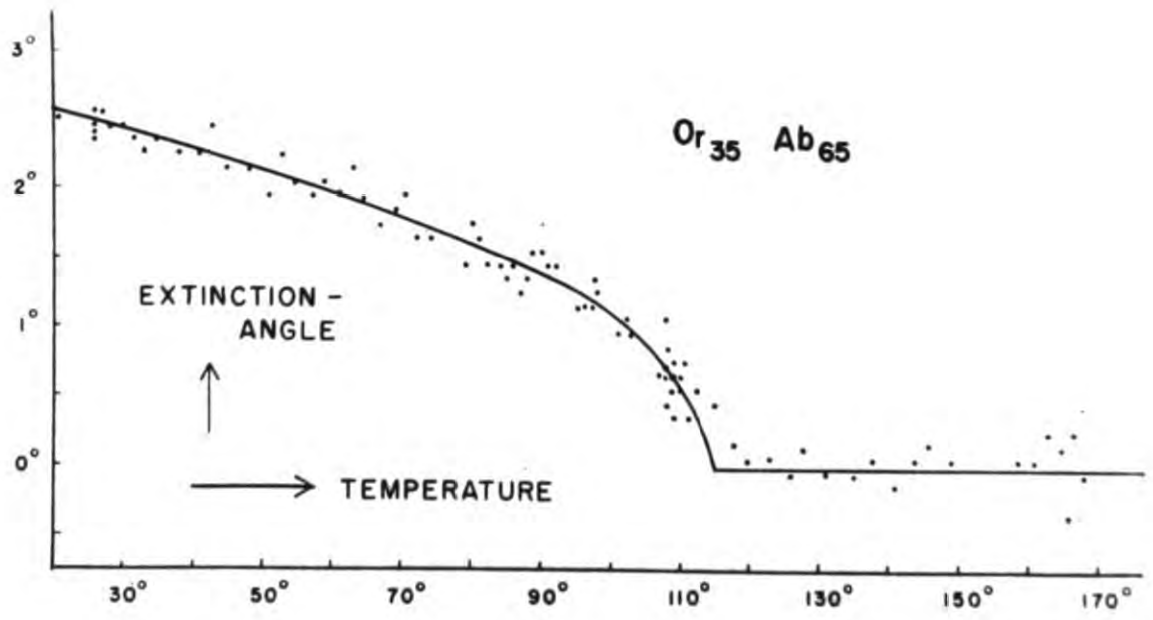

Fig. 10.7.

Fig. 10.6.

Spacing of the ($\bar{2}01$) planes in a series of alkali feldspars from Or_{100} to Or_{0}. (after Bowen and Tuttle 1950). These feldspars are all high temperature types.

Fig 10.7.

Diagram to show the location of the symmetry change between mococlinic sanidine, with straight extinction and triclinic albite (oblique extinction). The figure shows that the change is largely a function of temperature. (after Laves 1952).

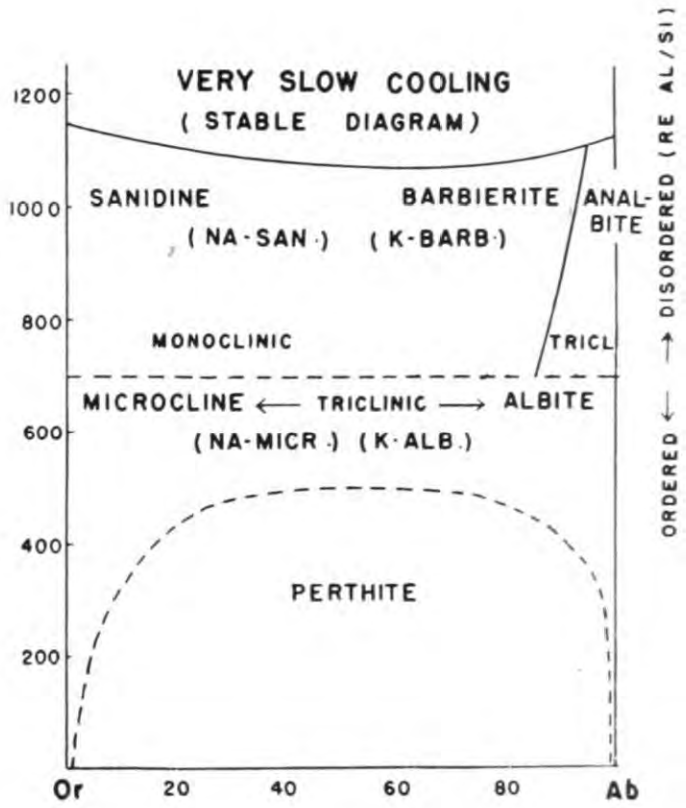

Fig. 10.8.

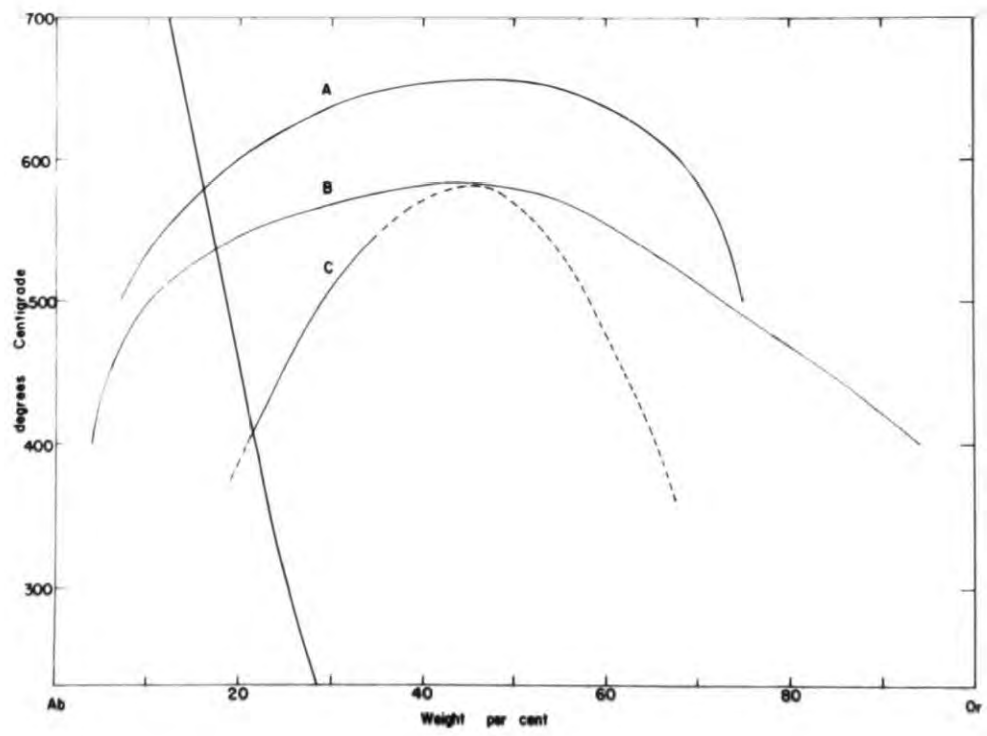

Fig. 10.9.

Fig. 10.8.

Phase diagram by Laves(1952,) for the Or - Ab system at normal pressure. Note the position of analbite and the deflection of the Barbierite - Analbite line so that all albites are suggested to be triclinic.

Fig. 10.9.

Curves representing determinations of the alkali feldspar solvus.

A: After Bowen and Tuttle(1950)

B: After Bowen and Tuttle(unpublished data)

C: After Smith and MacKenzie(1958), the dotted line being inferred.

The figure is after Smith and MacKenzie(1958).

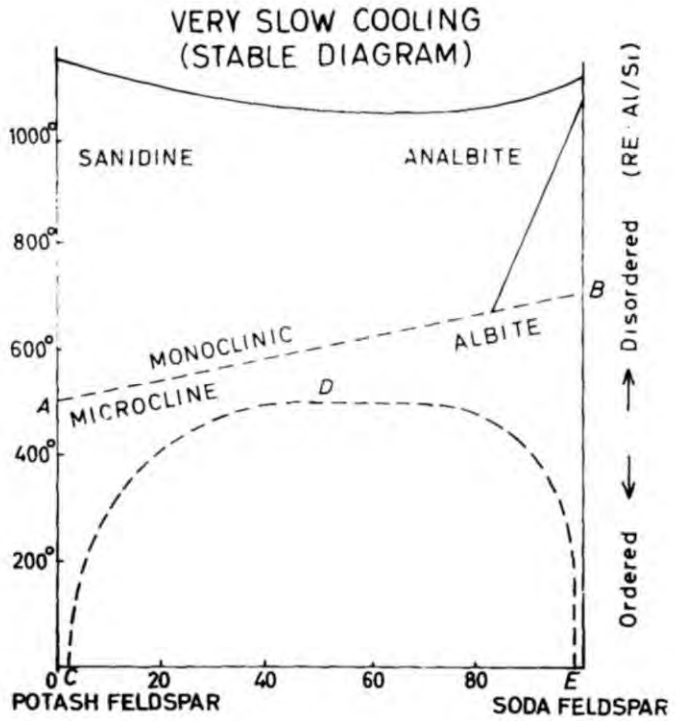

Fig. 10.10.

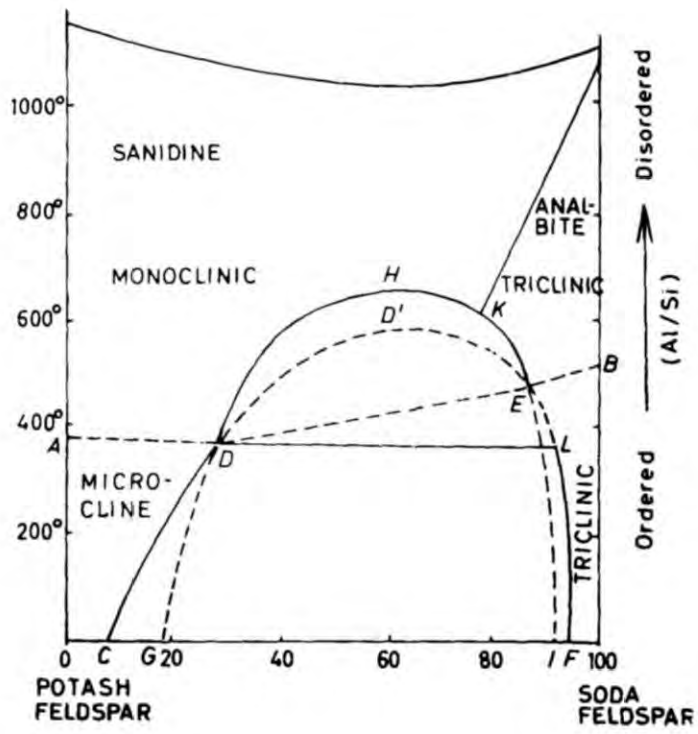

Fig. 10.11.

Fig. 10.10.

The phase diagram of Laves(1952) reproduced by Rao(1959). Note the position of analbite(c.f. Fig. 10.8.)

Fig. 10.11.

The phase diagram for the alkali feldspars proposed by Rao(1959). Note the position of analbite. The curve ADEB is the order-disorder boundary, CDEF the solvus for microcline and albite. DHKE the solvus for disordered feldspars.

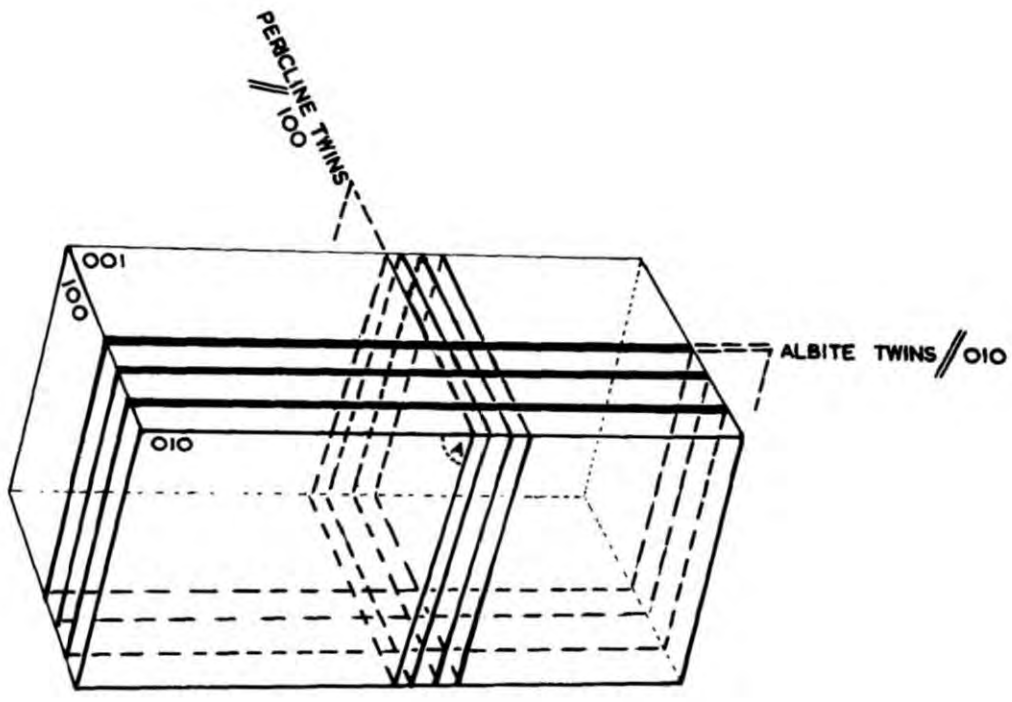

Fig. 10.12.

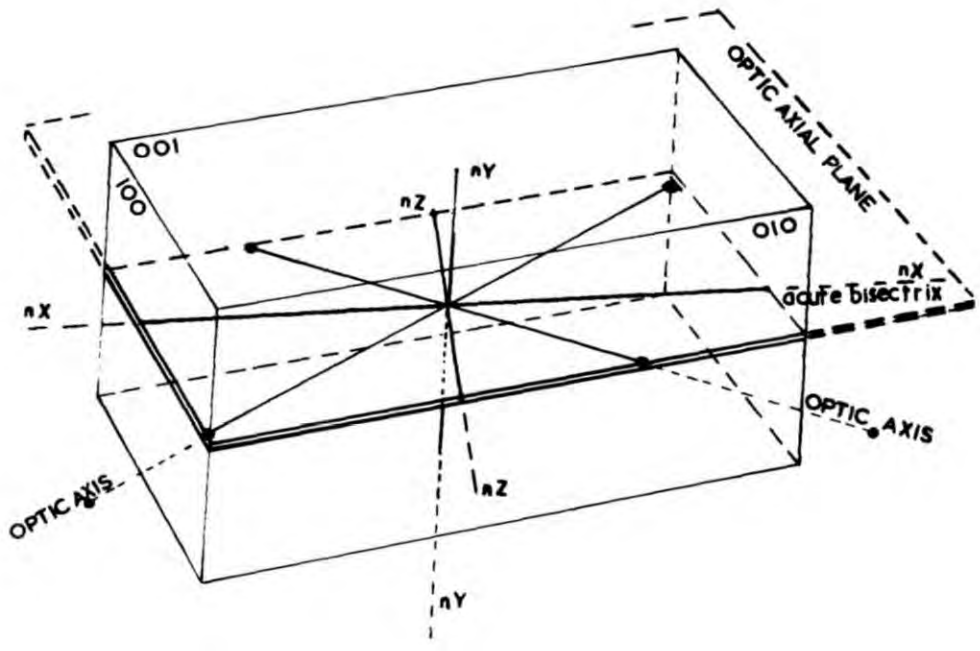

Fig. 10.13.

Fig. 10.12.

Block diagram to demonstrate the relationship of Pericline and Albite twin lamellae.

Fig. 10.13.

Block diagram to show the optical orientations of microcline.

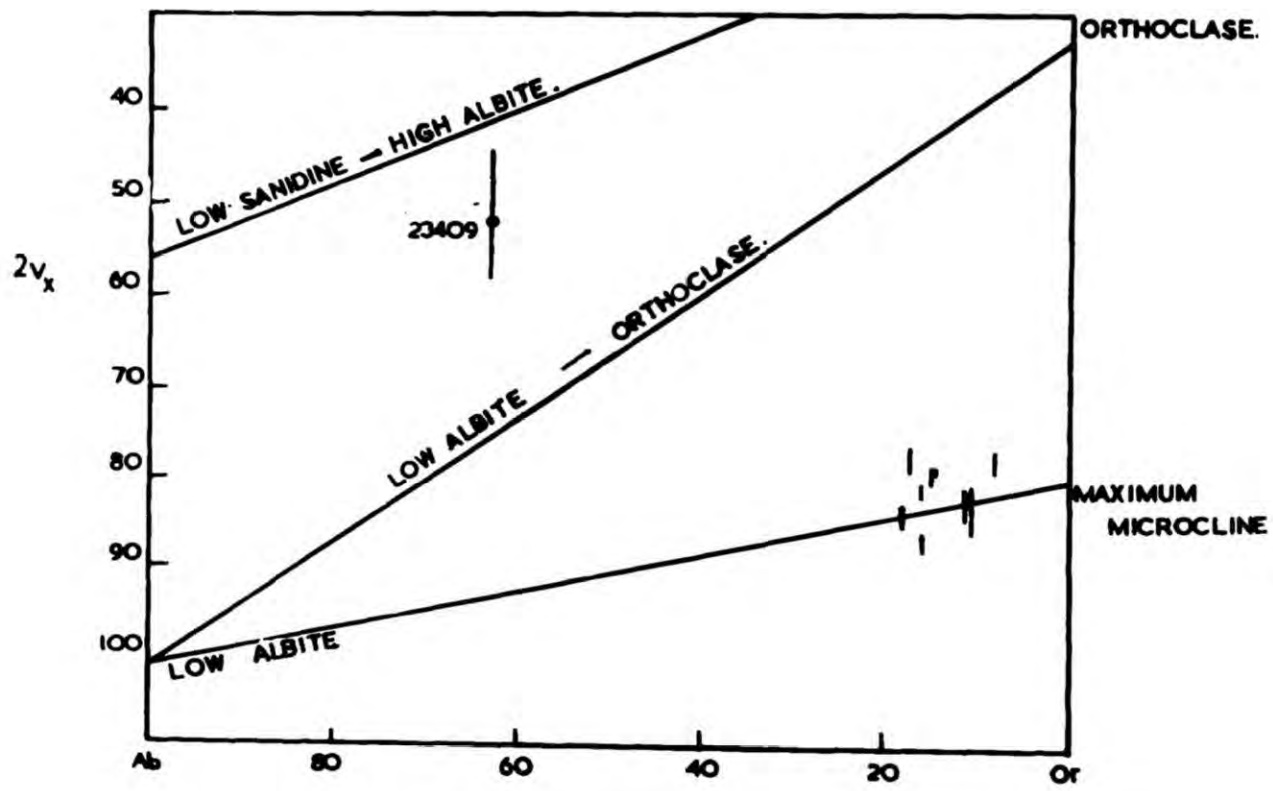

Fig. 10.14.

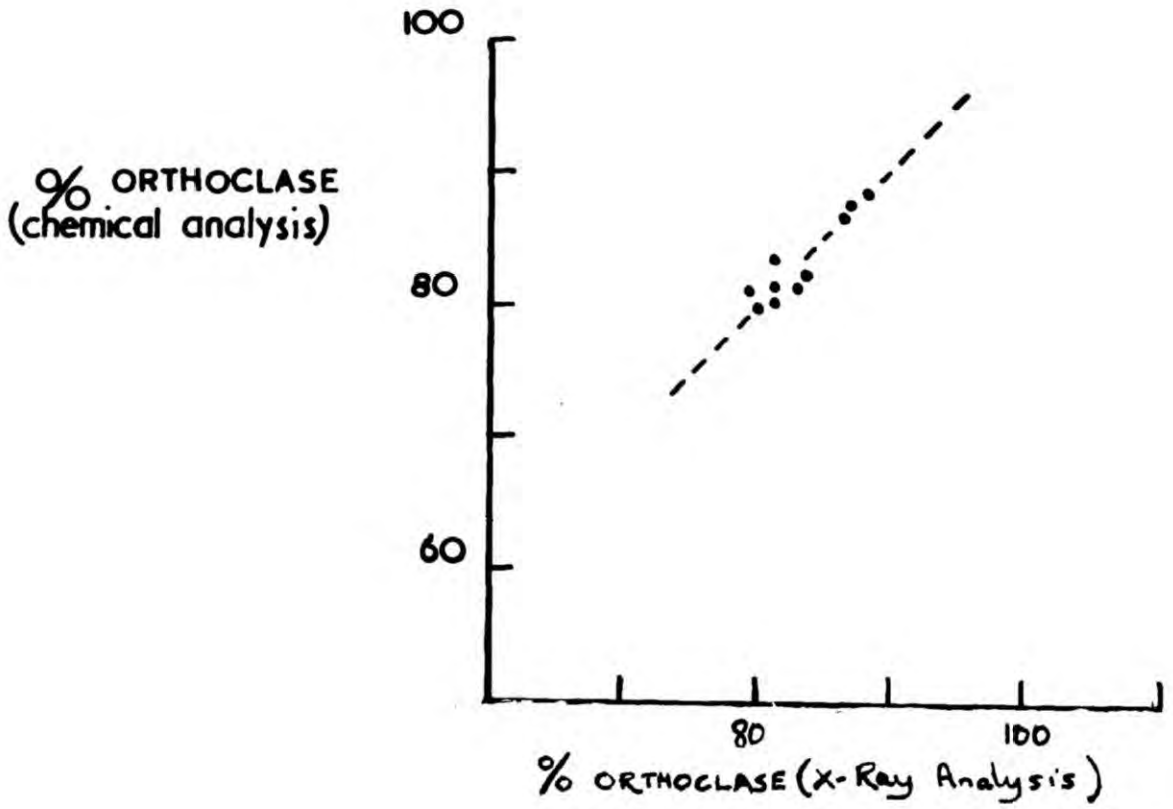

Fig. 10.16.

Fig. 10.14.

Optic axial angle $2V_x$, plotted against the chemical composition of the microclines used in the present study. The composition of 23409 was obtained using X -ray methods.(The diagram is after Emeleus and Smith, 1960, modified after Tuttle 1950).

Fig. 10.16.

Results of chemical analysis of ten microclines (recalculated to % Or.) against % Or. determined using X -ray techniques.

Fig. 10.15.

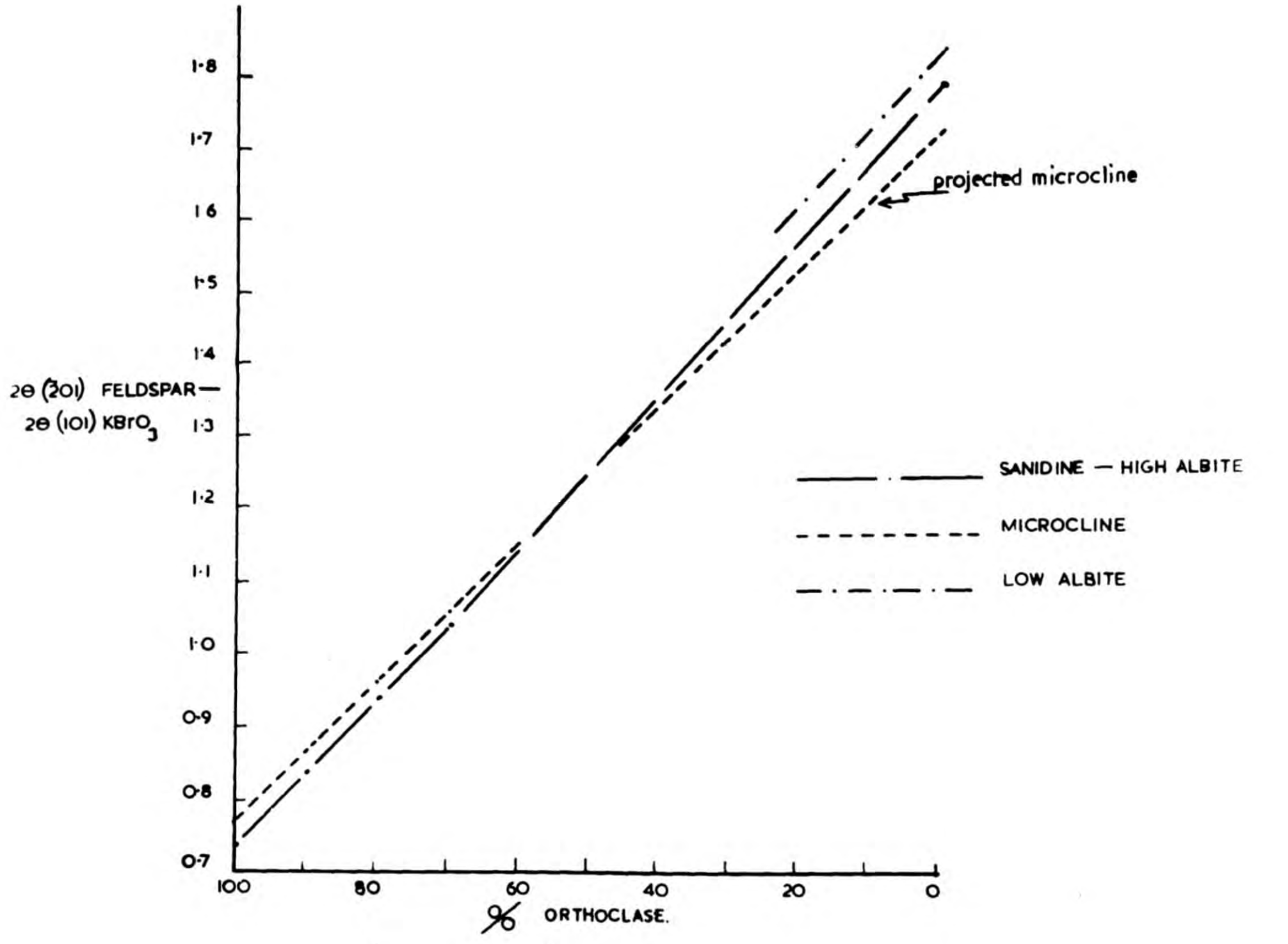
1·8
1·7
1 6
1·5
1·4
2θ (201) FELDSPAR
2θ (101) KBrO3
1·3
1·2
1·1
1·0
0·9
0·8
0·7
100
80
60
40
20
0
% ORTHOCLASE.
projected microcline
SANIDINE — HIGH ALBITE
MICROCLINE
LOW ALBITE

Fig. 10.15.

Determinative curves for the determination of % Or. using the difference between $2\theta(\bar{2}01)$ of the feldspar and the $2\theta(101)$ of $KBrO_3$. High Sanidine - High Albite and Microcline are after Orville(1957 and 1960) ,Low Albite,after Smith(1956).

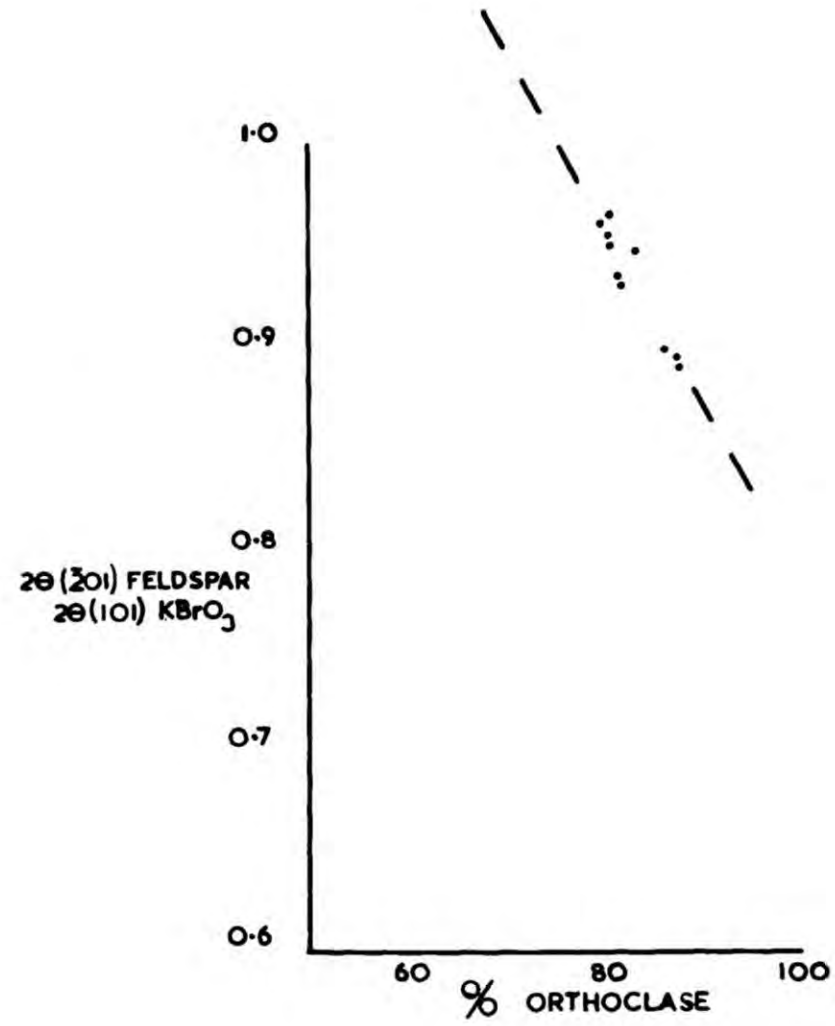
1·0
0·9
0·8
2θ(3̄01) FELDSPAR
2θ(101) KBrO3
0·7
0·6
60
80
100
% ORTHOCLASE

Fig. 10.17.

Fig. 10.17.

Determinative curve for the determination of the % Or. by the X-ray method, compiled by using the analyses of the ten Greenland microclines. This line agrees very closely with that suggested by Orville(1960).

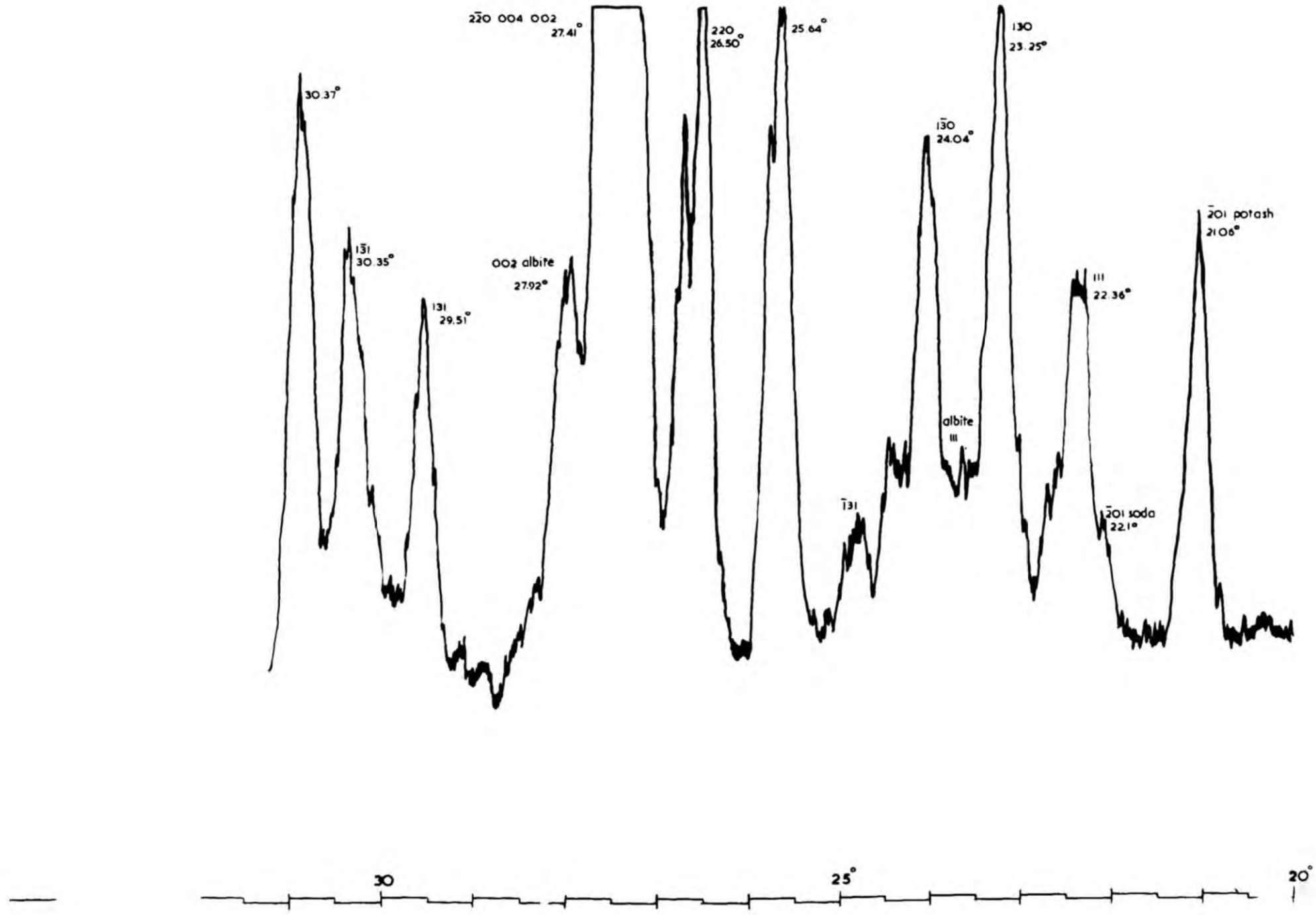
2$\bar{2}$0 004 002
27.41°
220
26.50°
25.64°
130
23.25°
30.37°
1$\bar{3}$0
24.04°
$\bar{2}$01 potash
21.06°
1$\bar{3}$1
30.35°
002 albite
27.92°
111
22.36°
131
29.51°
albite
111
$\bar{1}$31
$\bar{2}$01 soda
22.1°
30
25°
20°

Fig. 10.18.

Typical X -ray diffraction chart for microcline (42896) in the natural state.(Cu. radiation).

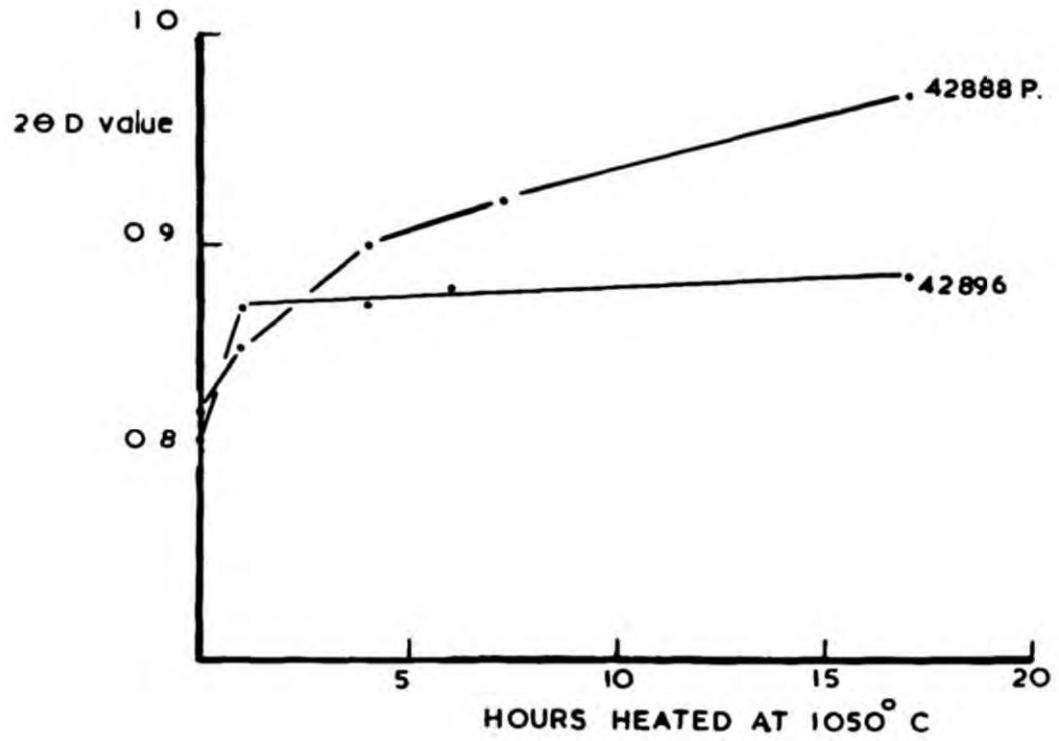

Fig. 10.19a.

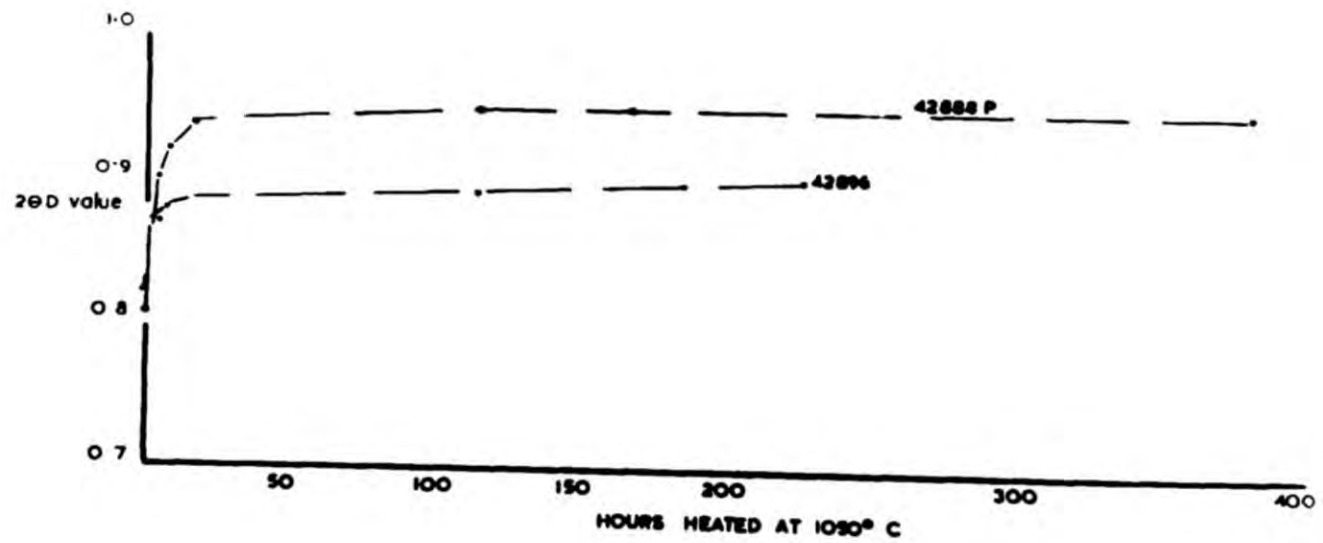

Fig. 10.19b.

Fig. 10.19a.

Homogenisation results for specimens 42888P and 42896 from 0 to 20 hrs. at 1050°C

Fig. 10.19b.

Homogenisation rates for specimens 42888P and 42896, from 0 to 400 hrs. at 1050° C.

The homogenisation is measured by the change in 2θ D value $\equiv 2\theta(\bar{2}01)$ feldspar - $2\theta(101)$ $KBrO_3$.

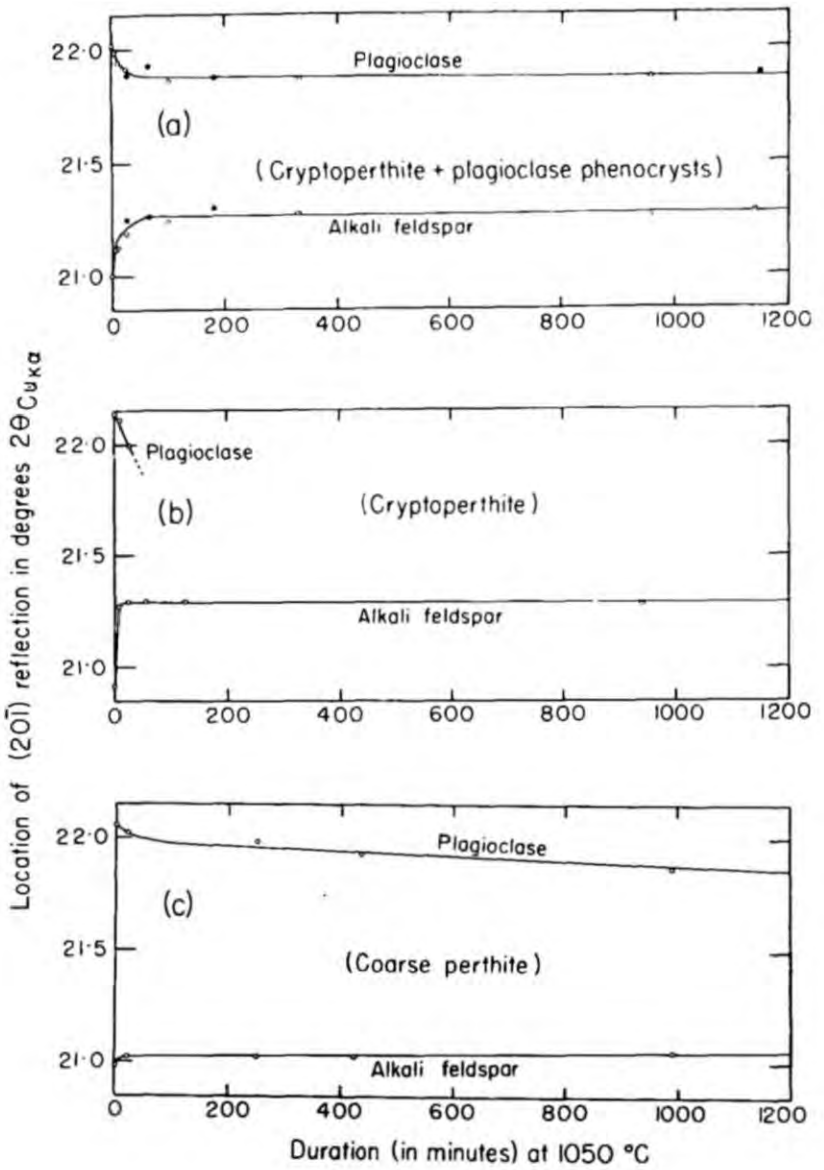

Fig. 10.20.

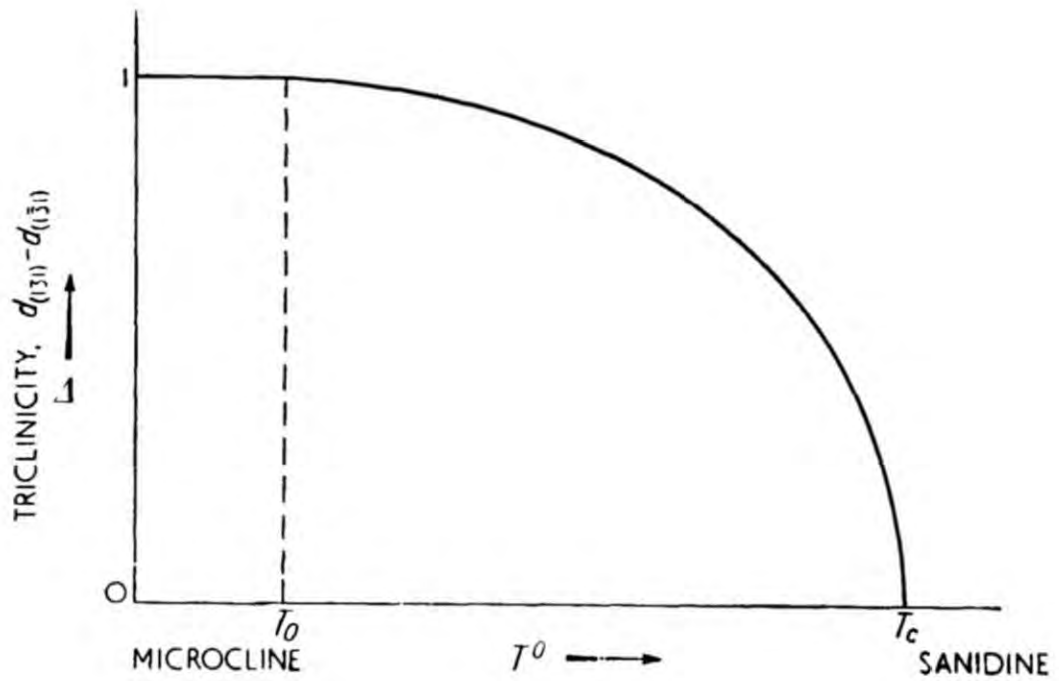

Fig. 10.21.

Fig. 10.20.

Homogenisation rates obtained by Ernst (1960) for
(a): crptoperthite + plagioclase phenocrysts.
(b): cryptoperthite
(c): alkali feldspar + plagioclase = coarse perthite.

Note the rapid homogenisation obtained within a few heating at 1050°C.

Fig. 10.21.

Relation between rate of cooling and triclinicity after Goldsmith and Laves(1954a).

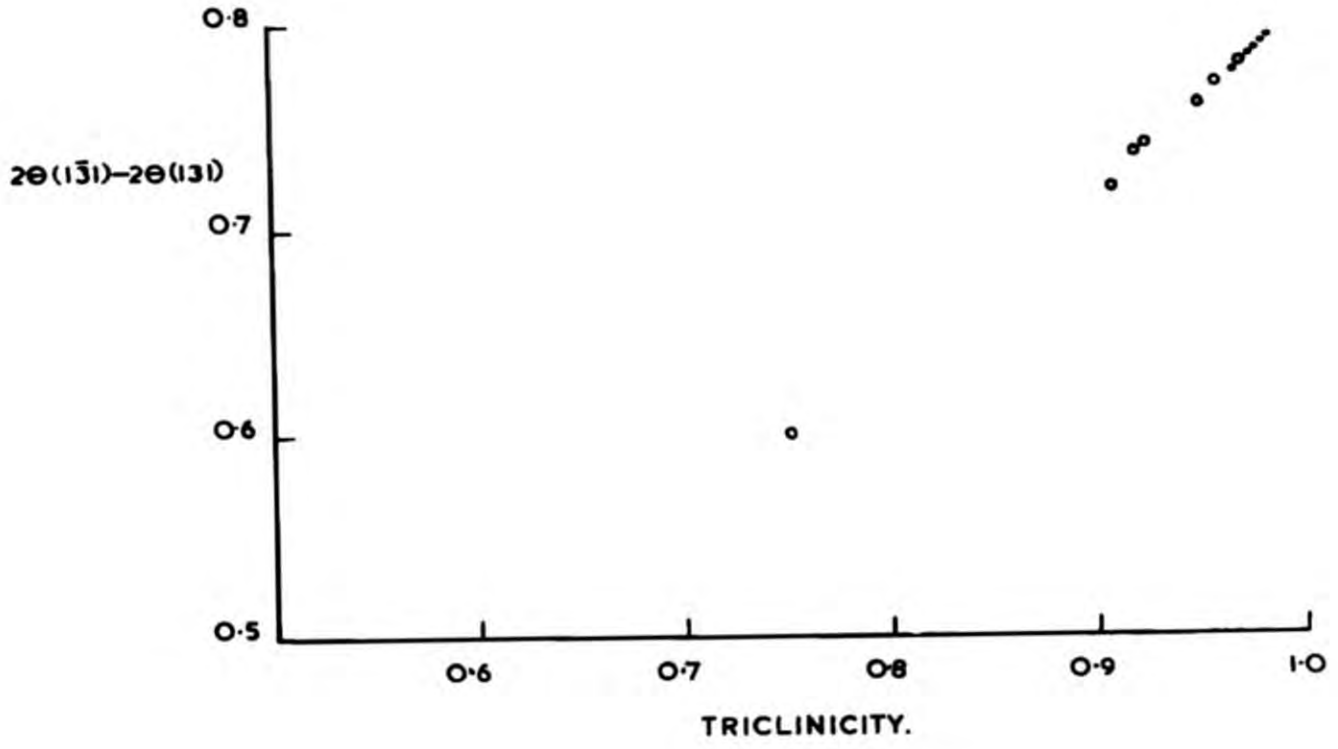

Fig. 10.22.

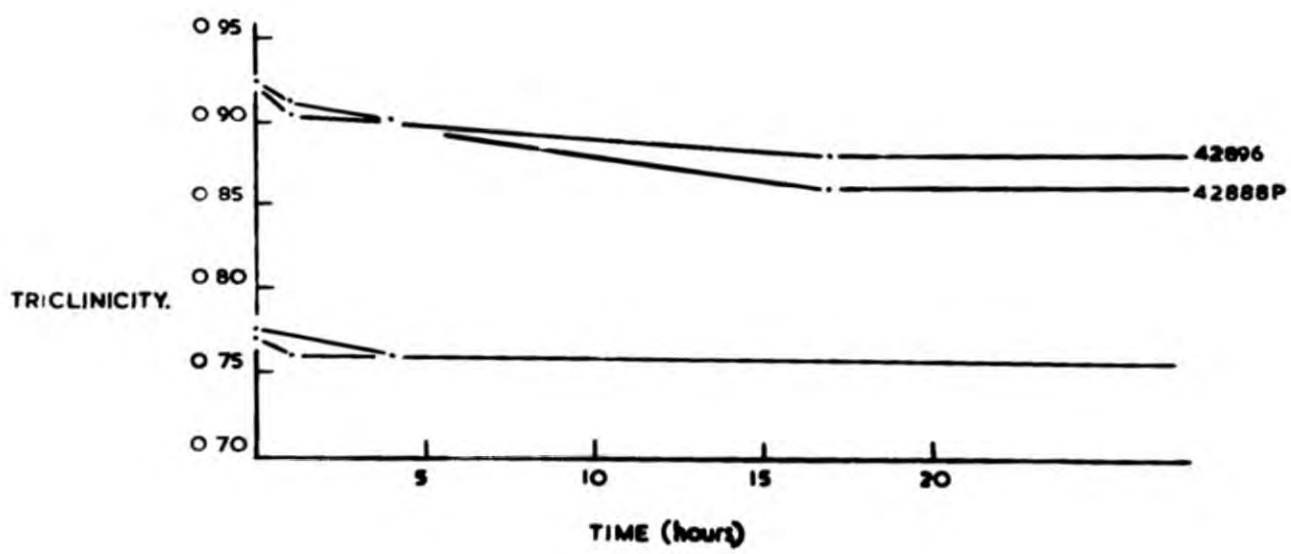

Fig. 10.23.

Fig. 10.22.

Linear plot of $2\theta(1\bar{3}1) - 2\theta(131)$ against triclinicity. This shows the broad difference between the Sanerutian Granites(dots) and the Ketilidian Granites and gneiss.

Fig. 10.23.

Changes in triclinicity and $2\theta(1\bar{3}0) - 2\theta(130)$ against time for specimens 42888P and 42896. The upper graphs are for triclinicity.(compiled from Table 10.16.)

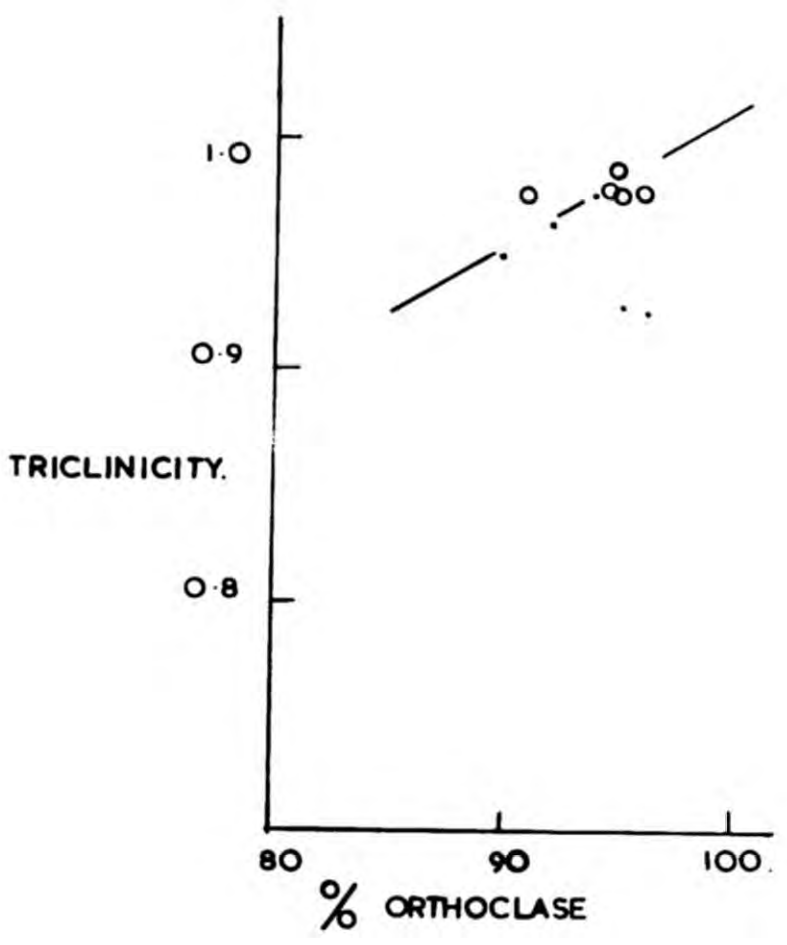

Fig. 10.24.a

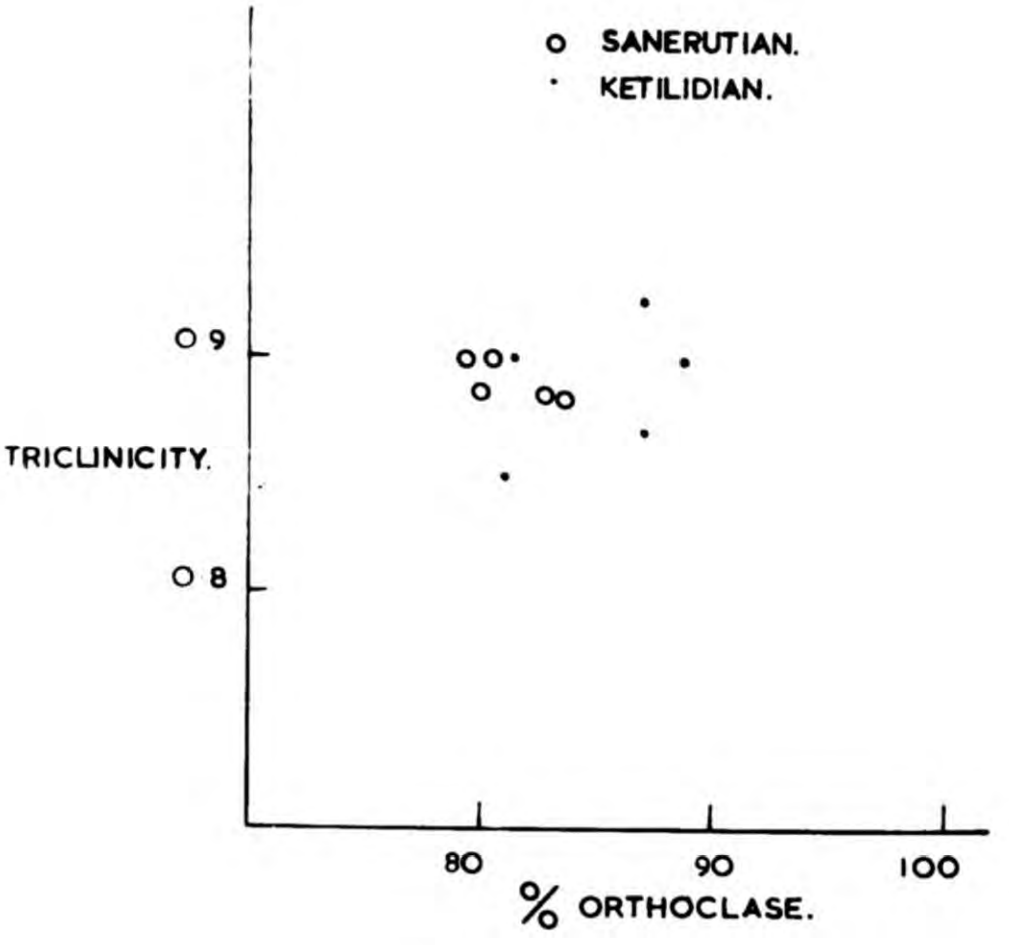

Fig. 10.24.b.

Fig. 10.24.

Graphs to show % Or. plotted against triclinicity before and after homogenisation. (a): before homogenisation.

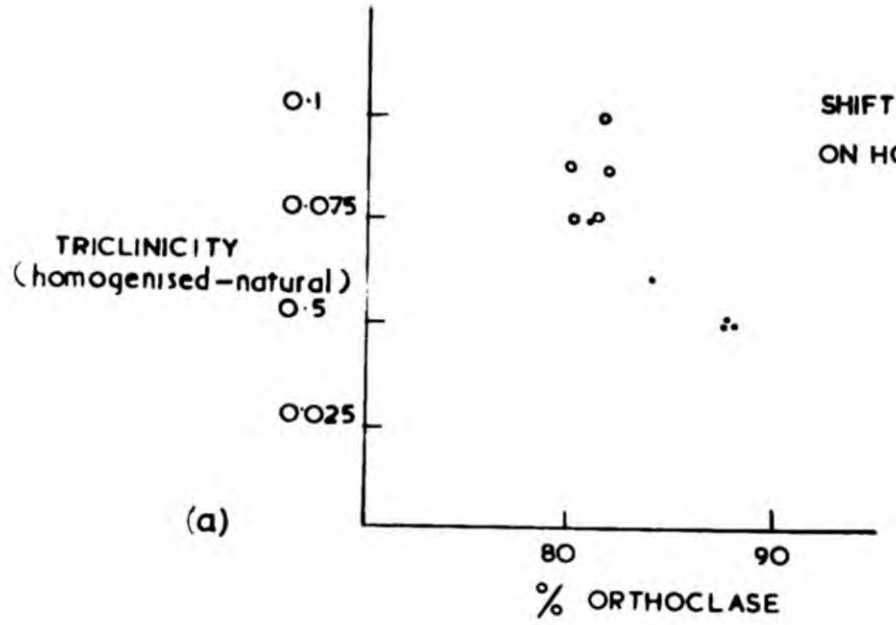
0·1
0·075
0·5
0·025
TRICLINICITY
(homogenised – natural)
(a)
80
90
% ORTHOCLASE

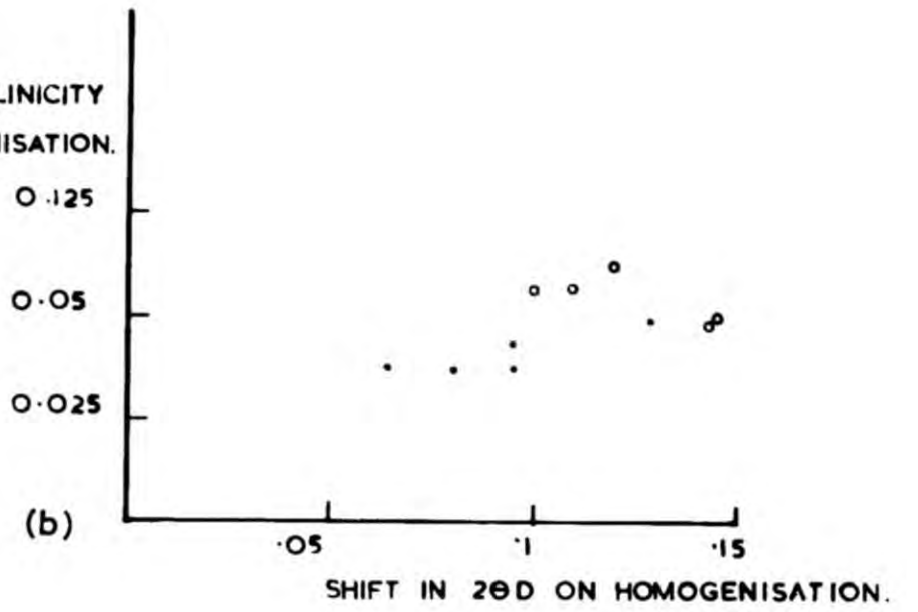
SHIFT IN TRICLINICITY
ON HOMOGENISATION.
0·125
0·05
0·025
(b)
·05
·1
·15
SHIFT IN 2θD ON HOMOGENISATION.

Fig. 10.25.

(a): Plot of the composition of ten microclines against the difference in triclinicity before and after homogenisation. This shows that as the % of Ab. increases so does the difference in triclinicity between the natural and homogenised specimen.

(b): Plot of the shift of triclinicity on homogenisation against the shidt in D 2θ on homogenisation. The diagram shows that the increase in shift of D 2θ(which indicates the incoming of the albite molecule), is matched by an increase in the shift in triclinicity. Thus, the greater the increase in albite taken into the feldspar the greater the decrease in triclinicity.

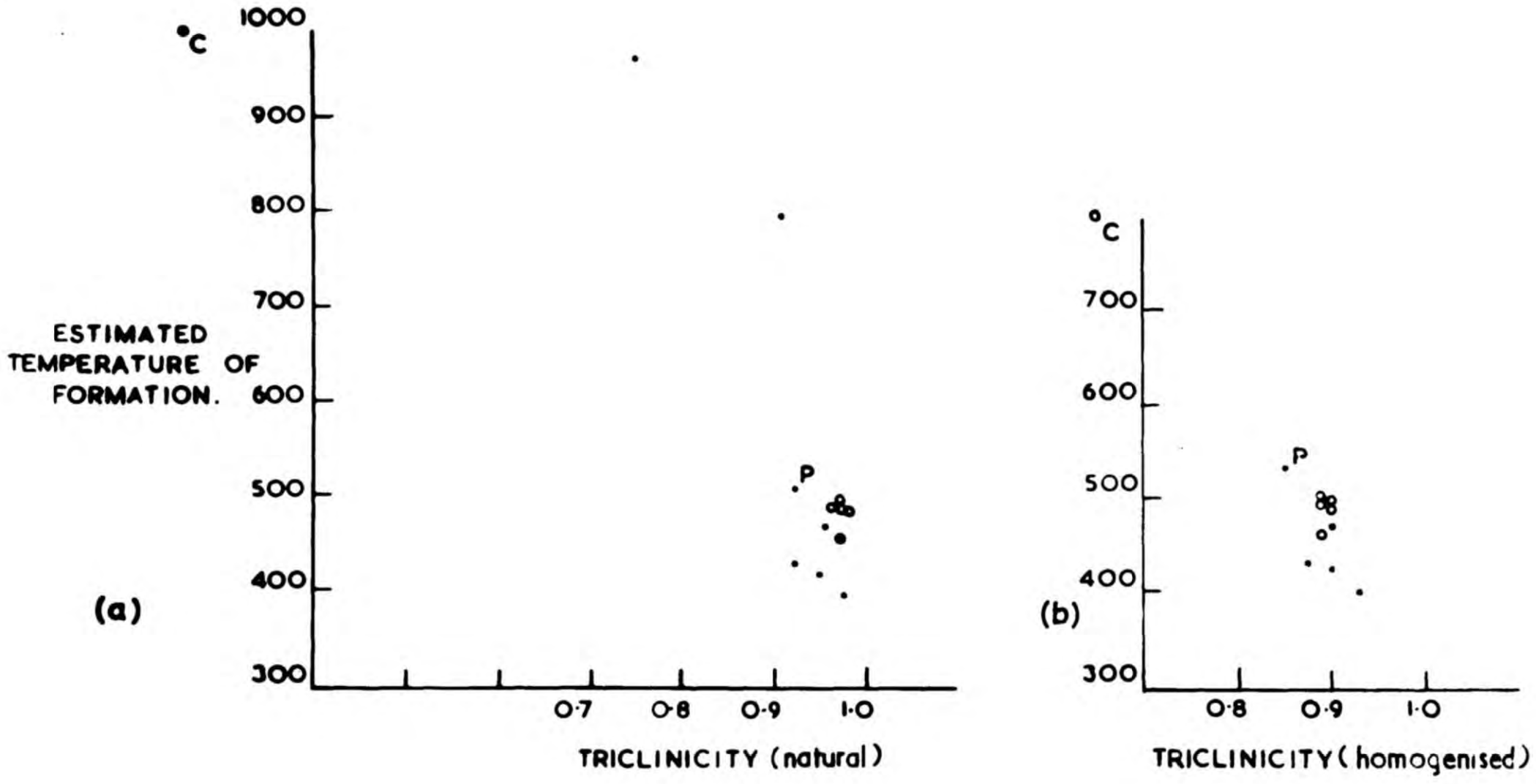
°C
1000
900
800
700
600
500
400
300
ESTIMATED TEMPERATURE OF FORMATION.
(a)
P
0·7
0·8
0·9
1·0
TRICLINICITY (natural)
°C
700
600
500
400
(b)
P
0·8
0·9
1·0
TRICLINICITY (homogenised)

Fig. 10.26.

Fig. 10.26.

(a): Estimated temperature of crystallisation against triclinicity in the natural specimens. Note the clustering together of the Sanerutian granite microclines.

(b): Estimated temperature of crystallisation against triclinicity of homogenised specimens. Note that the estimated crystallisation temp.-erature increases as the triclinicity decreases. P. represents the phenocryst from 42888

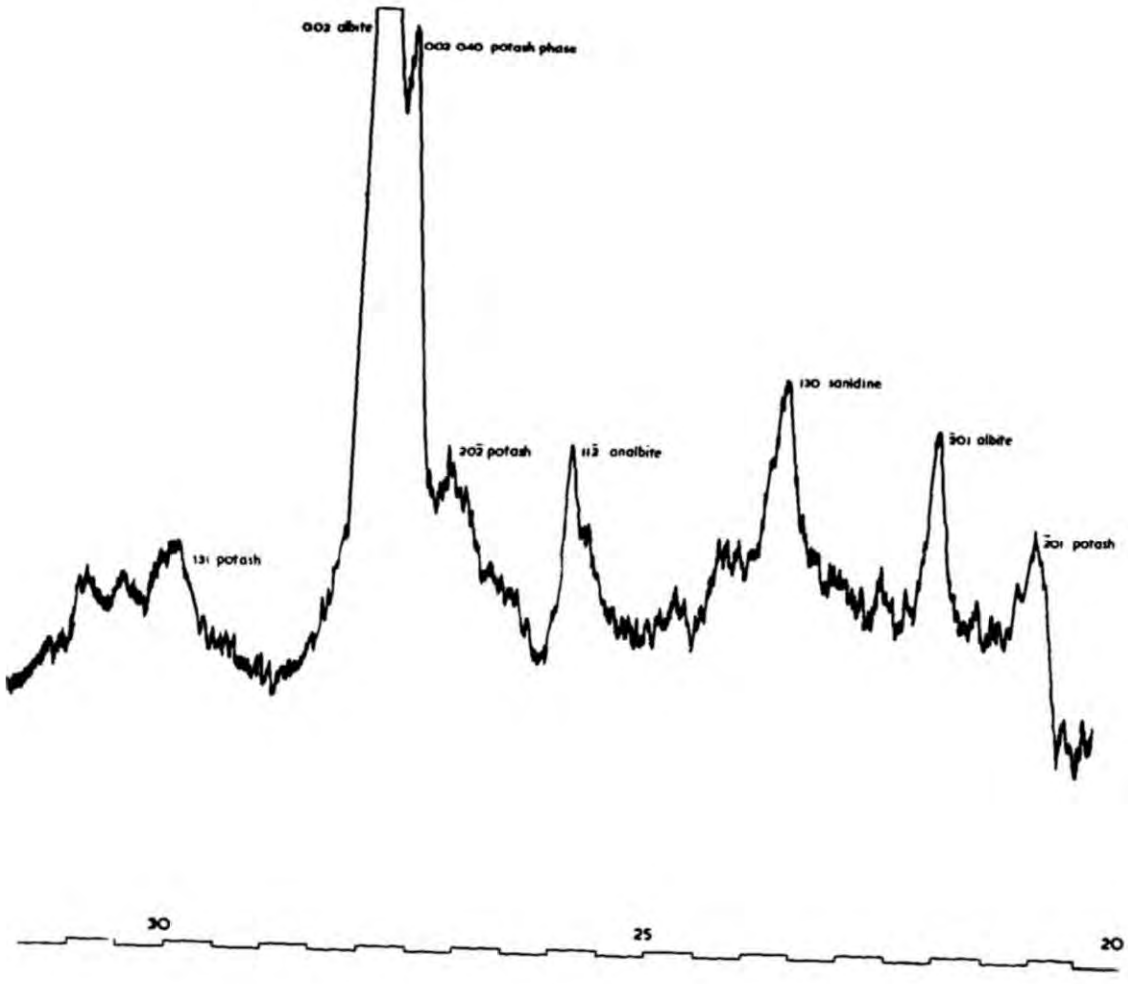
002 albite
002 040 potash phase
202 potash
11$\bar{2}$ analbite
130 sanidine
$\bar{3}$01 albite
131 potash
$\bar{2}$01 potash
30
25
20

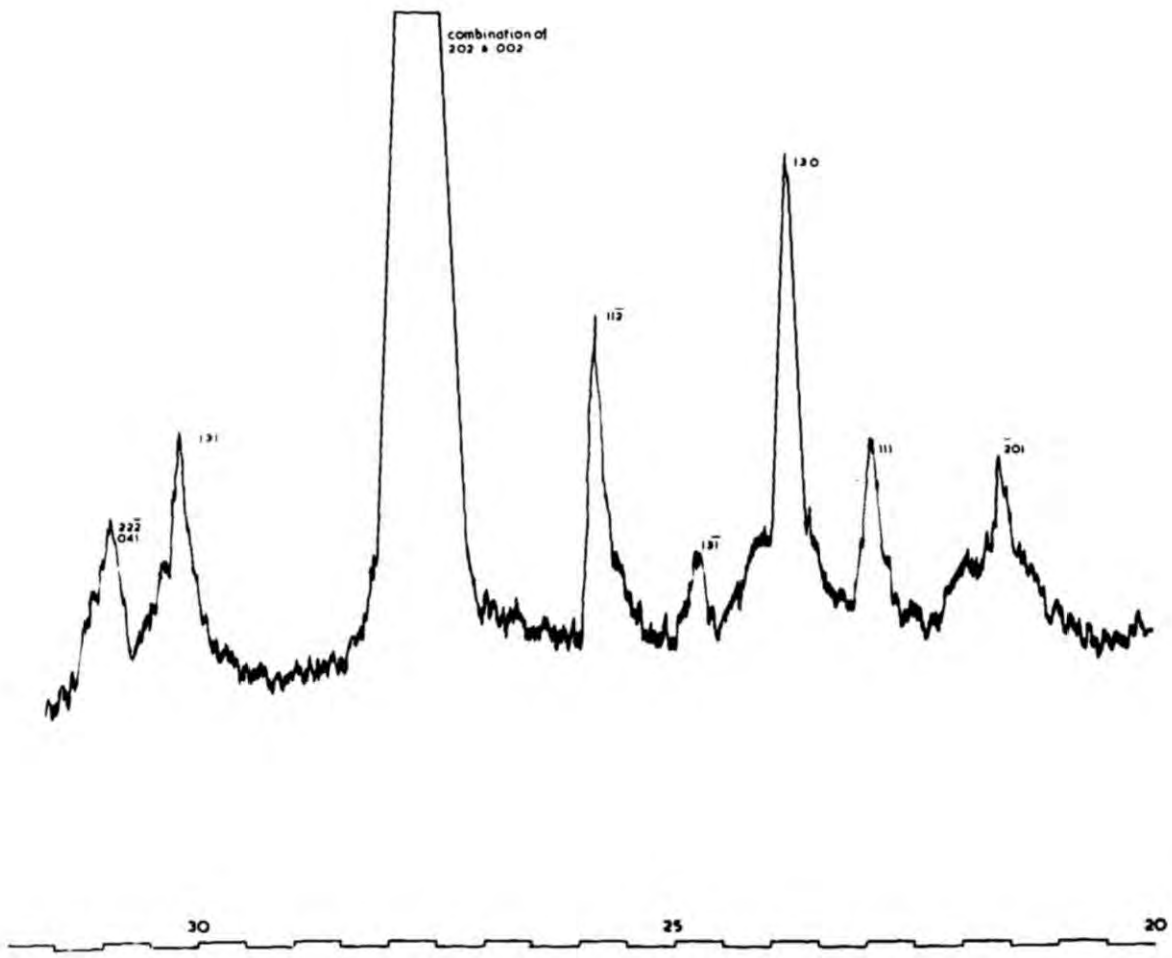
combination of
202 & 002
130
11$\bar{2}$
131
$22\bar{2}$
041
$13\bar{1}$
111
$\bar{2}$01
30
25
20

Fig. 10.27.

X -ray diffraction chart obtained on specimen 23409, (a phenocryst from an alkaline dyke). The upper diagram is the trace obtained on the natural specimen and the lower, the trace after homogenisation.

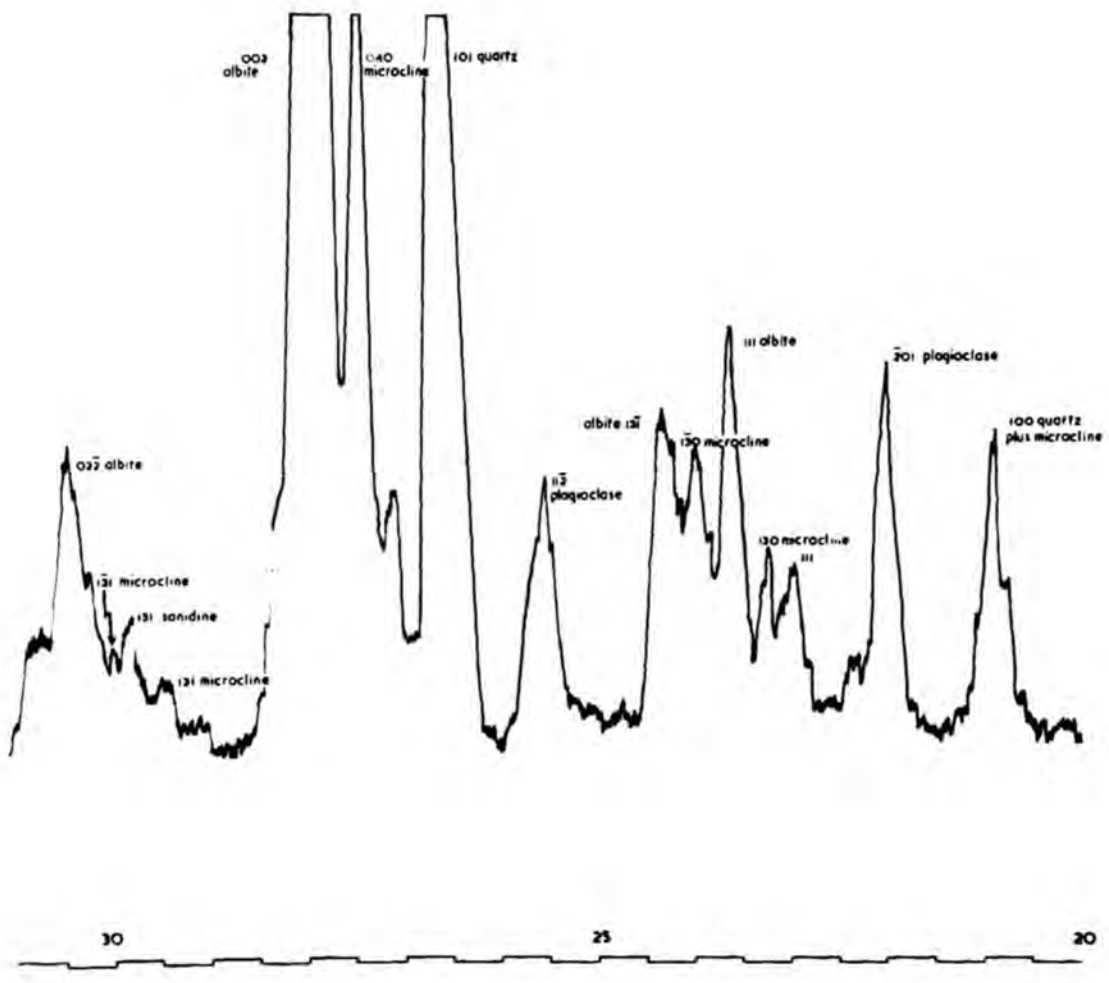
002
albite
040
microcline
101 quartz
022 albite
131 microcline
131 sanidine
131 microcline
11$\bar{3}$
plagioclase
albite 13$\bar{1}$
130 microcline
111 albite
120 microcline
111
$\bar{2}$01 plagioclase
100 quartz
plus microcline
30
25
20

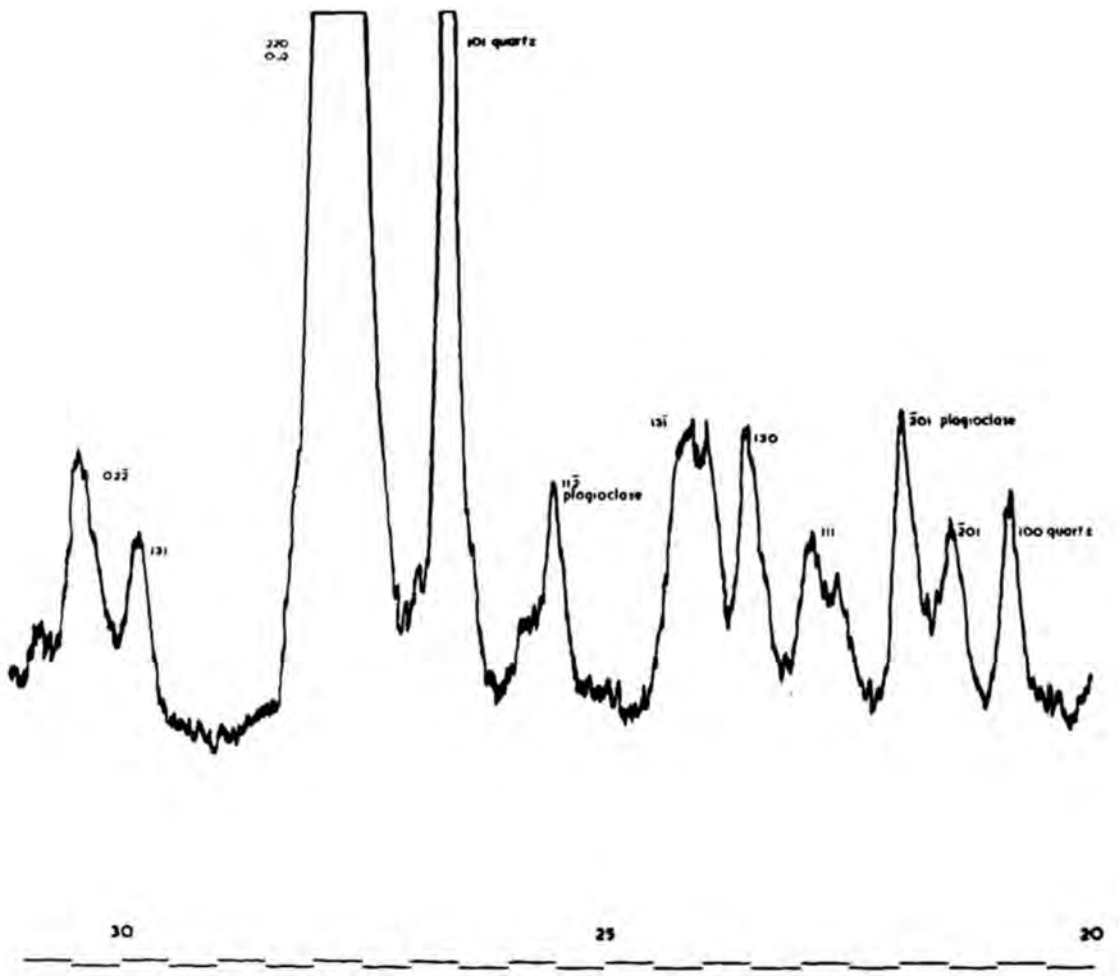
220
002
101 quartz
022
131
11$\bar{3}$
plagioclase
13$\bar{1}$
130
111
$\bar{2}$01 plagioclase
$\bar{2}$01
100 quartz
30
25
20

Fig. 10.28.

Fig. 10.28.
X-ray diffraction chart obtained on specimen 23848(a phenocryst from a hybrid dioritic gneiss). The lower trace is after homogenisation

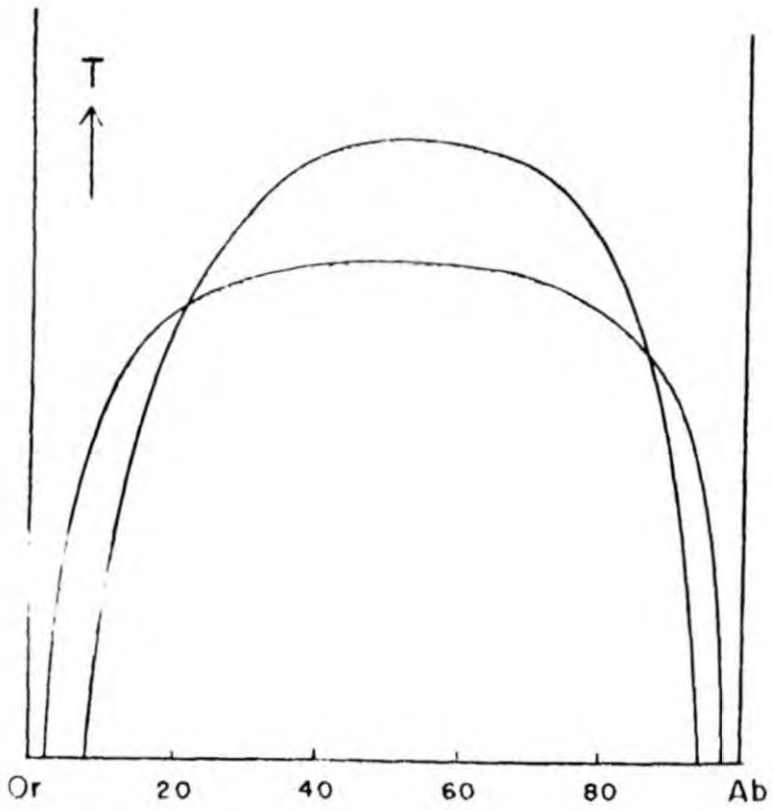

Fig. 10.29.

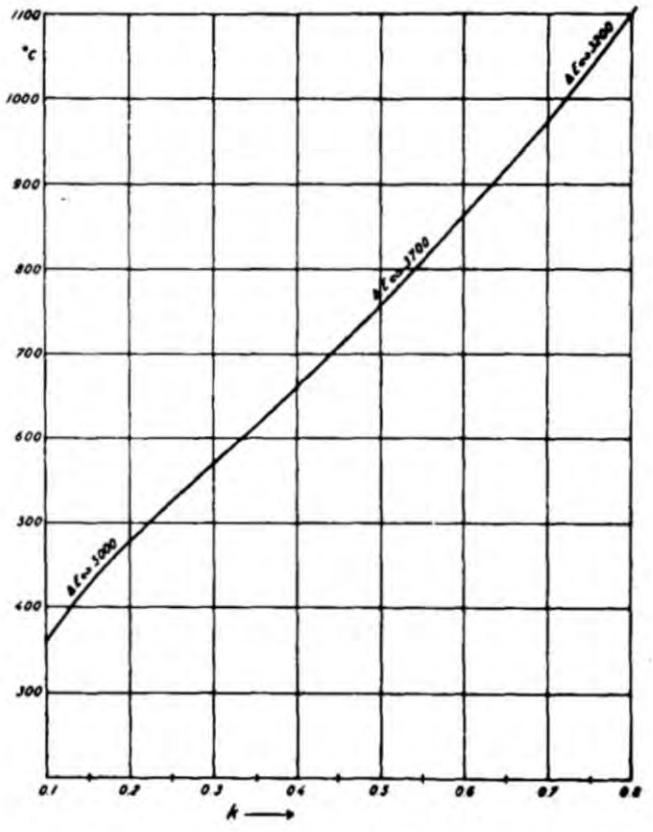

Fig. 10.31.

Fig. 10.29.

Diagram to show two solvii for the alkali feldspars (after Laves, 1952). The taller graph is for the monoclinic feldspars and the smaller for the triclinic.

Fig. 10.31.

Barth's diagram for the estimation of the temperature of crystallisation, where k = % Ab. in the alkali feldspar / % Ab. in the plagioclase feldspar.

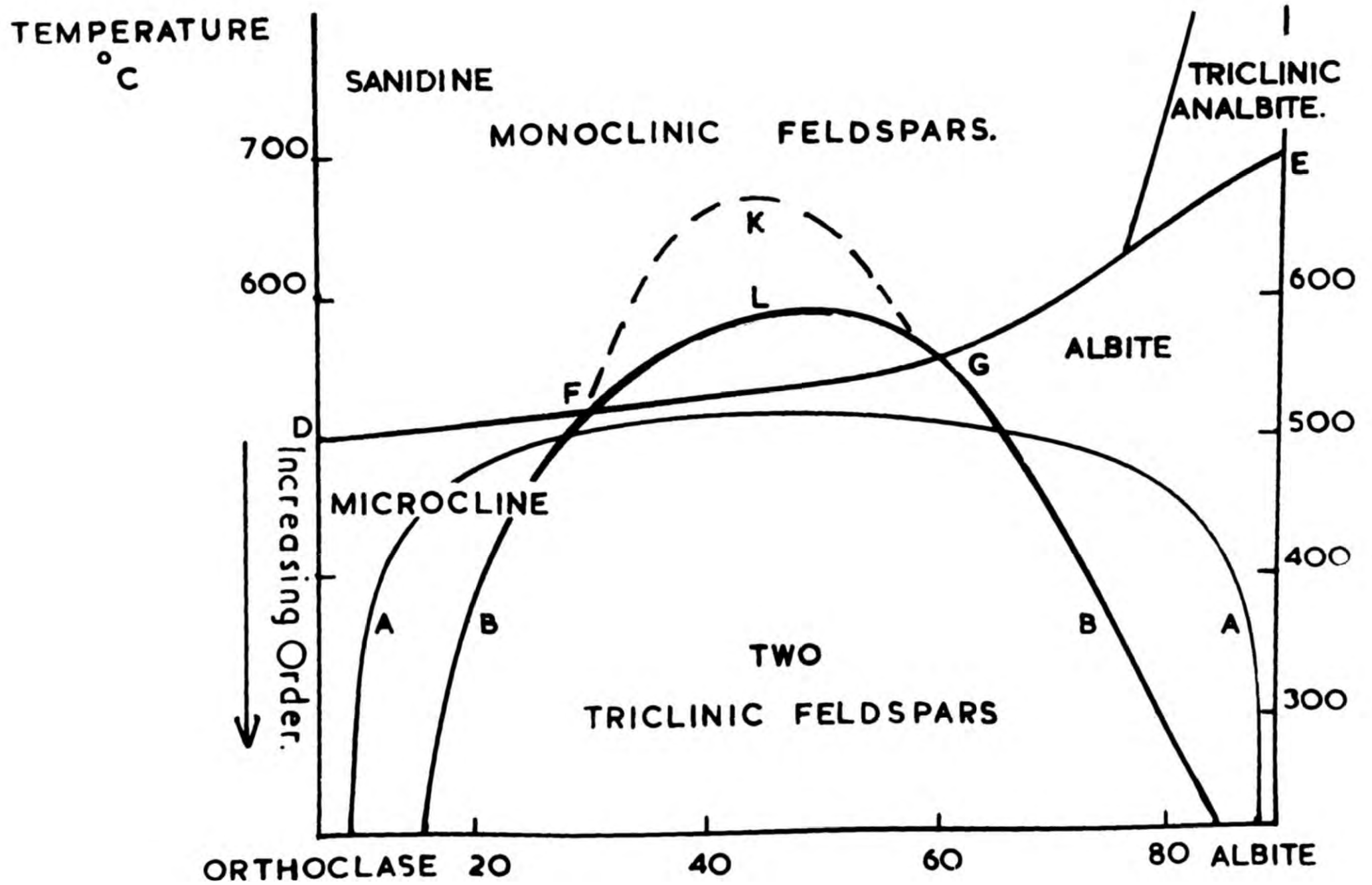
TEMPERATURE °C
SANIDINE
MONOCLINIC FELDSPARS.
TRICLINIC ANALBITE.
700
600
K
L
E
G
ALBITE
F
D
500
MICROCLINE
400
A
B
B
A
TWO
TRICLINIC FELDSPARS
300
Increasing Order.
ORTHOCLASE
20
40
60
80
ALBITE

Fig. 10.30.

Suggested phase diagram for the system Or - Ab. at normal pressure. Curve A. represents the solvus for the fully ordered microcline series. B. is the solvus for the sanidine - analbite series (partly after Smith and MacKenzie, 1958) and the line D - E is the order-disorder boundary, modified after Laves (1952). The solvus F - K - G is that suggested by Bowen and Tuttle (1950).

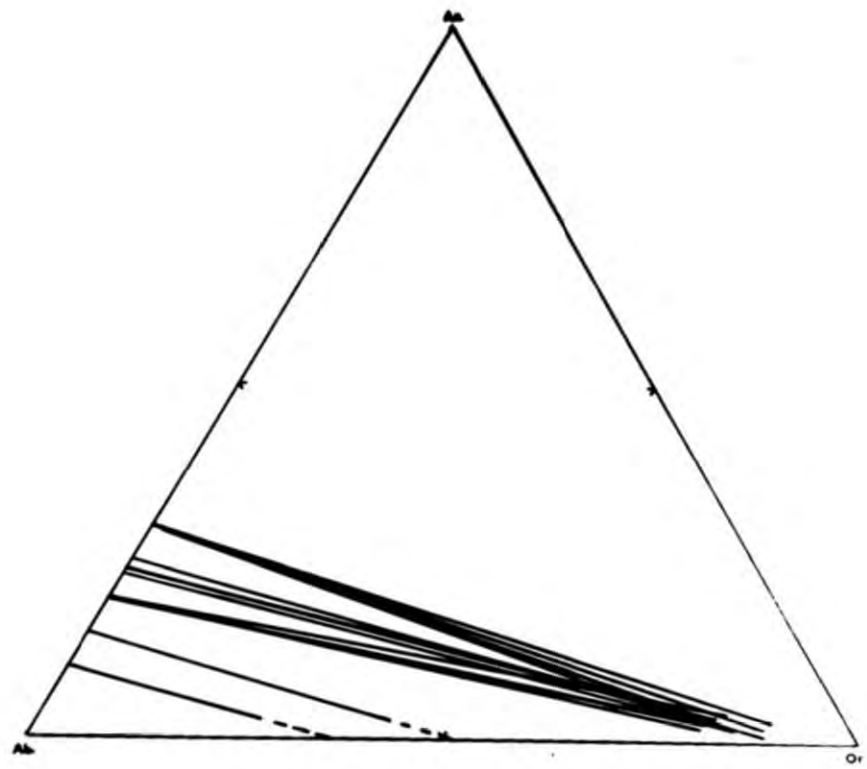

Fig. 10.32.

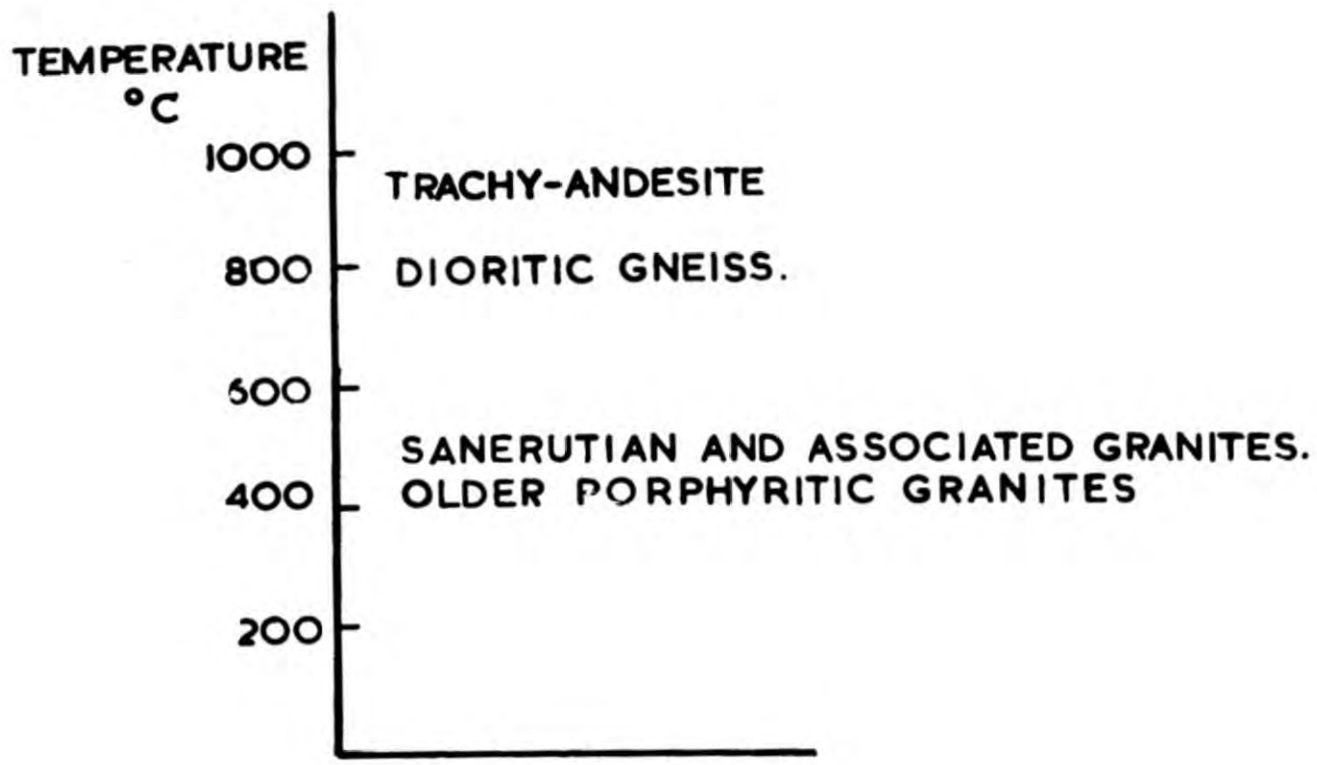

Fig. 10.33.

Fig. 10.32.

Diagram of the co-existing plagioclase - alkali feldspar phases in the representative granites, alkaline dyke and dioritic gneiss.

Fig. 10.33.

Diagram to show the estimated temperatures for the granite types, the alkaline dyke and the dioritic gneiss, using the Barth(1956) method. These temperatures represent the last temperature of crystallisation.

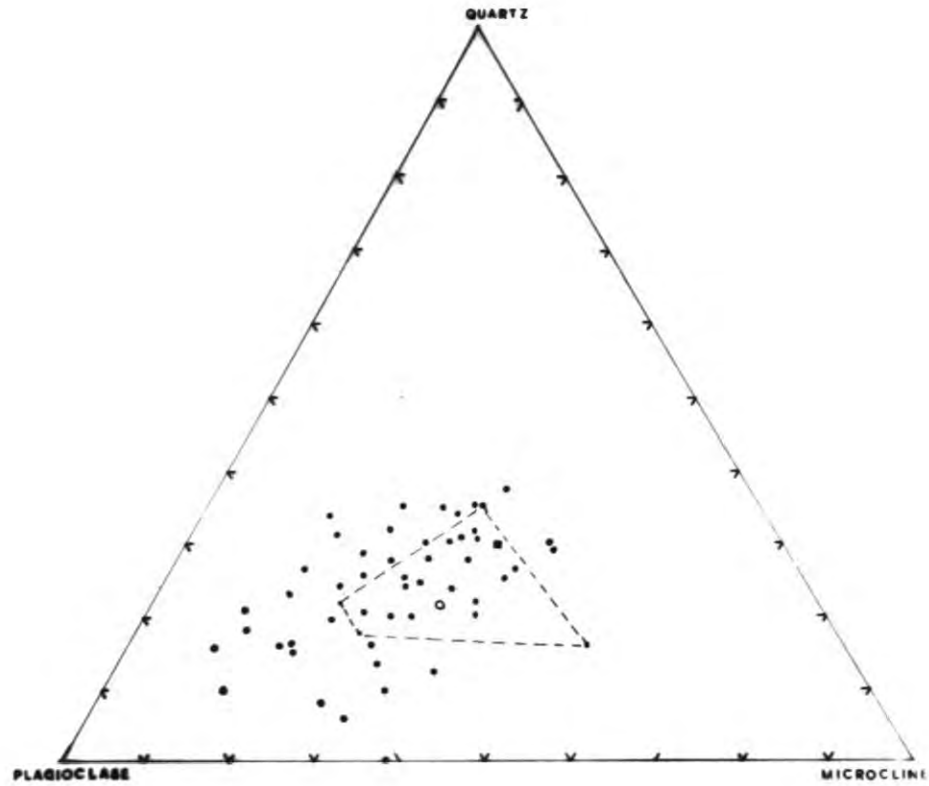

Fig. 11.1.

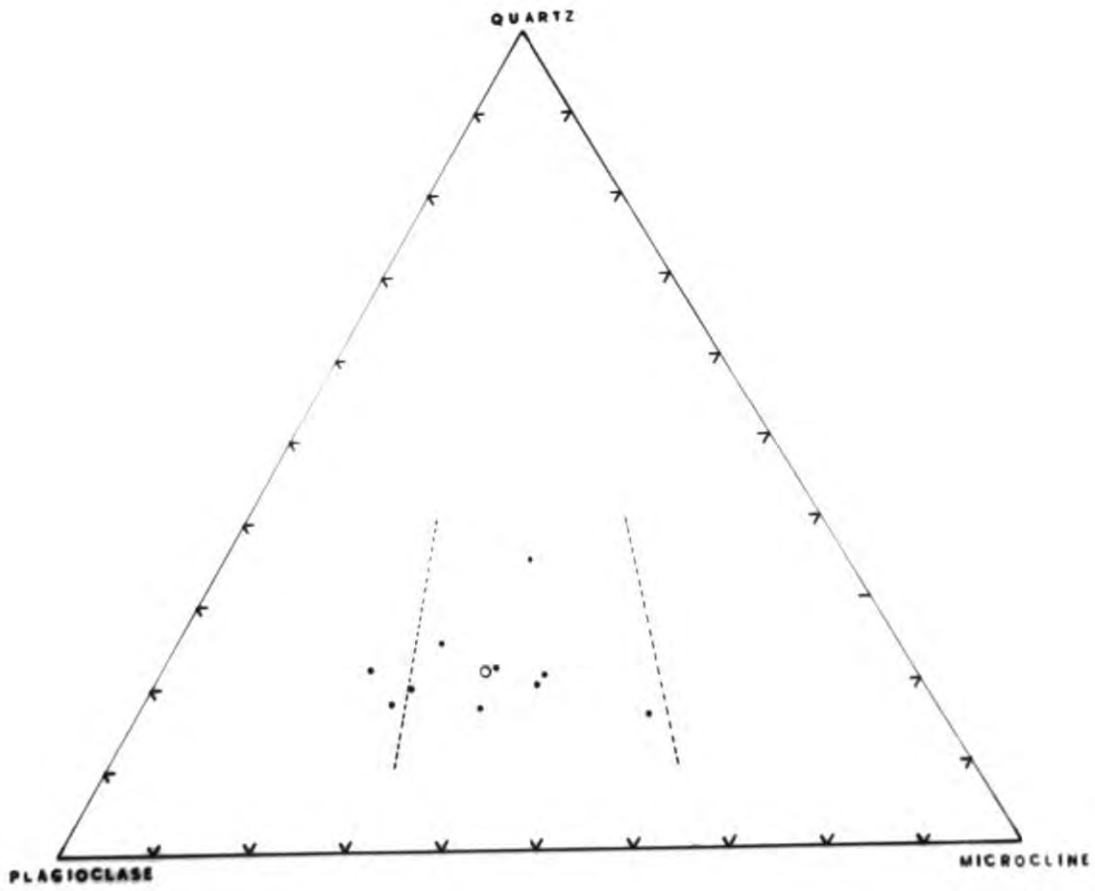

Fig. 11.2.

Fig. 11.1.

Modal anlysis results on over 40 granitic rocks. The dotted line represents the spread obtained when ten thin sections from the same rock were point counted. The values are plotted on a quartz-plagioclase-microcline diagram after these minerals have been totalled to 100%.

Fig. 11.2.

Modal analysis reuslts on ten thin sections from rock 42888. The open circle represents the average of the values obtained and the dotted lines, the granodiorite-quartz monzonite-granite fields.

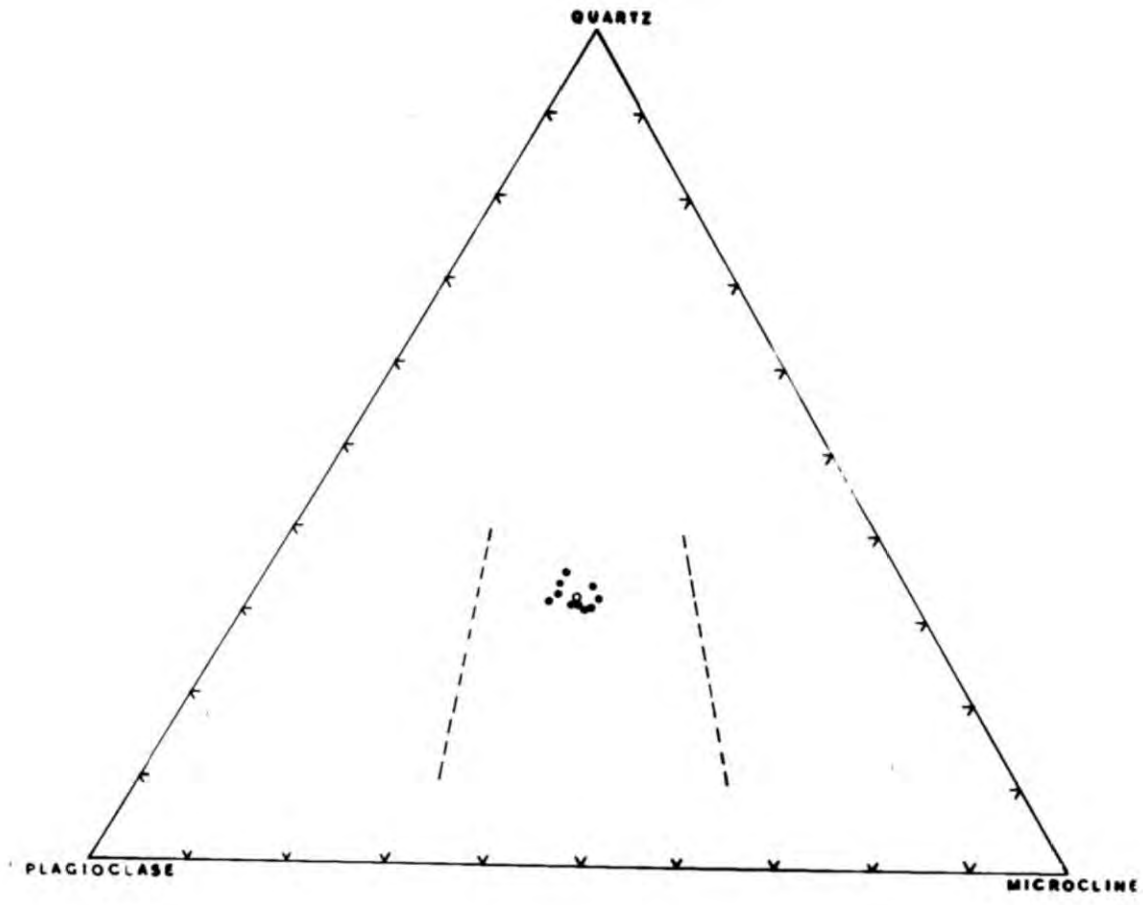

Fig. 11.3.

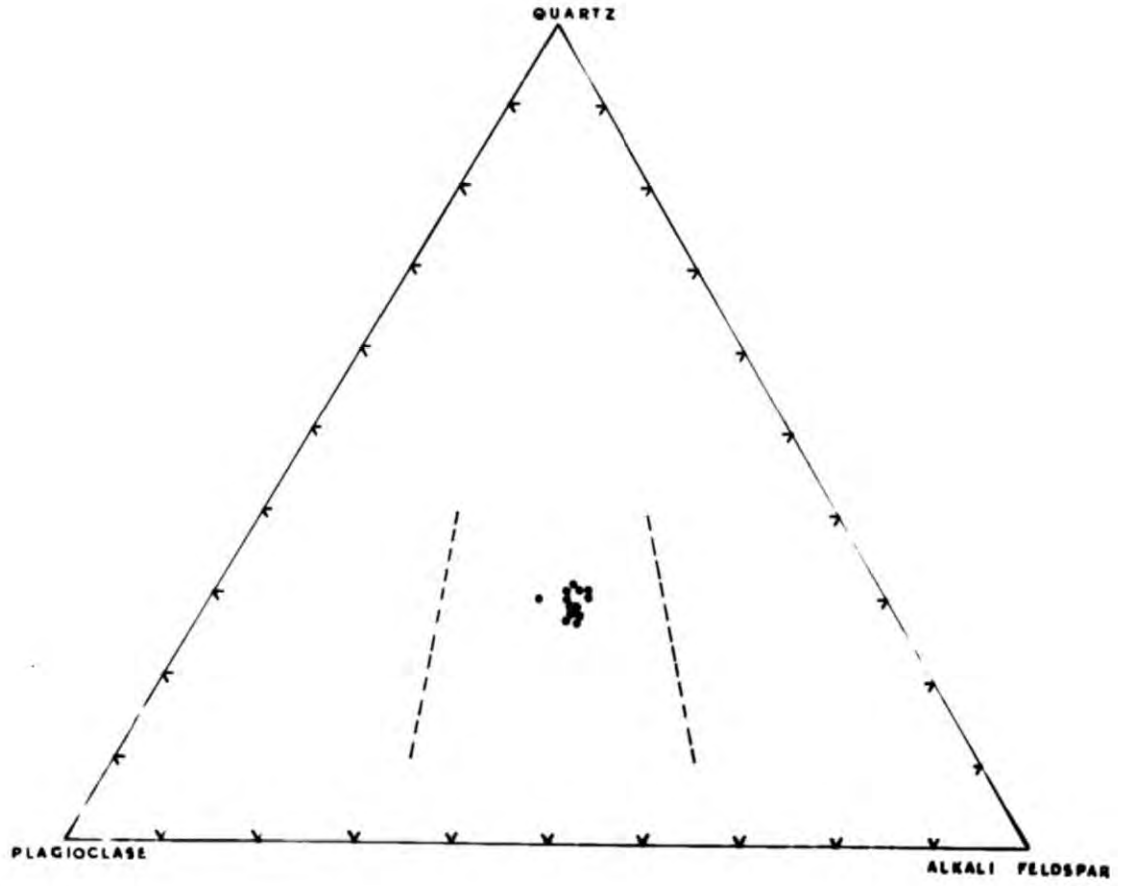

Fig. 11.4.

Fig. 11.3.

Modal analysis results on ten thin sections from the fine grained Sanerutian Granite(specimen 23882), the circle represents the average of the values.

Fig. 11.4.

Modal analysis results on 13 thin sections of the G 1. granite,recalculated from the data in Fairbairn et.al.(1950).

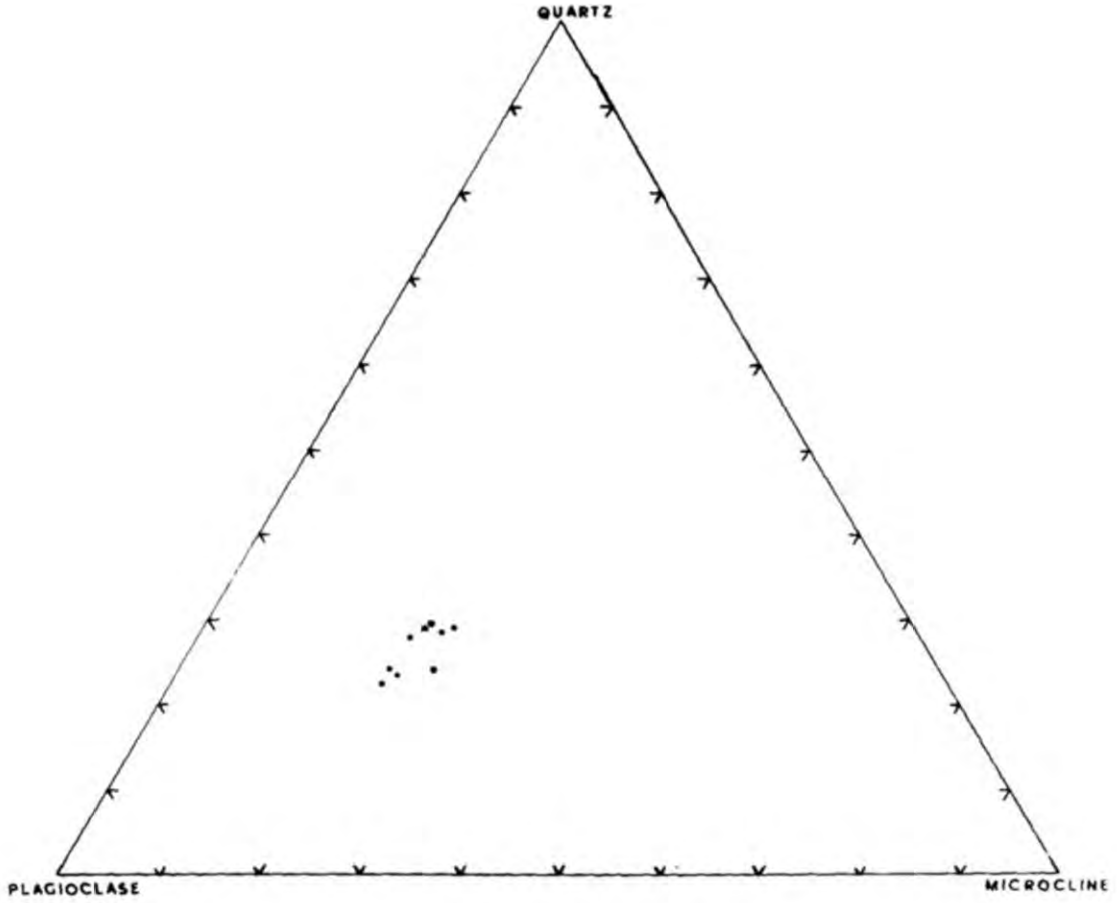

Fig. 11.5.

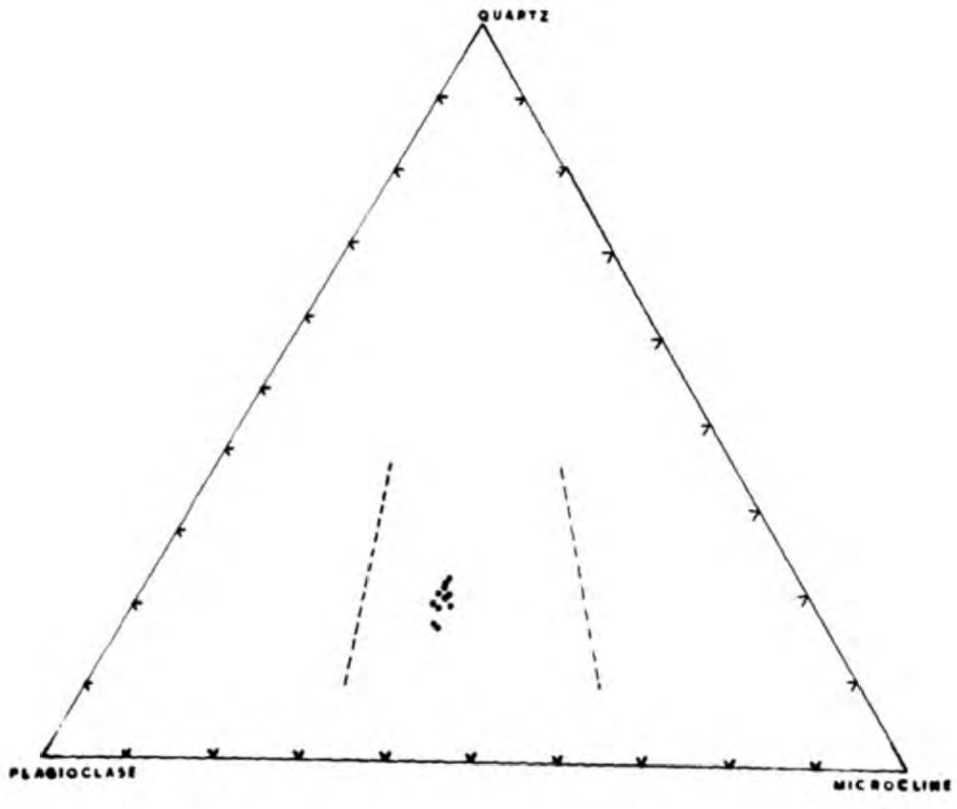

Fig. 11.6.

Fig. 11.5.

Modal analysis of one thin section(42888) carried out by several student operators.

Fig. 11.6.

Results obtained by a combined modal analysis technique on thin section and rock slab(42888) Open circle represents the average of the values obtained.

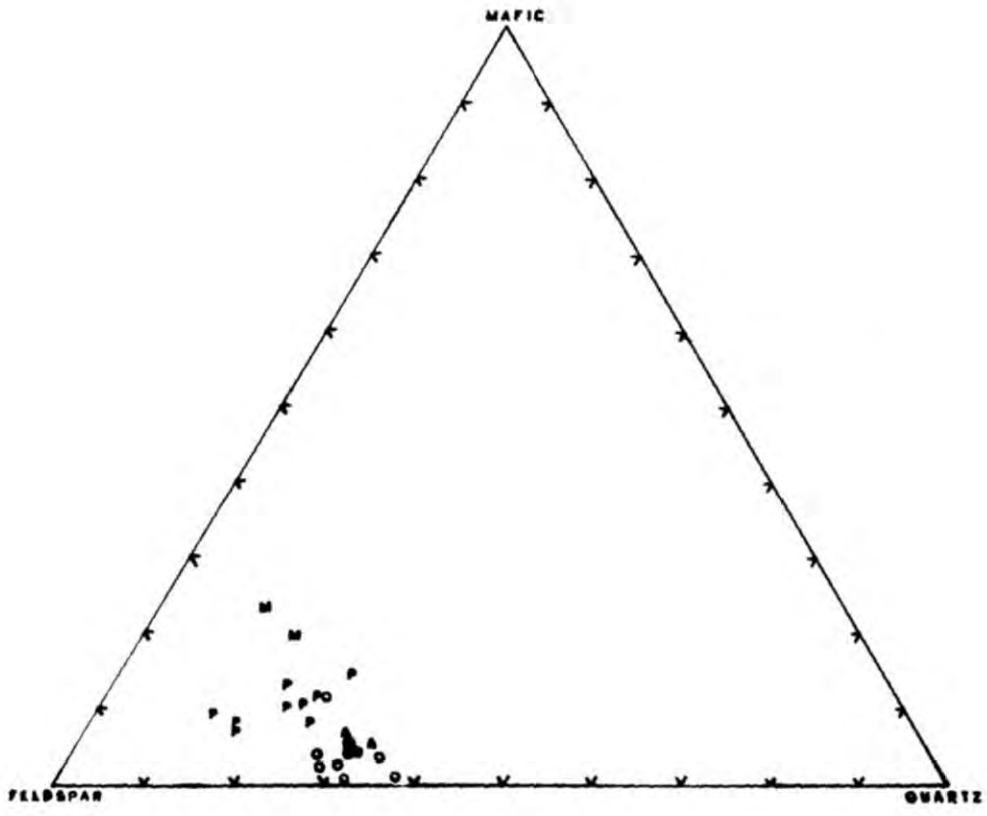

Fig. 11.7.

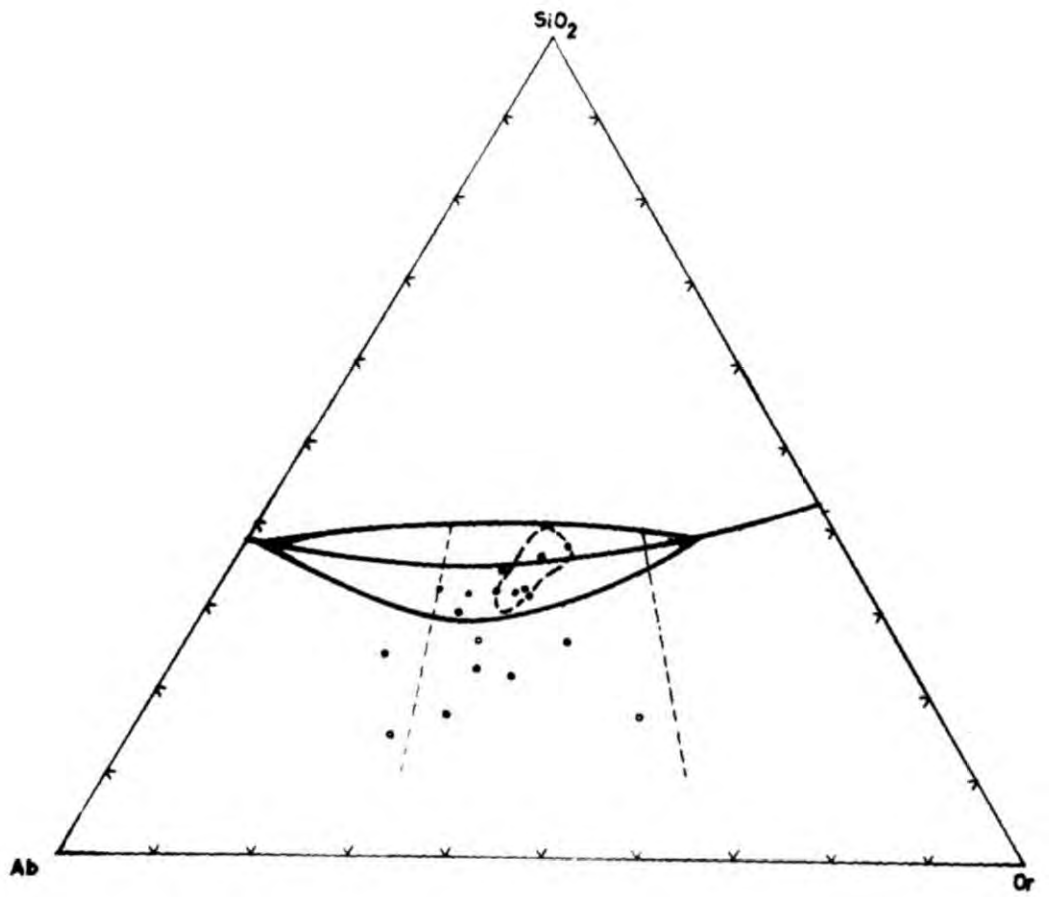

Fig. 11.8.

Fig. 11.7.

Modal analysis results on Sanerutian Granites(= open circle), Porphyritic Aplitic Granites(= A), Porphyritic Ketilidian Granites(=P.) and the microgranodiorite(= M.) These values are plotted on a mafic-total feldspar-quartz diagram.

Fig. 11.8.

Plot of modal analysis results of Sanerutian Granites(closed circles) and Porphyritic Granites of Ketilidian age(open circles) plotted on a quartz - Ab - Or. diagram. The values for the Ketilidian Granites were obtained by combined rock and thin section analysis.(For explanation of other symbols see text.).

Fig. 13.1.
Infrared absorption spectra for G1 Granite, microcline, oligoclase and quartz.

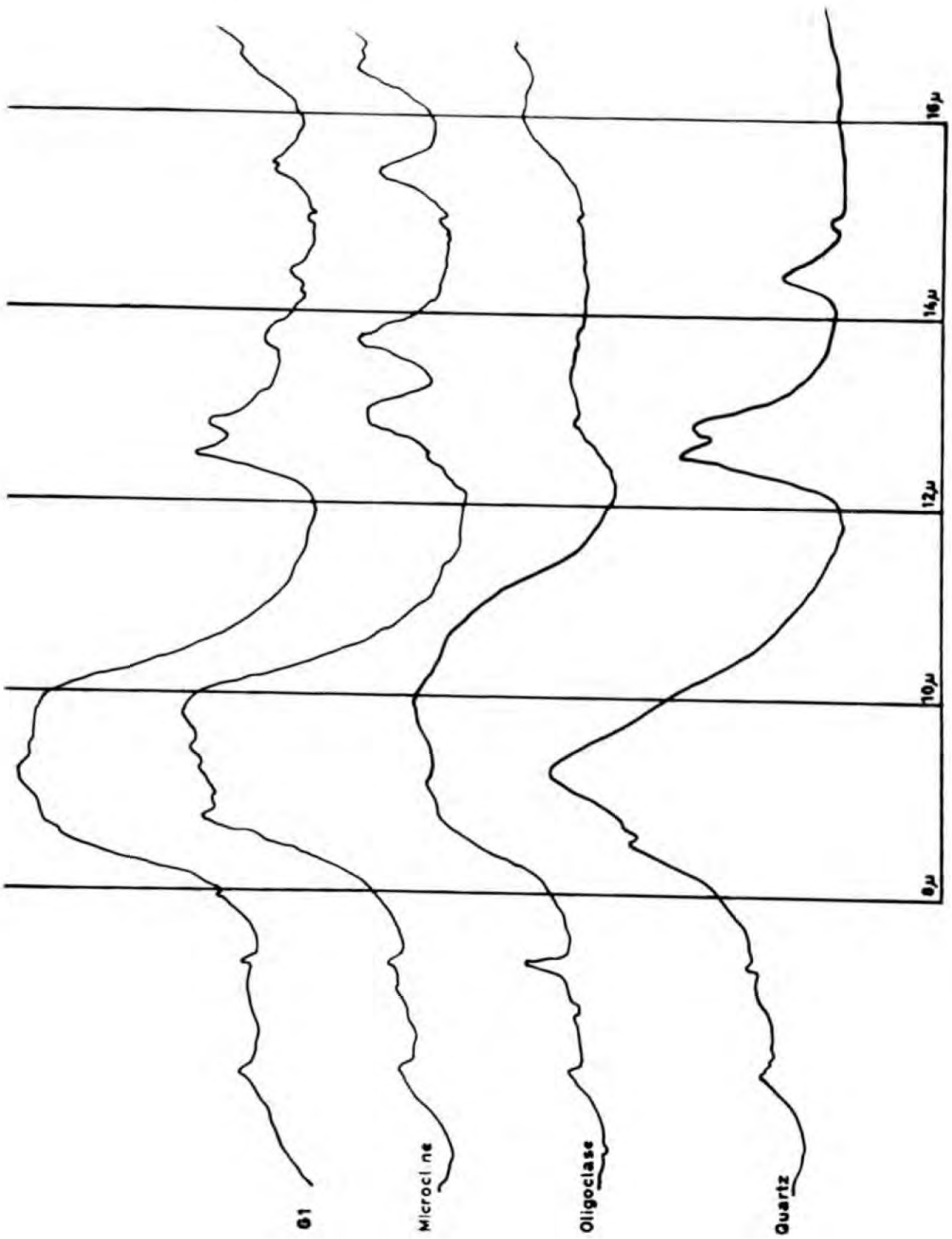

Fig. 13.1.

GEOLOGY OF THE JULIANEHÄB DISTRICT.

"GRANITES"

- Sanerutian Aplitic Granite.
- Porphyritic Aplitic Granite.
- Euhedral Feldspar Phenocryst Gr.
- Big Feldspar Phenocryst Gr.
- Small Feldspar Phenocryst Gr.
- Microgranodiorite
- Undifferentiated hornblende–biotite Gr.

OTHER ROCK TYPES

- Gneiss Band
- Amphibolitic facies of Gneiss Band.
- Fine grained Dioritic Gneiss.
- Amphibolitic xenoliths
- Amphibolite
- Gabbro–Norite.
- Diorite
- Granodiorite Gneiss.

SKOVFJORD

KANGERDLUARSSUK

TARTOQ

Faulted Syenite

Veins of Sanerutian Granite cutting porphyritic Granite

Veins of diorite cutting fine grained dioritic gneiss

Scattered patches of fine grained dioritic gneiss

Kuanitic dyke swarms

Breccia zone

Banded gneiss

BRECCIA PIPE

Strong alignment in xenoliths

Typical porphyritic granite

Numerous veins of Sanerutian Granite in Diorite

Copper Mine. (abandonned)

0 1 2 3 km.

STRUCTURAL MAP OF THE JULIANEHÄB DISTRICT.

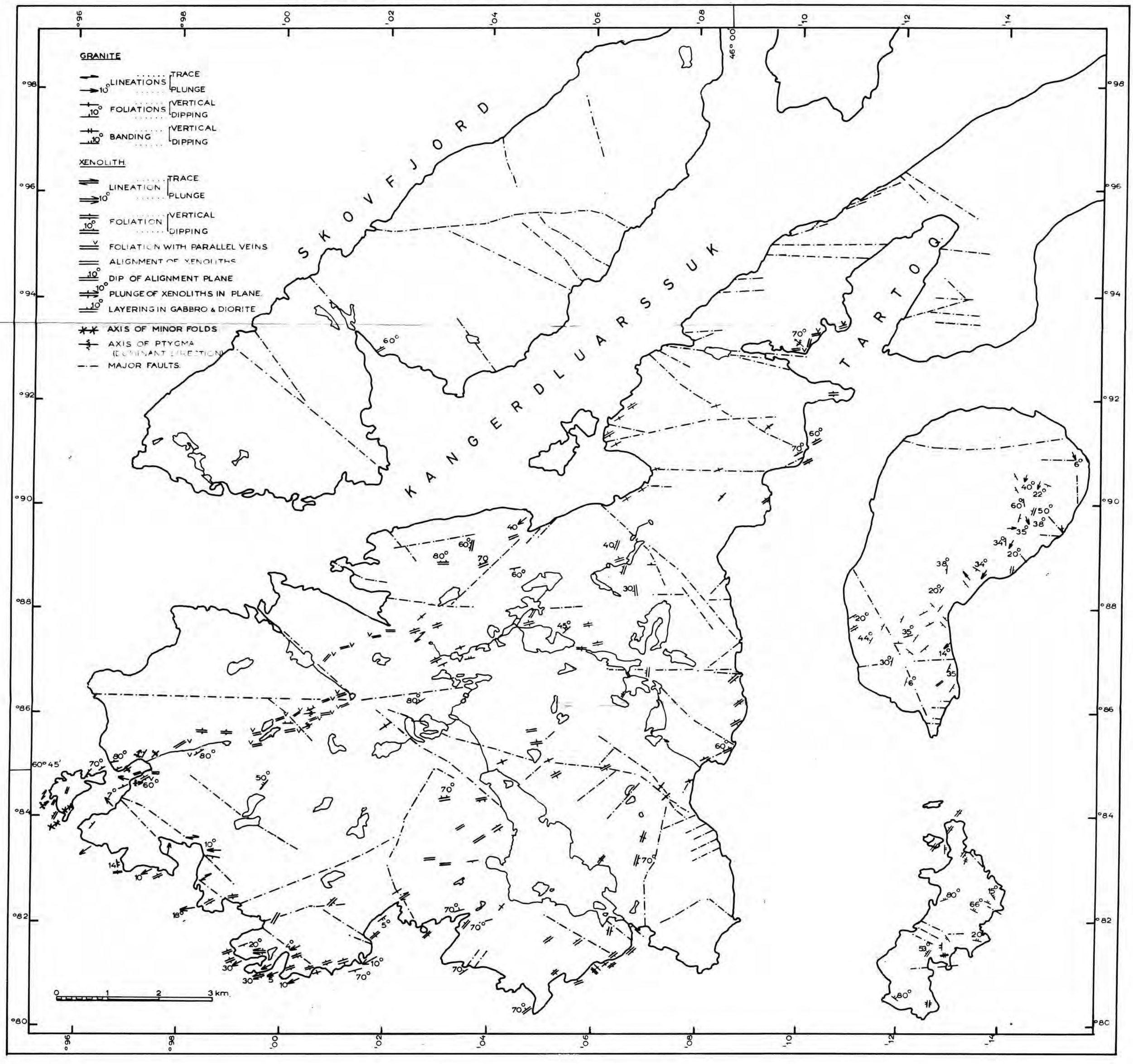

DYKE AND SILL DISTRIBUTION

JULIANEHÅB DISTRICT.

DOLERITE

TRACHY–ANDESITES

TRACHYTIC TYPES.

LAMPROPHYRIC SILL.

KUANITIC DYKES.

DYKE AND SILL THICKNESS NOT TO SCALE.

N

SKOVFJORD

KANGERDLUARSSUK

TARTOQ

46° 00'

60° 45'

0 1 2 3 km.